Surface modifications of nanocrystalline diamond films and their functionalization with phthalocyanines

Dissertation

zur Erlangung des akademischen Grades eines Doktors der Naturwissenschaften (Dr. rer. nat.)

vorgelegt im Fachbereich 10 - Mathematik & Naturwissenschaften der Universität Kassel

vorgelegt von: Dipl. -Ing. Hristo Petkov

Gutachter: Priv.- Doz. Dr. Cyril Popov
                      Prof. Dr. Ulrich Siemeling
Prüfer: Prof. Dr. Martin Garcia
                      Prof. Dr. Kilian Singer

Tag der Abgabe: 15.03.2016
Tag der Disputation: 06.06. 2016

Table of contents

List of tables

List of figures

Abstract

Boron-doped diamond is a promising electrode material for a number of applications providing efficient carrier transport, a high stability of the electrolytic performance with time, a possibility for dye-sensitizing with photosensitive molecules, etc. It can be functionalized with electron donor molecules, like phthalocyanines or porphyrins, for the development of light energy conversion systems. For effective attachment of such molecules, the diamond surface has to be modified by plasma- or photo-chemical processes in order to achieve a desired surface termination. In the present work, the surface modifications of undoped and boron-doped nanocrystalline diamond (NCD) films and their functionalization with various phthalocyanines (Pcs) were investigated. The NCD films have been prepared by hot filament chemical vapor deposition (HFCVD) on silicon substrates and were thereafter subjected to modifications with O_2 or NH_3 plasmas or UV/O_3 treatments for exchange of the H-termination of the as-grown surface. The effectiveness of the modifications and their stability with time during storage under different ambients were studied by contact angle measurements and X-ray photoelectron spectroscopy (XPS). Furthermore, the surface roughness after the modifications was investigated with atomic force microscopy (AFM) and compared to that of as-grown samples in order to establish the appearance of etching of the surface during the treatment. The as-grown and the modified NCD surfaces were exposed to phthalocyanines with different metal centers (Ti, Cu, Mn) or with different side chains. The results of the Pc grafting were investigated by XPS and Raman spectroscopy. XPS revealed the presence of nitrogen stemming from the Pc molecules and traces of the respective metal atoms with ratios close to those in the applied Pc. In a next step Raman spectra of Ti-Pc, Cu-Pc and Mn-Pc were obtained with two different excitation wavelengths (488 and 785 nm) from droplet samples on Si after evaporation of the solvent in order to establish their Raman fingerprints. The major differences in the spectra were assigned to the effect of the size of the metal ion on the structure of the phthalocyanine ring. The spectra obtained were used as references for the Raman spectra of NCD surfaces grafted with Pc.

Finally, selected boron doped NCD samples were used after their surface modification and functionalization with Pc for the preparation of electrodes which were

Abstract

tested in a photoelectrochemical cell with a Pt counter electrode and an Ag/AgCl reference electrode. The light sources and electrolytes were varied to establish their influence on the performance of the dye-sensitized diamond electrodes. Cyclic voltammetry measurements revealed broad electrochemical potential window and high stability of the electrodes after several cycles. The open circuit potential (OCP) measurements performed in dark and after illumination showed fast responses of the electrodes to the illumination resulting in photocurrent generation.

Zusammenfassung

Bordotierter Diamant ist ein vielversprechendes Elektrodenmaterial für eine Vielzahl von Anwendungen, da er einen effizienten Ladungsträgertransport erlaubt, seine elektrolytischen Eigenschaften zeitlich extrem stabil sind, eine Sensibilisierung mit photosensitiven Farbstoffmolekülen möglich ist u.a.m. Für die Entwicklung von Systemen zur Umwandlung von Lichtenergie kann er mit Elektronen-liefernden Molekülen wie Phthalocyaninen oder Porphyrinen funktionalisiert werden. Für eine effektive Anlagerung derartiger Moleküle müssen Diamantoberflächen mithilfe plasma- oder photochemischer Prozesse modifiziert werden, um eine geeignete Oberflächenterminierung zu erhalten. In dieser Arbeit wurden undotierte und bordotierte nanokristalline Diamantschichten (NCD) sowie deren Funktionalisierung mit verschiedenen Phthalocyaninen (PCs) untersucht. Die NCD-Schichten wurden mithilfe der chemischen Heißdraht-Gasphasenabscheidung (HFCVD) auf Siliziumsubstraten abgeschieden; anschließend wurden sie mit O_2- oder NH_3-Plasmen bzw. UV/O_3-Behandlungen modifiziert, um die H-Terminierung der Schichten nach dem Wachstum zu ändern. Die Effektivität dieser Modifizierungen sowie deren zeitliche Stabilität während der Lagerung in verschiedenen Umgebungen wurden mithilfe von Kontaktwinkelmessungen sowie der Röntgenphotoelektronenspektroskopie (XPS) untersucht. Darüber hinaus wurde die Oberflächenrauheit nach der Modifizierung mittels der Rasterkraftmikroskopie (AFM) bestimmt und mit der von unmodifizierten Proben verglichen, um festzustellen, ob während der Oberflächenbehandlung Ätzprozesse stattgefunden haben. Schließlich wurden unbehandelte und modifizierte Oberflächen Phthalocyaninen mit verschiedenen zentralen Metallatomen (Ti, Cu, Mn) und/oder verschiedenen Seitenketten ausgesetzt. Die Ergebnisse dieser Pc-Anlagerung wurden mithilfe der XPS und der Raman-Spektroskopie untersucht. Aus XPS-Spektren ergab sich die Anwesenheit von Stickstoff auf den Oberflächen, der von den Pc-Molekülen stammt, sowie Spuren der jeweiligen Metallatome, wobei die Verhältnisse relativ genau mit denen in den jeweiligen Pcs übereinstimmten. In einem weiteren Schritt wurden Raman-Spektren der Ti-Pc-, Cu-Pc- und Mn-Pc-Moleküle bei zwei Anregungswellenlängen (488 und 785 nm) aufgenommen, um deren Raman-Fingerabdrücke zu erhalten. Dazu wurden Tropfen der Pcs auf Si-Substraten nach Verdampfen des Lösungsmittels verwendet. Die größten Unterschiede in den Spektren

konnten auf Effekte der Größe der Metallionen auf die Struktur der Phthalocyaninringe zurückgeführt werden. Die dabei erhaltenen Spektren wurden als Referenzen für die Raman-Spektren von NCD-Oberflächen verwendet, an die Pcs angelagert worden waren.

Abschließend wurden auf der Grundlage ausgewählter bordotierter NCD-Proben nach entsprechender Oberflächenmodifizierung und Pc-Funktionalisierung Elektroden hergestellt, ´die in einer photoelektrochemischen Zelle mit einer Platin-Gegenelektrode und einer Ag/AgCl-Referenzelektrode charakterisiert wurden. Dabei wurden verschiedene Lichtquellen und Elektrolyte verwendet, um deren Einfluss auf die Eigenschaften der Farbstoff-sensibilisierten Diamantelektroden zu untersuchen. Zyklische Voltammetrie-Messungen ergaben ein weites elektrochemisches Potentialfenster und, nach einigen Zyklen, eine hohe Stabilität der Elektroden. Messungen des Leerlaufpotentials (OCP) im Dunkeln sowie unter Beleuchtung zeigten eine schnelle Antwort der Elektroden auf die Beleuchtung, wobei Photoströme erzeugt wurden.

1. Introduction

Nanocrystalline diamond (NCD) attracts attention as a promising material for many applications in various fields, such as photonics, biosensing, biomedicine and mechanics. In addition to the excellent mechanical properties, some other outstanding features of diamond, like a large band gap of 5.4 eV, high breakdown electric field and high thermal conductivity, are attractive for semiconductor applications because these properties open up a new field of research. The electron and hole mobilities of diamond at room temperature are among the highest of all semiconductors. The material is also biocompatible, nontoxic, chemically inert, and environmentally benign. In addition, it is considered for a number of advanced optical applications such as adaptive micro optics, optical sensors or material basis for quantum information processing.

Part of the surface properties of the NCD films can be adjusted during the deposition process, for example simply by using different gas mixtures and/or deposition pressures to influence the crystallinity and the surface topography can be influenced. Furthermore, the surface of the films can be modified after the deposition (with respect to the surface termination, which effects the surface composition and wettability) using different techniques. All this makes NCD a promising material for different (bio)sensors, field effect transistors (FET) and micro-electro-mechanical systems (MEMS). The surface properties determine the interaction between the diamond films and bio-species or cells. Usually the diamond layers prepared by chemical vapor deposition (CVD) possess hydrogen termination, due to the H_2 ambient during the deposition, the surface is hydrophobic, stable and inert. This inertness can be beneficial for many application areas (i.e. manufacturing of electrodes for harsh environment), but is also making the immobilization of molecules on the surface difficult. Hence, photo- or electrochemical processes are required to change the surface chemistry in order to make possible the attachment of functional groups. Exposure to O_2 or NH_3 plasma is not only making the surface hydrophilic, but also improves the chance to immobilize molecules and increases the chemical versatility of the NCD layer.

Introduction

The possibility to harvest solar energy replicating natural photosynthesis has attracted considerable attention of the scientists in the last decades. Different strategies are currently being followed in order to develop technologies to capture sun light and utilize it for light-driven interactions leading to the generation of photocurrent or to the formation of clean fuels like hydrogen or methanol. The development of light-energy conversion systems, such as photoelectrochemical cells, requires selection and detailed investigation of electrode materials, of catalysts (required for the splitting of water into hydrogen and oxygen) and photosensitizers (i.e. dyes). Porphyrins and phthalocyanines, organic compounds akin to chlorophyll, can be applied as light harvesters and/or electron donors, and have already shown promising effects in solar photovoltaic cells. On the other hand, the electrode materials have to possess a number of properties, including an efficient electron transport, stability of the electrolytic performance with time, possibility for dye-sensitizing, etc.

Diamond doped with boron with concentrations of ca. 3×10^{20} cm^{-3} can be used for the fabrication of electrodes. Boron doped diamond (BDD) electrodes show high chemical stability working in contact with liquid phases, even under extreme pH conditions, and possess a large electrochemical potential window superior to those of the common electrode materials. The BDD surface can be modified by plasma- or photo-chemical processes in order to achieve desired surface terminations and subsequently functionalized with photosensitive dyes.

The goal of the current work was to investigate the growth of undoped and boron doped nanocrystalline diamond (NCD) films, their surface modifications by UV/O$_3$ treatment or O$_2$ and NH$_3$ plasmas, the stability of the achieved different surface terminations and the possibility for anchoring of phthalocyanines (Pc) as dye molecules. Phthalocyanines different metal ions and/or side chains synthesized by the group of Prof. Siemeling (Dept. of Metallorganic Chemistry, Institute of Chemistry, University of Kassel) were applied to NCD with H-, O- and NH$_2$-terminations. The results of the surface modifications and functionalizations were investigated by contact angle measurements, X-ray-photoelectron spectroscopy (XPS) and Raman spectroscopy. Selected samples of boron doped NCD modified and grafted with Pc were used for preparation of electrodes and subjected to photoelectrochemical tests. Cyclic voltammetry and open circuit

potential measurements varying the light source and the electrolyte were exploited to study the electrochemical performance of the diamond electrodes and the possibility to generate photocurrent upon light irradiation.

2. Diamond as material

The diamond has been well - known to the humanity since before Christ. It was discovered in India in rivers and streams about 4 century BC. The extraordinary properties of diamond like, extreme e.g. hardness, have been disclosed in China in the second century BC. Historians assume that Alexander the Great has brought the precious gem to Europe. The history of cutting diamonds dates back to the beginning of the 15-th century in Paris. Diamonds have become popular in jewelry and since this time their usage has accelerated. The position of the diamonds as fashionable accessories for Europe's elite has strengthened and a lot of famous diamonds have been cut and polished.

The structure of the diamond contains only carbon atoms covalently bonded and ordered in a face-centered cubic (fcc) lattice. In the past diamonds have been classified based on properties, such as color, fluorescence or visible absorption spectra. Robertson et al. [1], [2] reported the first classification of diamonds on the basis of the difference in transparency in both ultraviolet (10 nm to ~400 nm) and infrared (over 700 nm) region. The diamond crystals from the first group (type I) show UV opaque below 300 nm wavelength and absorb strongly at higher wavelengths (in the range of 7000- 20 000 nm). The second group is composed of type II diamonds, which transmit in the UV region and display small or no anomalous birefringence when viewed between crossed polarizers. Therefore the diamonds from the type II possess nearly perfect crystal structure [3]. However, this classification was not precise enough. In 1954 Sutherland et al. suggested that a carbon atom in interstitial lattice positions, carbon vacancies, or clusters of vacancies or cavities in the diamond structure might be reason for the existence of two types of diamonds. Later it was proposed that the presence (in type I) or the absence (in type II) of nitrogen atoms in the diamond structure was the cause for the differences [4]. Next studies of the optical bands with a prism spectroscope revealed a relation in the optical properties: a dependence of the diamond color on the UV fluorescence [5], [6]. Various properties, like color, transparency and luminescence [7], were deeply investigated and the data collected were the corner stone in the modern IR spectroscopy to determine the diamond types. In 1959 Kaiser and Bond [8] proved the relationship between several optical characteristics (yellow coloration, blue fluorescence, and a

particular IR absorption spectrum) and the presence of nitrogen atoms in the crystal lattice. The nitrogen impurity in levels detectable by IR absorption spectroscopy is the main difference between the diamonds from type I and type II.
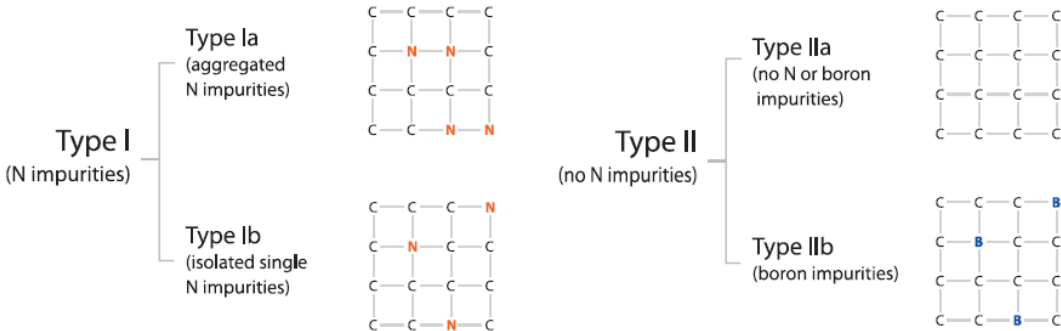
Figure 2.1 *Classification of the natural diamonds respective the impurities in the crystal lattice [9]*

Two forms of nitrogen impurities were distinguished - aggregated and isolated- using IR spectroscopy [10]. Based on these results the diamond from type I was divided into two further groups - types Ia and Ib (see figure 2.1). Type Ia is the most common type (>95%) of natural diamond, containing up to 0.3% nitrogen, while type Ib is rare. Very few natural diamonds are from the latter type (~0.1%), but nearly all synthetic industrial diamonds belong to it. These diamonds contain up to 500 ppm nitrogen.

The types Ia and Ib differ also by the nature of the nitrogen inclusion (figure 2.1). The most common configuration for type Ia diamonds involves two N atoms adjacent to each other in the lattice [9]. In type Ib a single N atom is incorporated in the crystal lattice. In the literature this defect is called an isolated N or single substitutional N atom. In contrast, type Ia diamonds contain N atoms that are in close proximity to one other in one of two spectroscopically detectable configurations.

Diamonds belonging to type II are also very rarely present in the nature and can also be split into two groups - IIa and IIb [11], [12]. Type IIa diamonds contain negligible content of nitrogen which is very difficult to be detected using infrared or ultraviolet absorption methods. The nitrogen content in type IIb diamonds is even lower than in type IIa. The unique properties (such as electrical conductivity and the p-type semiconductor behavior) of this type of diamonds are due to the boron impurity [13].

2.1. Deposition of diamond films

The high quality natural and synthetic diamonds are well known as a popular jewelry accessory and those with low quality can be used for cutting, abrasive or polishing tools. Besides of undeniable value as precious gem stones, diamond possesses a remarkable set of superior physical properties, which makes it very attractive as a material for applications in various areas.

Diamond is a metastable allotrope of carbon, where the carbon atoms are arranged in a variation of the face-centered cubic crystal structure called a diamond lattice. The diamond is thermodynamically less stable than the graphite. The conversion rate from diamond to graphite is negligible at ordinary conditions. Diamond is well-known as a material with superlative physical qualities, most of which originate from the strong covalent non-polar bonding between its atoms. The fact that diamond is composed of pure carbon was discovered in the 18th century. From this time originated the first information about diamond formation, which requires hard conditions: high pressure and high temperature.

Due to these extreme conditions, the first synthetic diamond was produced in a laboratory only in the 20th century after the carbon phase diagram had been discovered (figure 2.2).
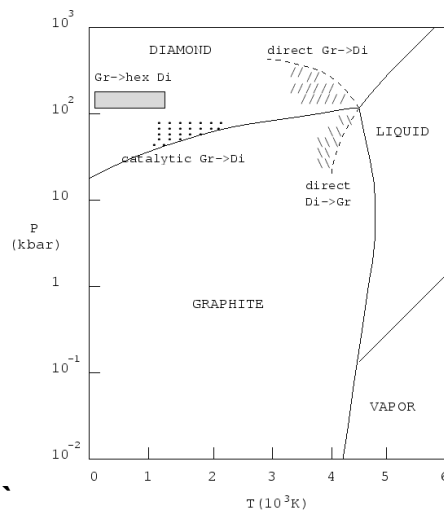
Figure 2.2 *Carbon phase diagram [14]*

O.I. Leipunski described the conditions of the diamond synthesis in a theoretical work in the 1940's [15]. The first machine, able to produce diamonds appeared only in

1950 and ever after diamonds can be reproducibly obtained. Since the second half of the 20th century a new preparation technique has been discovered- diamonds have been produced from graphite under very high pressure and high temperature (HPHT). The first synthetic diamonds were not good enough to be used for jewelry but still good for technical applications due to their hardness. The HPHT synthesis was considerably improved in the recent years and nowadays the growth of crystals up to 5 millimeter is possible.

Parallel to the HPHT technique another method, namely Chemical Vapor Deposition (CVD), was developed for diamond synthesis. In this method a gas mixture with carbon-containing species is used for a chemical reaction on the heated substrate surface and an external excitation is needed to start the process. The external source of excitation can be thermal (heating with hot filaments), or by radiation (using microwave generator). Further, the chemical reaction proceeds, generating the film-forming species (figure 2.3).
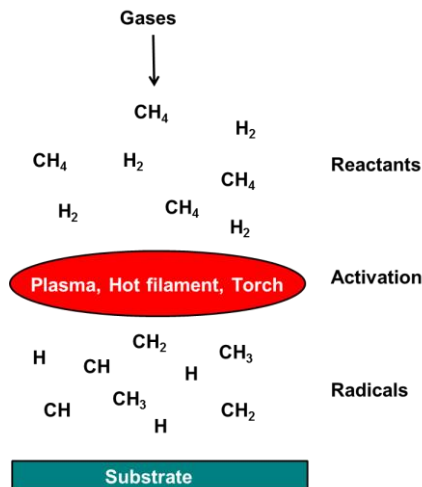
Figure 2.3 *Schematic CVD diamond process*

2.1.1 Low pressure synthesis

Diamonds can be deposited by low pressure synthesis at 1-100 kPa pressure and temperatures between 650 and 1000 °C. At these conditions the diamond phase is metastable and the graphite stable. That is due to the small difference in the free enthalpy (its value at standard conditions is 0.03 eV per atom) [16]. Graphite and diamond are simultaneously deposited on the substrate and because of the high activation energy

required a diamond to graphite conversion is impossible. This conversion occurs initially at 1450 °C. If the graphite formation is further suppressed, only the desired metastable phase will grow. All techniques for diamond deposition at low pressure are based on the activation of a gas mixture from hydrocarbons and hydrogen thereby carbon containing species and atomic hydrogen are formed [17].

The atomic H is known to etch graphitic sp^2 carbon many times faster than the diamond-like sp^3 carbon. As a result the H atoms serve to remove back to the gas phase any graphitic clusters that may form on the surface, while leaving the diamond clusters behind. Thus, the growth of diamond from carbon containing molecules diluted in hydrogen consists of two processes: (i) carbon deposition primarily in the form of graphite with a small amount of diamond, (ii) selective etching of graphite by atomic hydrogen. By optimization of the CVD process one can produce atomic hydrogen from molecular hydrogen close to the surface of the growing film.

Several deposition techniques are known for preparation of diamond: microwave plasma enhanced chemical vapor deposition (MWCVD), plasma jet CVD [18], hot filament CVD [19] and acetylene torch CVD [20] but none of them is considered as the most beneficial.

2.1.2 Hot Filament Chemical Vapor Deposition (HFCVD)

Hot filament chemical vapor deposition is one of the most used techniques for production of diamond films. The simplicity of the process makes it very reliable and preferable. The process is based on the thermal decomposition of carbon containing gases, like methane, propane and other hydrocarbons, in free radicals. These radicals are energetic activated for the diamond growth. A typical HFCVD set up is shown on figure 2.4. It consists of a gas chamber, substrate holder, gas line for introduction and distribution of the gas mixture and several metal wires, located at a constant distance from the substrate. The filaments are made of tungsten or tantalum, because of their high melting points. In order to avoid contamination from the metal wires, a carburization process is desired. During the carburization process metal carbide is deposited on the wire aiming to decrease the vapor pressure of the filaments. The last pre-deposition procedure is the heating of the filaments to temperature above 2000 °C by current

application. Such high temperatures are needed for the decomposition of the carbon containing gas and the molecular hydrogen.
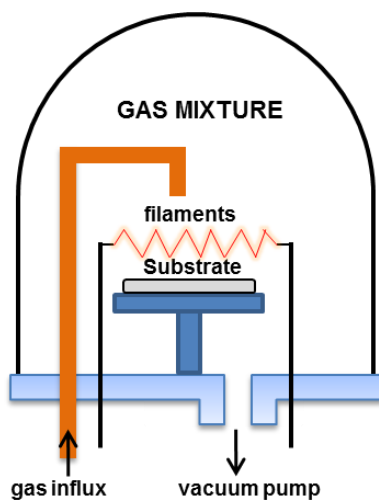
Figure 2.4 *Principle scheme of a hot filament CVD set-up*

The composition of the gas mixture used during the growth process is of importance for the quality and the properties of the NCD film. M. Amaral et al. reported that the smoothness of the NCD film increases with the concentration of noble gases /Ar/. The increase of the hydrocarbon amount and of the amount of noble gases (Ar, Xe, He) or the presence of nitrogen lead to decrease of the surface roughness due to lower amount of atomic hydrogen and the enhanced quantity of non-diamond or amorphous phase. If the C/H ratio is too high, a graphitic material is predominantly deposited [21].

2.1.3 Microwave Plasma Chemical Vapor Deposition (MWCVD)

Generally speaking the deposition conditions in the microwave plasma CVD (MWCVD) reactor are similar to those in the hot filament set-up. MWCVD is the most commonly used diamond growth technique. Schematic representations of microwave reactors of NIRIM type and of ASTeX type are shown in figure 2.5.

Microwave plasma assisted CVD applies electric discharge to produce the radicals required for diamond growth. Microwave power coupled to the growth chamber via a quartz window generates discharge and ignites the plasma [22]. The exited electrons collide with the molecules from the gas mixture. This process leads to heating and dissociation of the gas molecules and generation of high ionization fractures (active

species) needed for the diamond growth. The products from this activation process are hot electrons, cold ions and neutrals.

In the NIRIM type MWCVD system [23] the CH_4/H_2 plasma is generated in a cylindrical quartz tube, perpendicularly connected to a rectangular waveguide (figure 2.5a). The intensity maximum of the electric field is in the center of the discharge tube, creating a stable plasma. The plasma position can be changed by slight shift of the wavelength. The substrate is placed in the discharge tube using a dielectric rod to prevent microwave leakage and is heated by the plasma. The main advantages of the NIRIM type reactors are the simplicity of the reactor design and the flexibility of the substrate position toward the plasma. Disadvantage is the limitation in the size of substrate to few cm^2 by the inner diameter of the cylindrical quartz tube [24].
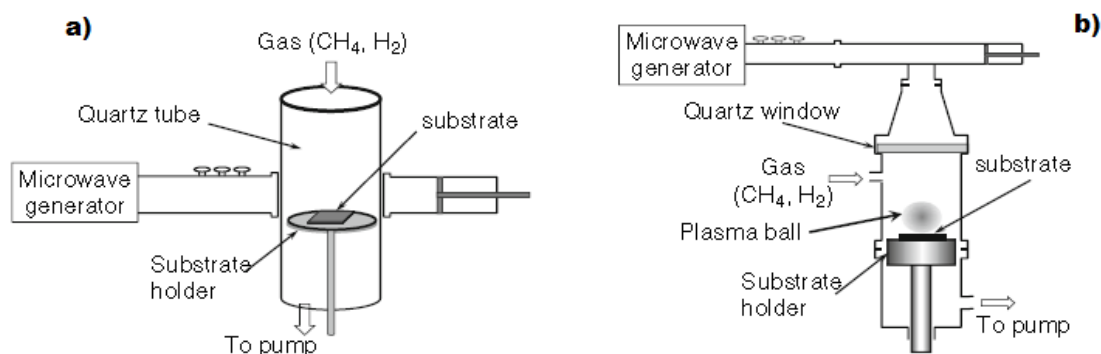
Figure 2.5 *Schemes of microwave plasma-enhanced CVD reactors: (a) NIRIM type, (b) ASTeX type [25]*

The second type of reactors (shown on figure 2.5b) firstly designed by Bachmann et al. [26], and later commercialized be Applied Science Technology, Inc. consists of a cylindrical stainless steel chamber coupled with a microwave generator (2.45 GHz) via an axial antenna through a quartz window. A discharge called "plasma ball" is generated close to the substrate providing the substrate heating. Substrates with size 10 cm in diameter can be coated in this type of reactors. Microwave power up to 5 kW can be used to achieve growth rate higher than 10 µm/h. If the pressure is too high or microwave power too low, the plasma is not stable and tends to jump to the quartz window, occasionally resulting in destruction of the window. The same appears also if the microwave power is too high for a given pressure.

The advantages of the microwave system are the high power and hence the higher growth rates, the usage of a wide variety of gas mixtures, including mixtures with high oxygen content or containing chlorinated or fluorinated gases [24].

2.1.4 Diamond growth mechanism

The diamond growth is a complex process, which can be viewed from chemical and physical aspects. The simplified schema of the growth mechanism is presented in figure 2.6. The mixed reaction gases are flowed into the chamber passing through an activation region– plasma, electric discharge, hot filaments, etc. This excitation causes dissociation of the gases into reactive atoms and radicals and their partial ionization.
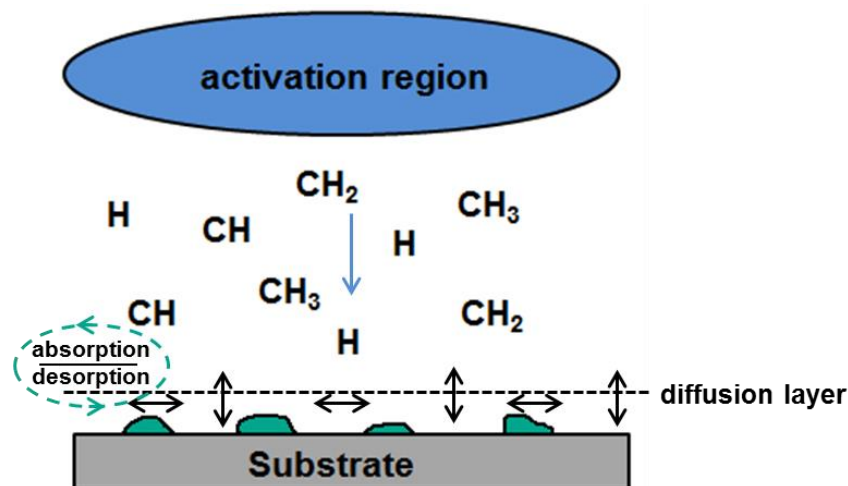
Figure 2.6 *Physical and chemical processes during diamond growth*

On the other hand the ions and electrons are heated and this leads to the heating of the gas mixture and the whole chamber. The activated fragments continue to mix and react with the substrate surface and a so-called diffusion layer is built. The adsorption and desorption processes in this layer continue together with the surface diffusion of the film-forming species until an appropriate reaction (nucleation) location on the substrate is found. When the conditions are fulfilled, the diamond growth can begin. The chemical processes in the gas phase during the CVD process are a subject of investigations during the last decades. A lot of scientists [27] have studied these processes in order to understand better the diamond growth. For example, Bachman et al. [28] have investigated the diamond growth mechanism and its dependence on the gas compositions and reactor types.

The C-H-O phase diagram presented on figure 2.7 reveals the narrow diamond growth region limited by the oxygen and carbon contents in the gas phase. If the oxygen level is too high the diamond growth is not possible.
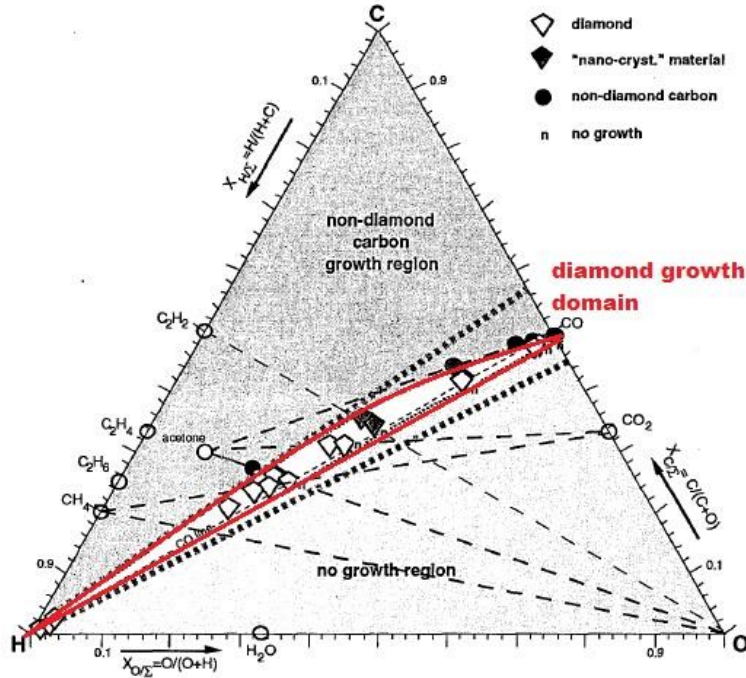
Figure 2.7 C-H-O gas phase diagram of diagram CVD *[28]*

In the carbon-rich gas domain non-diamond amorphous carbon species are prior deposited [28]. Diamond growth is feasible when the gas composition lies in diamond growth domain (defined by red lines on the diagram). The diamond growth domain is available by 0.3 - 5% CH_4 in hydrogen atmosphere.

The diamond growth is relatively independent on the precursors, however, there is no unanimity about the species involved in the process: C, CH, C_2, C_2H, CH_3, C_2H_2 [29], [30]. Even today the growth species chemistry is still not completely clear but the importance of the CH_3 radicals is doubtless [31] as evidenced from Equations 1-4 viewing the reactions in the activation region:

$$CH_4 + H \rightleftarrows CH_3 + H_2 \tag{1}$$

$$2CH_3 \rightleftarrows C_2H_6 \tag{2}$$

$$C_2H_6 + H_2 \rightleftarrows C_2H_4 + 2H_2 \tag{3}$$

$$C_2H_4 + 2H \rightleftarrows C_2H_2 + 2H_2 \tag{4}$$

The schematic growth mechanism is illustrated in figure 2.8. During the growth process the reaction chamber is saturated with hydrogen and the diamond surface is mostly hydrogen terminated. The bond between carbon and hydrogen is very stable, the possibility of the surface to adsorb hydro carbon species, like CH_3, is limited and the species migration between different nucleation sites (migration in x-direction) is reduced (figure 2.8). Atomic hydrogen is able to react with the hydrogen from the surface, creating a free nucleation site.
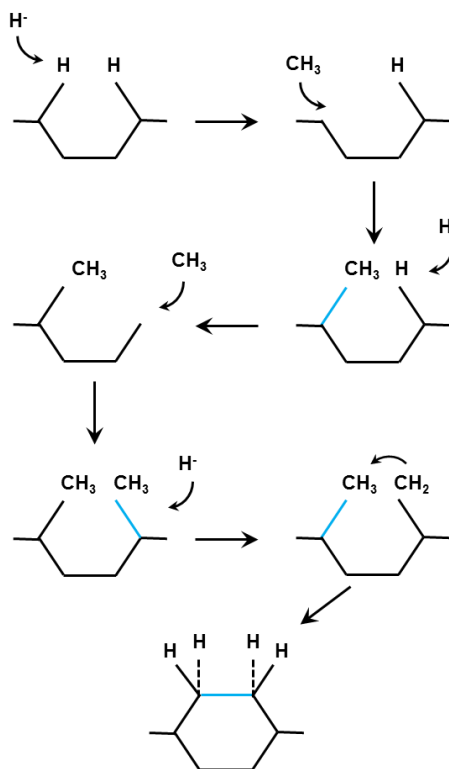
Figure 2.8 *Diamond growth mechanism – desorption and adsorption processes on the surface (in blue color - the new bonds formed during the process) after [28]*

The adsorption of free hydrogen atom is energetically the most likely further reaction, thus stabilizing the surface. Simultaneously adsorption of methane radicals from the gas phase on the free surface and addition of a carbon atom to the lattice is also possible thereby the process (adsorption of CH_3 at the expense of hydrogen) can occur very closely to the adsorbed hydrogen or attached methyl radical. The chemisorption process continues with H-abstraction from the already bonded to the surface methyl radical and the adsorption of a new free radical with addition of two new carbon atoms to the diamond lattice. The

13

growth mechanism can be described as a process, in which separate carbon atoms are stepwise incorporated in the diamond lattice. Thereby the atomic hydrogen is playing the role of a "catalyst". If there is oxygen in the system, OH radical groups are formed and they etch the amorphous carbon away thus increasing the growth rate and preparation of diamond film with better quality.

2.1.5 Diamond nucleation

Diamond nucleation is the first stage of the growth process. The formation of sp^3 tetrahedral lattice starts after the diamond nucleus appears on the surface. The nucleation is crucial for the size of the diamond crystals, film thickness, morphology and homogeneity. The process is influenced by the presence or absence of defects, surface roughness and the adhesion between the deposited film and the substrate. The diamond nucleus is the smallest unit needed for the diamond growth. The nucleation process can occur:

> ➢ in the gas phase – homogeneous nucleation,
> ➢ on the substrate surface – heterogeneous nucleation.

The classical nucleation theory has introduced the term nucleus size - the critical cluster size above which the growth process is dominating over the etch process. In case of homogeneous nucleation this size can be evaluated from the change in the free energy between the gas and solid phases (both bulk and surface contribution). Based on the classical nucleation theory, Derjaguin and Fedoseev [32] have defined the theoretical requirements for the homogeneous nucleation. Frenklach and co-workers [33] published for the first time the conditions of homogeneous nucleation considering the theoretical work of Fedoseev and co-workers [34] and assumed that the hydrogen atoms should reach a state of super-equilibrium. Frenklach et al. extended further the conditions with the suggestion that the hydrogen abstraction is the slowest process and the limiting step for the diamond growth [33].

Matsumoto and coworkers proposed in 1983 that small hydrocarbon molecules, like adamantane, bicyclooctane, tetracyclododecane, hexacyclopenta-decane, and dodecahedrane, shown on figure 2.9, can act as nuclei in a homogeneous diamond

growth [35]. The molecule of adamantane is the simplest arrangement of carbon atoms needed for the stable diamond lattice. Tetracyclododecane and hexacyclopentadecane can be considered as twin diamond nuclei. They both are supposed to be the precursors of the fivefold twinned diamond microcrystals predominant in CVD diamonds. Diamond lattice can be generated from all of the mentioned molecules only by hydrogen abstraction and excess of carbon introduced to the structure [36].
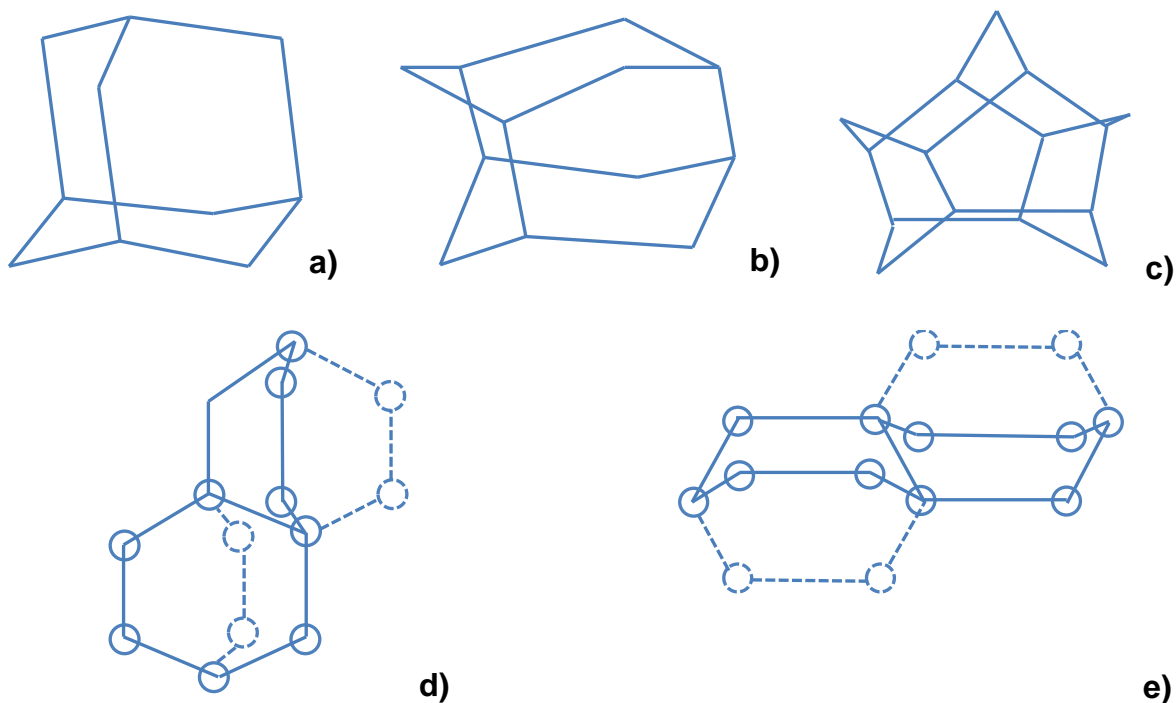
Figure 2.9 *Schematic illustration of the different hydrocarbon cage molecules: a) adamantane; b) tetracyclododecane ; c) hexacyclopentadecane; d) cis boat-boat bicyclodecane; e) trans boat-boat bicyclodecane*

From thermodynamic point of view, such hydrocarbons are unstable at the specific conditions of the CVD (temperatures over 600 °C and low pressure) [37], [38] but it still can be assumed that a nucleus might be built in the gas phase, reach the surface and participate in the growth process. The role of the nucleus as a core for the successive diamond growth is more theoretical and highly questionable but its influence over the nucleation density is undoubted.

When the nucleation appears on a non-diamond surface (like metal or silicon surface), a carbide interlayer is initially formed - MeC or SiC. This interlayer is required for the formation of the first diamond nuclei (figure 2.10). The first stage of the nucleation process is called carburization: all available carbon atoms cover completely the surface and form a carbide surface layer [39].
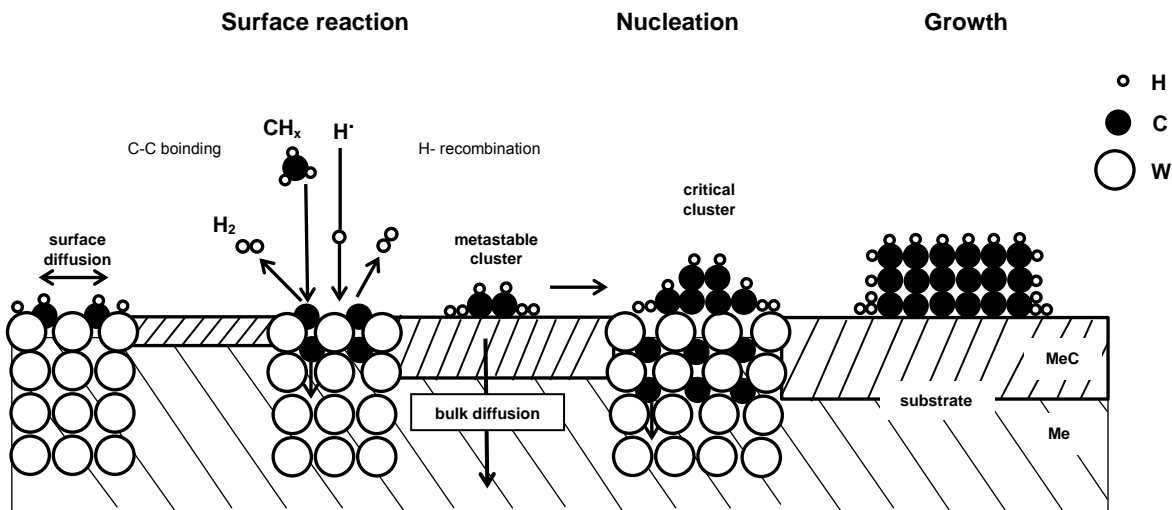
Figure 2.10 *Heterogeneous nucleation on a non-diamond surface (in this case W)*

The lack of carbon atoms on the surface is the reason why the nucleation process is impossible at the beginning. The carbon transport rate is in inverse proportion to the thickness of the interlayer - when the layer thickness increases, the transport rate decreases and the C-concentration on the surface increases, as a result metastable clusters are built. For the purpose of diamond nucleation two conditions should be fulfilled:

- the carbon concentration must exceed the critical level for diamond nucleation,
- the metastable cluster should be large enough (the critical size must be reached).

The nucleation process at atomic level can be described by the following characteristics:

- atoms from the gas phase interact with the substrate surface and become adsorbed onto it;
- the small adatoms may desorb or diffuse over the surface;
- adatoms accumulate atoms from the gas phase and clusters are formed;

- increase or decrease of the adatoms concentration leads to growth or decay of the new formed cluster;

- the cluster remains unstable until exceeds the nucleus (or critical) size; at this size the growth is more probable than the decay;

- stabilized cluster can assure the needed nucleation site for further growth. Both simple nuclei as adatoms and molecules from the gas phase can be adsorbed and incorporated. The time needed for the formation of such a cluster is called incubation period.

A lot of work has been invested over the years into the study of the dependence between the substrate properties and the nucleation process. Several studies without pretreatment of the surface have revealed two main trends. The carbon diffusion into the bulk material and the formation of the carbide layer have a big impact on the carbon concentration on the surface [40]. Both the carbide layer formation and the low diffusion benefit the existence/appearance of carbon surface concentration, sufficient to start the nucleation [41]. The second trend is the assumption that a nucleation occurs mainly or only at the so-called defect sites on the surface. The nucleation is an important stage of the diamond deposition process. It is strongly influenced by the substrate material and the initial surface conditions. Silicon is preferred as a material for thin film diamond deposition because of its good semiconductive and mechanical properties. The high lattice mismatch (α_{Si}= 0.543 nm, α_{NCD}= 0.356 nm) and high surface energy difference (1.5 - 6 J.m^{-2}) between the Si and nanocrystalline diamond (NCD) appear to be an issue for the nucleation process [42] and the reason why diamond nuclei growth on a polished silicon surface is very difficult. This can be solved by additional pretreatment of the silicon substrate [43] to reach the required diamond growth nucleation density (between 10^9 and 10^{11} cm^{-2}). Two techniques are commonly used: (i) scratching of the substrate with a diamond powder using mechanical and ultrasonic techniques, (ii) bias enhanced nucleation (BEN). The first method is applied before the diamond deposition and it is pure mechanical one - the nucleation sites are achieved by scratching and/or seeding the substrate with diamond powder [44] or diamond paste. Thus a higher nucleation density can be achieved due to the creation of defects (nucleation sites) on the surface (min. 3 orders of magnitude higher compared to a substrate without any pretreatment) [45].

During this scratching, fragments from the seeding diamond remain on the substrate, damaging the surface, which make this technique not appropriate when the surface should be intact. In order to protect the substrate and to minimize the scratches, a diamond suspension can be used. The common size of the diamond particles for pretreatment is 0.1-20 µm, recently stabilized suspensions with crystallite sizes down to 10 nm are also available. With time evolution morphology change from large randomly spread crystals to smaller crystals with higher density [46].

The bias enhanced nucleation (BEN) has been demonstrated for the first time in 1991 by Yugo et al. [47]. This method provides a high nucleation density up to 10^{10} cm^{-2} even on mirror-polished substrates and stable conditions for oriented or epitaxial growth. Bias voltages from +100 to -200 V were applied to the substrate for a various time. Stoner and Jiang reported the first ever successful high textured (100) diamond growth in microwave plasma assisted set-up using BEN [48], [49]. This method was further developed and a new nucleation model was suggested by Yugo et al. [50]. The sp^3 carbon atoms form clusters due to low energy implantation and these clusters provide nucleation sites for the growth. The negative bias charges attract positive ions from the gas phase and the ions bombard the substrate thus removing the contaminations and favoring the sp^3 cluster formation on the surface enhancing further the nucleation.

2.1.6 Poly-, nano- and ultrananocrystalline diamond films

Natural and synthetic diamonds are limited in size, while for many applications much larger surfaces are required. The solution of this problem are diamond coatings on different substrates which possess the excellent properties of diamond. According to their crystallinity the diamond films are divided into polycrystalline (PCD), nanocrystalline (NCD) and ultrananocrystalline (UNCD), displayed on figure 2.11.

The PCD films (called also microcrystalline) are composed of diamond crystallites with a size of several microns and different crystographic orientation. The major disadvantage of the PCD films is the high surface roughness (figure 2.11,a) which requires an expensive and time consuming mechanical polishing. The surface roughness can be decreased with the deposition of smaller crystallites, like NCD films. In this case

the diamond crystallites grow from the nucleation sites on the substrate but due to the higher nucleation density they are smaller in size (figure 2.11,b).

a)   b)   c)
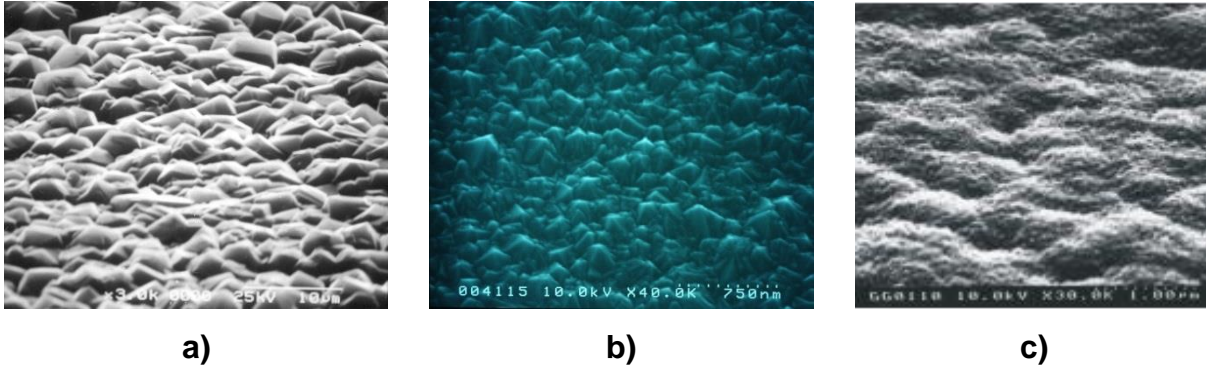
Figure 2.11 *SEM top view pictures of: a) PCD film; b) NCD film; c) UNCD film*

Even in this case the surface is still rough dominated by diamond facets. A further step toward smoother diamond coatings can be done by deposition of UNCD films. These films differ in outer appearance from PCD and NCD, as seen on figure 2.11,c. Their growth is characterized by a high secondary nucleation rate, which means that the crystallite growth is interrupted, followed by new nucleation and growth steps. High secondary nucleation rates can be achieved by variation of the deposition conditions, e.g. use of gas mixtures without or with small concentrations of hydrogen, decrease of the substrate temperature, etc. The result is diamond crystallites with a size up to 10 nm, embedded in an amorphous carbon matrix. The ratio between the crystalline and amorphous phase can vary depending on the deposition conditions as well as the content of sp^2- bonded carbon atoms in the grain boundary material.

In this work NCD films were deposited and subjected to further investigations.

2.1.7 Atomic hydrogen

Atomic hydrogen can be produced from molecular hydrogen at different conditions: heating up (up to several thousand degrees), electrical load with high current density at low pressures, irradiation with UV or microwaves or by electron beam excitation with energy of 10-20 eV.

The reverse reaction of agglomeration and molecular hydrogen creation, however, is also possible. The reactions can be described with the following equation:

$$H_2 \leftrightarrow 2H \qquad \Delta H_R^o = 435 \text{ kJ/kmol} \qquad (5)$$
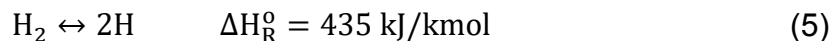
After excitation the hydrogen is scattered in atomic form. The atomic hydrogen etches preferably graphite phase according to the so called "selective etching model" during the diamond growth (Fig. 2.12). The different rates of etching of graphite and diamond define the diamond growth from thermodynamic and kinetic points of view [51]. This means if carbon and hydrogen are simultaneously introduced in the gas mixture, the result will be the formation of pure diamond. The requirement for these "etching recipes" is the hydrogen concentration to be higher than the equilibrium ones since below 1250 °C (i.e. the temperature range of diamond CVD) the graphite phase can be etched away only with extremely high concentration of atomic hydrogen.
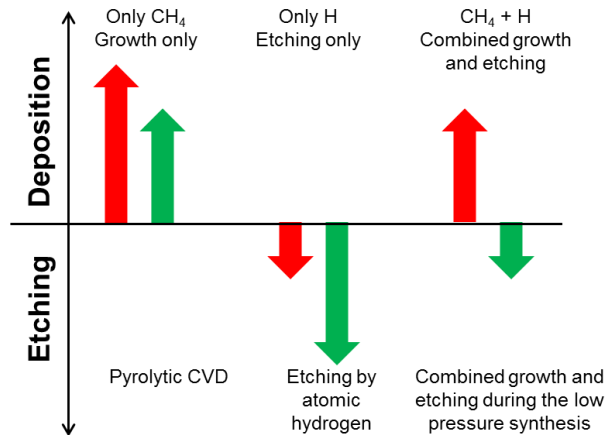
Figure 2.12 *Relative etch and deposition rates of diamond (red arrows) and graphite (green arrows)*

Zhang and co-workers reported [52] that the hydrogen etching varied with the diamond crystallites orientation. The efficiency of etching on plain different from [001] orientation is much higher that on [001], which can provide a novel method for growth of [001]-oriented diamond films with small thickness.

2.2. Diamond properties

2.2.1 Mechanical properties

Diamond is the hardest known natural, single phase material. The precise value of its hardness depends on the crystalline direction: for the synthetic polycrystalline diamonds (PCD) the value can reach 100 GPa. The hardness reported for nanocrystalline

(NCD) and ultrananocrystalline diamond (UNCD) films is similar, in the range up to 95 GPa. There is a considerable spread of hardness values for these types of films, depending on the deposition conditions, leading to different crystallite sizes, fraction of amorphous phase, etc.

The strong covalent C - C bonds in the fcc crystal lattice, the small distance between the atoms and a crystal lattice without defects are also contributing for the pronounced hardness value. The hardness can be characterized as:

- Qualitative – using the Mohs scale, a rough measure of the resistance of a smooth surface to scratching or abrasion, devised by the German mineralogist Friedrich Mohs (1812). The hardness value is determined by surface scratching using a substance with defined hardness. The materials are ranked along the Mohs scale, which is composed of 10 minerals with arbitrary hardness values [53]. Diamond can scratch all minerals involved in the scale; therefore it has number 10 in this scale.

- Quantitative – using the Vickers/Knoop hardness test method. A pyramidal diamond prism is pressed to the surface of the material with an exact known load, the resulting imprint measured with a microscope   can be used for calculating of the hardness [54]. The Knoop hardness measured for diamond is 7000 kg/m².

Other important diamond features are the exceptional wear resistance and the low coefficient of friction. These properties allow the application of CVD diamond on cutting tools from non-ferrous materials, surgical knives and as wear resistant coatings.

The extreme hardness of the diamond is in direct correlation with the elastic properties of the material - it can be hardly deformed until a fracture occurs, when it is exposed to a load. Therefore diamond is associated with the family of the brittle materials. The break resistance of a single crystalline diamond is about 2500 MPa and exceeds all other materials. For example, the break resistance of germanium is 90 MPa and of zinc sulfide 100 MPa.

The elastic properties of the diamond can be defined by measuring the elastic modulus E (Young modulus). The relationship between the tensile load and the resulting

deformation reveals the value of the E modulus, which for monocrystalline diamond is between 1050 and 1207 GPa depending on the lattice orientation [55].

2.2.2 Electrical properties

Natural diamond is an excellent electrical isolator with a wide band gap of 5.47 eV. After doping (introducing of small amounts of impurities to the crystal lattice) with different elements, the most common of which are boron, nitrogen and phosphorus, it can be turned into a semiconductor material (figure 2.13).
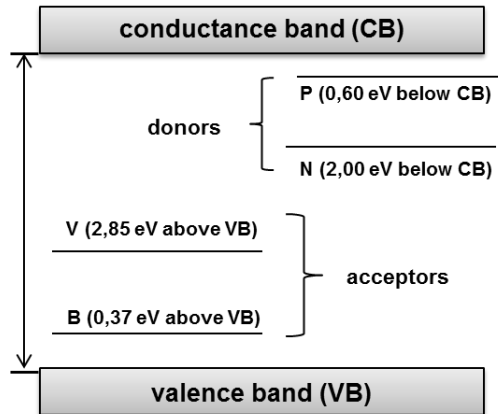
Figure 2.13 *An energy diagram of selected states in the band gap of diamond*

The doping of diamond with an acceptor type of material, such as boron, induces p-type semiconductor behavior [56]. At low doping levels, the diamond acts as an extrinsic semiconductor, while at high doping levels the material acts as a semi-metal. The boron dopant atoms can be easily incorporated into both natural and synthetic diamond prepared by CVD without any changes in the crystal orientation. The boron acceptor level was determined to be ~0.37 eV above the top of the valence band as shown in figure 2.13. The boron doped CVD diamond films can reach a hole mobility of ~1800 cm^2 V^{-1} s^{-1} at 300 K determined by Hall-effect measurements, a value close to the maximum one of ~2010 cm^2 V^{-1} s^{-1} obtained for IIb crystals [57].

Diamond shows n-type semiconductor properties after doping with a donating material (such as phosphorus). The incorporation of large atoms into the tight layout of the diamond lattice is challenging, a group in NIMS, Japan succeeded to synthesize diamond by high-pressure high-temperature (HPHT) technique, using phosphine as a

dopant source in 1997 [58]. The n-type diamond film doped with low phosphorus content possessed electron mobility of about 780 cm^{2}V^{-1}s^{-1} at room temperature [59].

Diamond poses high hole mobility, high saturation velocity and high breakdown field. A comparison between the material properties of diamond and other semiconductor materials [60], like Ge (p-type) and GaAs (n-type) is shown in Table 1.

Table 1 *Electrical and semiconductive properties of diamond in comparison with other semiconductors [20]*

	diamond	Ge	GaAs
Electical resistivity	$\leq 10^{18}$ Ωm	10^3 Ωm	
Dielectric constant at 300 K	5.70	11.9	12.9
Band gap at 300 K	5.47 eV	1.12 eV	1.42 eV
Electron Hall mobility at 300 K	2800 cm^{2}V^{-1}.s^{-1}	3900 cm^{2}V^{-1}s^{-1}	8500 cm^{2}V^{-1}s^{-1}
Hole mobility	130 to 2010 cm^{2}V^{-1}s^{-1}	1900 cm^{2}V^{-1}s^{-1}	400 cm^{2}V^{-1}s^{-1}
Electron saturation velocity	2.2×10^7 cm/s	0.9×10^7 cm/s	1.8×10^5 cm/s

In the nature boron impurities are rare but in the CVD diamonds boron is widely used for doping. The easiest way for doping is to introduce boron-containing gas directly in the deposition chamber during the growth process. The doping level can be easily varied from 10^{16} to 10^{20} cm^{-3} and some properties of the boron-doped diamond (BDD) films, like hydrophobicity, reversibility (the rate at which the electron transfer occurs between the working electrode and the solution redox species), and work potential window are related to the doping level [61].

The resistivity of boron-doped diamond films decreases with the increase of the doping level. For example, when the boron-carbon ratio in the gas source increases from zero to 0.5% (5000 ppm), the resistivity of the BDD film declines from 1×10^{12} Ω cm to

1.6×10^{-2} Ω cm. The resistivity of more heavily boron-doped diamond film can be reduced to a value of 5×10^{-3} Ω cm and keep nearly a constant value afterward [62].

2.2.3 Electrochemical properties

The electrochemical behavior of the diamond has been studied since 1987, when the first paper on the electrochemistry of a CVD-diamond electrode was published [63]. The diamond electrochemistry is a very specific matter due to the unique properties of the material.

Several groups (Fujishima in Japan, Pleskov in Russia, Tenne in Israel, Angus and Miller in the USA, and Compton in England) have spent a lot of time and efforts in investigation of the factors that influence the electrochemical response of the diamond electrodes [64]. Some of these factors are:

- doping material, type and level – this affects directly the potential-dependent density of the electronic states;
- surface chemistry - different molecules or atoms can be attached to the surface;
- morphology and microstructure;
- impurity and defect density - dependent on the gas mixture during the diamond deposition different atoms can be introduced to the diamond lattice, causing defects into the perfect diamond structure;
- presence of an amorphous phase (for example sp^2 hybrid carbon atoms).

Each of these factors can change the electrode properties and influence the charge transfer mechanism. The properties of the electrode can be manipulated by the selection of the appropriate deposition conditions. For example, the presence of nitrogen in the gas mixture in the reactor can result in a change of the electrochemical performance due to the shift from semiconductive to a metal-like behavior [65]. Difference in other pre- or post-growth procedure (surface cleaning in acidic bath, cooling or annealing) could lead to variability in the electrode properties and performance.

Boron doped diamond (BDD) electrodes show good electrochemical activity in inorganic and organic redox systems, such as $[Fe(CN)_6]^{3-/4-}$, Ce^{3+}/Ce^{4+}, quinone/hydroquinone and others. A typical voltammetry curve of boron doped diamond presented in figure 2.14 reveals that the potential window defined by the hydrogen

evolution reaction at cathodic (negative) potential and by the oxygen evolution reaction at anodic (positive) potential is higher than 3 V [66]. The differences between the diamond and the platinum electrodes are well visible. The potential window for platinum is approximately 1.2 V, similar to those of carbonaceous materials, like glassy carbon, graphite, etc. [67] commonly used in the industry. For diamond it is considerably higher - in the range of 3-3.5 V, due to the chemical inertness and the negligible interaction between the diamond surface and the aqueous electrolytes.
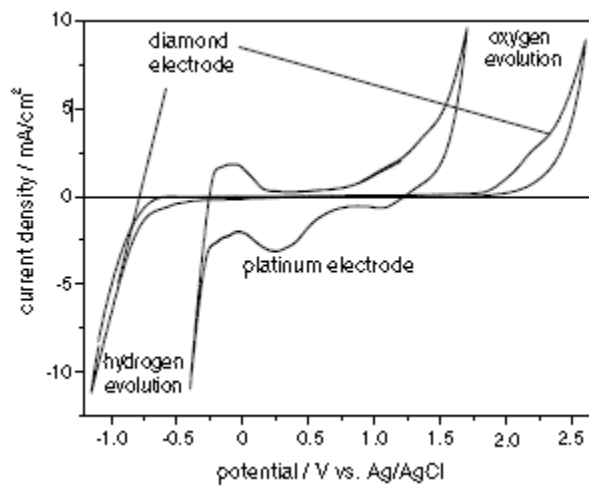
Figure 2.14 *Cyclic voltammogram of diamond and platinum in 0.1 M H$_2$SO$_4$ [68]*

The electrochemical behavior and kinetics of the processes are strongly influenced by the surface termination of the diamond film. For example, if the diamond film is hydrogen terminated the surface will be relatively hydrophobic. Reactions, that required adsorption, will be prohibited from the diamond surface. This is a precondition for a broad potential window. The diamond quality is also important for the electrochemical properties. The amount of sp^2 carbon (amorphous phase) affects the size of the potential window - it decreases with the increase of the non-diamond part.

A new branch in the electrochemistry was developed, namely the electrochemistry of diamond electrodes, related with the fundamental and application research of the diamond films during the last 15 years. It is due to the outstanding properties of the boron-doped diamond thin films, like large potential window, high efficiency of oxidation process, maximum current efficiency for OH radicals generation in water on account of extremely high overvoltages (cathodic -1.2 V vs. SHE and anodic +2.6 V vs. SHE), low background current and adsorption. The excellent electrochemical properties together with a high

resistivity to aggressive environment and chemical inertness make the diamond an ideal candidate for electrode manufacturing e.g. for photoelectrocemical cells and (bio)sensors [69]. The material can be used in electroanalysis for the detection of low concentration analytes with high precision and stability, for high current density electrolysis (1-10 A/cm^2) in aggressive solution environments without any microstructural or morphological degradation, as a corrosion-resistant electrocatalyst support, and as optically transparent electrodes for spectroelectrochemical measurements [70]. The use of diamond as electrode material has many benefits. In comparison to conventional sp^2 carbon electrodes, the diamond electrodes provide improvements in terms of linear dynamic range, limit of detection, response precision, and response stability. The deposition costs dropped significantly in the last decades, which makes diamond more attractive for commercial uses.

Currently three industrial areas for application of BDD electrodes should be mentioned: waste water treatment [71], [72] electro-analysis and electrochemical energy technology.

BDD electrodes are commonly applied for water purification. The organic pollution can be completely oxidized to CO_2, while the toxic non-organic waste can be oxidized or converted to biocompatible compounds, if the oxidation process is difficult [73]. These electrodes are able to operate under hard conditions and to degrade pollutants, like cyanides, phenol, chlorophenols [74], nitrates [75], aniline and others.

Diamond electrodes can be used for different electro-analytical applications depending on the tasks. Compared to the standard gold or platinum electrodes, BDD electrodes possess several advantages, additionally to already mentioned large potential window between oxygen and hydrogen evolution in aqueous solutions and enhanced signal to background rations due to the low capacitive currents, also no formation and reduction of surface oxides, which leads to low surface adsorption (no contamination with foreign atoms or molecules) and better stability in long term aspect [76]. BDD electrodes show an excellent response stability and electrochemical activity even without further surface treatments [77]. These excellent properties allow the usage of diamond electrodes for anodic stripping voltammetry (ASV) [76], [78], [79], cathodic stripping

voltammetry (CSV) [76], [80], amperometric detection [81], [82], abrasive stripping voltammetry (AbrSV) [76], [83] and square wave voltammetry [84].

Recently researches have proved that diamond films are very promising candidate as a material in the electrochemical energy technology, for example in the solar cells conversion systems, in super capacitors and lithium energy storage devices. Honda et.al. [85], [86] have demonstrated the possibility to use diamonds as a double layer capacitor. The commercial double capacitors are complicated systems, with carbon electrodes for the fast exchange of electrical energy. However, a high voltage should be applied (but not higher than the breakdown voltage of the electrolyte) and a very large surface area is necessary for high storage capacity. Therefore acetonitrile is used in commercial double layer capacitors. This makes the device expensive and unfriendly for the environment. Boron doped diamond with it unique properties is the ideal candidate for a novel electrode material. The problem with the large area can be solved by nanostructuring. A so-called nano-honeycomb structure diamond electrode provides a 200-fold increase of the active area [85]. Diamond can be also used as an intercalation electrode for lithium ion batteries. Almeida and co-workers [87] have demonstrated such a device with a capacity up to 370 mAh/g. The capacity can be enhanced up to 890 mAh/g by a combination of nano-honeycomb doped diamond with carbon nanotubes introduced into the pores of the honeycomb structures.

2.2.4 Optical properties

Pure diamonds are transparent from the UV (around 230 nm) to the deep IR-region of the spectrum. Slight absorption bands resulting from two photon absorption exist between 2.5 and 6 μm. The optical properties of the diamond films are determined by:

- the high reflective index of 2.41 at 591 nm, which is the reason for reflectance losses in the UV-Vis range;
- the absorption attributed to foreign atoms, most common boron doping, in the visible and IR spectral regions;
- the rough surface, which causes the scattering losses in the UV-visible spectrum;

- the absorption of the chemical impurities and defect centers, such as sp^2-bonded non-diamond carbon and the incorporated nitrogen and silicon (for NV or SiV centers);

The highest transmission of the diamond does not exceed 71.2% (figure 2.15) due to the interface between diamond and air and the high refractive index of the diamond.
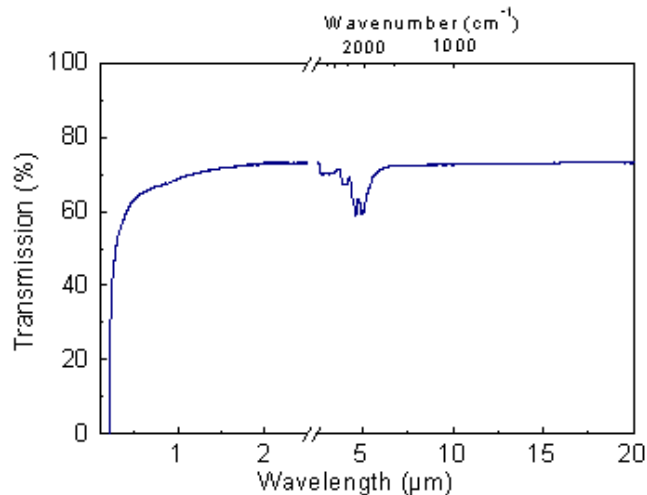
Figure 2.15 *Transmission spectrum of a diamond film [88]*

For wavelengths higher than the fundamental cut-off at 220 nm the transmission rises to values close to the theoretical (reflectivity limited) values of approximately 71% above 680 nm. The reduction in the transmission at shorter wavelengths can be partly attributed to scattering while the drop in the transmission close to the fundamental edge can be associated with bulk absorption mechanism [89]. The large band gap (5.45 eV) prevents thermally generated charge carriers at elevated temperatures. Therefore diamond remains transparent even at very high temperatures and radiation intensities.

Due to the remarkable optical properties, diamond is an ideal material for optical components, for example, it can be used in harsh environments as an infrared window. The commonly used IR materials in the 8–12 µm wavelength range (ZnS, ZnSe and Ge) are very brittle. Dischler & Wild [90] have shown that the disadvantages of these materials can be overcome by using diamond possessing its high wear resistance, thermal stability and transparency.

3. Surface modifications of diamond

The surface termination is a very important feature of the diamond films. It can strongly affect the properties of the material as the nature of the surface termination is capable to change completely the electrical properties and the electron affinity: the film can be converted from insulator to semi-conductor relying on the surface conductivity. For example, the hydrogen termination of the diamond surface causes p-type conductivity with a negative electron affinity of the film while after an oxygen modification the film shows insulating properties with a positive electron affinity [91]. The possibility to control and reverse the surface termination is very useful for applications of diamonds in (bio-)sensor devices, ion-sensitive field effect transistors, and electrochemical sensors [92].

The oxygen termination can be accomplished by various techniques: oxygen plasma, contact with boiling oxidizing acids, cathodic treatment or ultraviolet (UV)/ozone treatment [93]. The hydrogen termination occurs every time during the CVD growth of the sample due to the hydrogen present in the gas mixture during the process [94]. Ammonia plasma treatment of as-grown diamond resulted in amino-termination [95]. This termination is particularly of interest for immobilization of biomolecules, such as DNA, for biotechnological applications. Schematic presentations of the surface terminations described above are shown on figure 3.1.
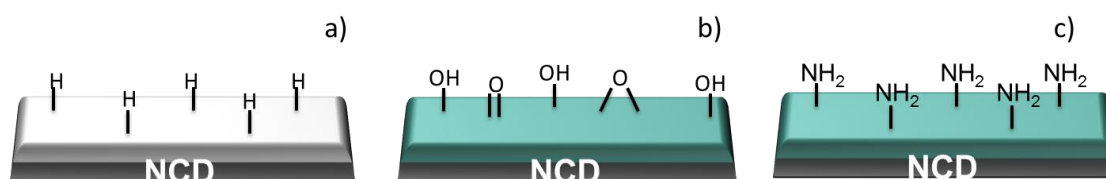
Figure 3.1 *Different diamond surface terminations: a) as-grown (H-termination), b) oxygen termination, c) amino termination*

3.1. Surface of as-grown CVD diamond

As-grown diamond thin films possess a hydrogen terminated surface due to the hydrogen containing atmosphere during the CVD. The films are hydrophobic because of the unipolar H-terminated surface. The hydrogen termination is very stable and can

sustain for very long time in air. It can be used for the manufacturing of electrodes stable at each pH value of the solution or diamond based FETs [96]. Such films possess carrier density of 10^{13} cm^{-2}, hole mobility and the hole sheet concentration in air of $\sim$150 cm^2/(Vs) and $\sim$5×10^{12} cm^{-2} at room temperature [96], respectively and unpinned surface potential. The carbon XPS core spectra are dominated by the sp^3 carbon bonds. Carbon atoms bonded to oxygen from surface contamination cause a shift towards higher energies, for example -C-OH or –C-O-C- are shifted by 1.3 ± 0.1 eV with respect to the main peak, oxidation to –C-O or -COOH groups leads to a further shift. In case of a carboxyl group (COOH) the binding energy can be shifted by 3.5–4.5 eV or higher [97].

3.2. Oxygen termination

The oxygen termination brings very high thermal and chemical stability to the diamond film, the procedure is useful for the manufacturing of high power electronic devices [98]. The diamond films with oxygen termination have different surface properties due to the variety of chemical groups (-C-O, -C-OH, -C-O-C-, -COOH), that can be formed on the oxygen terminated surface. These groups possess different types of bonds resulting in variation of the electronic and electrochemical properties. The oxygen terminated diamond surface shows hydrophilic behavior in contrast to the as-grown (H-terminated) one which is hydrophobic.
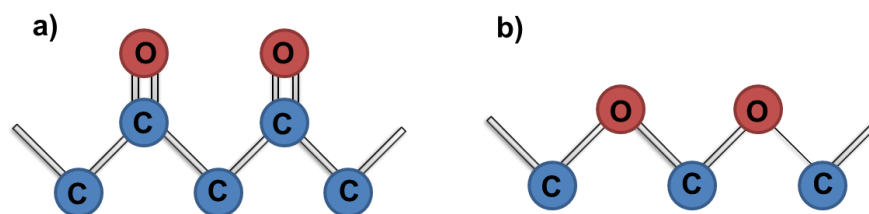
Figure 3.2 Atomic geometries for the O-terminated diamond surfaces: a) ketone and b) ether

The oxygen atom can saturate simultaneously two dangling bonds, as shown on figure 3.2 and therefore two different models are assumed to define the structure: (i) ketone (C=O) with a double bond between oxygen and carbon atoms; (ii) ether (C-O-C), where oxygen is connected via single covalent bonds to two carbon atoms. The changes

in the chemical bonding nature of the diamond surface after modification with oxygen can be well illustrated by X-ray photoelectron spectroscopy study (XPS).

Figure 3.3 represents the XPS C 1s spectra of two differently terminated surfaces described by Seshan et al. They reported about a slight shift in the peak position after the oxygen termination [95]. This is due to the difference in the band bending of both samples. Besides the main peak at 284 eV (attributed to the hydrogenated and non-hydrogenated diamond surface i.e. C-C and C-H bonds) additional peaks can be observed, particularly at the higher binding energy side.
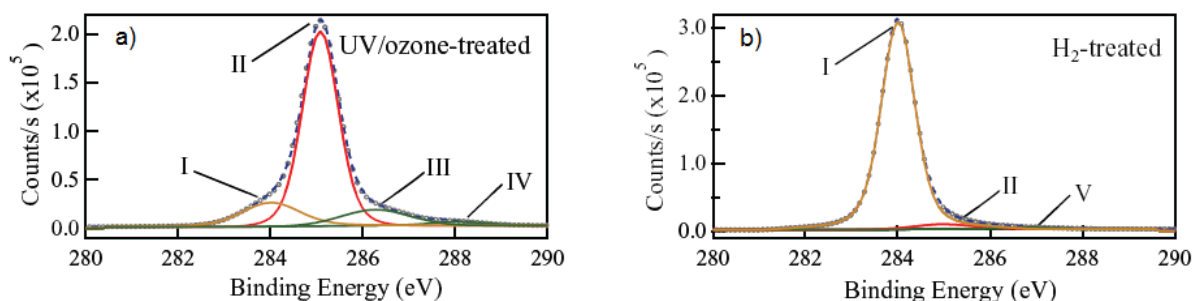
Figure 3.3 *XPS C 1s core spectra of an undoped CVD diamond film after: (a) UV/ozone treatment, (b) H_2-treatment [95]*

3.2.1 Chemical oxidation

The process of oxygen termination can be accomplished by chemical oxidation, for example by cooling of the sample with pure oxygen instantly after the growth. Another method of chemical surface oxidation is the purification by immersion in boiling acid (e.g. $HNO_3/H_2SO_4/H_2O_2$). As a result, carboxyl-, hydroxyl-, ketogroups and additional anhydrides can be expected on the surface. After an electrochemical oxidation with sulfuric acid, oxygenated carbon species are visible in the XPS C 1s spectrum. The new peaks in the spectra may be attributed to C=O and C-O groups, as reported by Simon and co-workers [99]. Capacitance voltage (C–V) measurements show a potential shift towards the positive region. This is due to the presence of C-O functional groups and the increased oxygen content [100]. With the help of high-resolution electron energy loss spectroscopy (HREELS) it could be also proved that the immersion of NCD in boiling acid is resulting in the creation of C-O groups on the film surface. No OH- vibrational bands were observed on the surface of this film, suggesting that C-O-C bonds cause the

recorded C-O stretching vibration. The most likely result of the reaction between acids and carbon atoms from the diamond surface is the formation of ether bonds. However, if the diamond film is immersed for a longer period the surface can be etched, which is of benefit for the ketone (C=O) groups creation [101].

3.2.2 UV-light/ozone treatment

UV/ozone treatment is considered as a convenient way for surface modification. The strong oxidant ozone provides active radicals needed for the oxidation in the form of single oxygen atoms. The ozone is the best oxidizing agent after fluorine, better than oxygen. Its polar O_3 molecule is very unstable, but much more reactive than O_2. The ozone is usually manufactured by passing an electrical discharge through oxygen gas or dry air. The resulting mixture of ozone and O_2 is usually suitable for most industrial applications. For surface modifications ozone is activated by UV light in the reaction chamber (see figure 3.4).
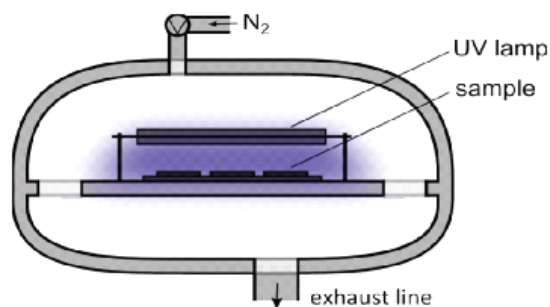
Figure 3.4 *UV/O_3 treatment set up*

A UV light with a definite wave length (ozone forming λ is below 200 nm) is used to excite and dissociate the oxygen molecules. The so-called UV/ozone treatment does not require expensive vacuum system or any heating, it can be carried out at room temperature in oxygen atmosphere or in air. Beside that it causes less damage to the surface in comparison to other oxidation methods (like oxidation in chemical solutions or oxygen plasma). Wang and coworkers reported identical morphology of the nanodiamond film before and after UV/ozone treatment. Thus this technique is suitable to define selectively non-conductive regions on FET devices [102]. The resistance of the modified surface is higher than that of the as grown one reported by Sakaia et al [103]. The oxidation level of the diamond can be controlled with the variation of the ozone treatment time.

3.2.3 Oxygen plasma

Oxygen termination of diamond surface can be achieved also by oxygen plasma, for example in oxygen plasma asher. This type of process is usually used in the industry mainly for cleaning and resists removal. After plasma treatment with a mixture of oxygen and inert gas such as nitrogen (see figure 3.5) the diamond surface is not only oxygen terminated but also completely free from ketone groups. HREELS measurements show only peaks that can be assigned to C-O-C and C-OH groups [101].
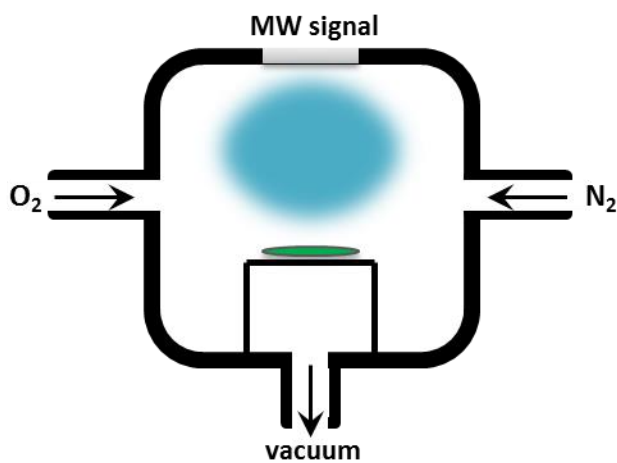
Figure 3.5 *Schematic illustration of an oxygen plasma asher*

Oxygen plasma treatment has almost no effect on the morphology of the diamond film. However, if the treatment time is long enough, significant roughness on surfaces can be observed. This will be discussed later in chapter 6.1. Microwave and RF plasma methods are very efficient methods for oxidation and are appropriate to achieve hydrophilic surface with contact angle under 20° for a short time of treatment [104].

3.3. Amino termination

The amination of the diamond surface is not so frequently used as the oxygen termination but still attracts the interest of many scientists. The amination process can be described as functionalization of the surface with nitrogen containing groups, mainly with $-NH_2$ groups. The presence of C-N bond makes the surface beneficial for biotechnological applications. The attached amine terminal functional groups on the

surface stimulate the immobilization of biomolecules and other organic molecules. The amino termination can be accomplish with chemical reaction [105], UV irradiation (λ= 254 nm) in ammonia gas [106] or with radiofrequence plasma of mixtures from He and NH_3 [107]. The plasma process affects very strongly the properties of the diamond surface without damaging the bulk material: the hydrophobic surface becomes hydrophilic, the surface energy is modified, biocompatibility and adhesion to other materials is improved. The variations of the gas mixture composition as well the treatment conditions are subject of significant research during the last years due to their strong influence on the surface chemistry and properties. Arefi-Khonsari et al. have shown that the plasma mixture of He/ NH_3 can enhance the adhesion on the film surface and stay stable over time [108], due to the high energetic electrons, ions and the metastability of the helium [109]. Depending on the diamond structure various groups might be built on the surface: the C-H bonds on the (111) facet surface will be replaced with NH_2 groups, while the (100) facets will be terminated with C≡N or C–N–C bonds [110]. The adhesion is very stable with the time.

4. Photosensitive molecules

4.1. Chlorophyll

Chlorophyll is a green compound, which can be found in the leaves of the plants. In 1864 Stokes verified that the chlorophyll is a mixture of compounds by the means of spectroscopy and thus disproved the assertion that it is a single compound. "Crystalline" chlorophyll can be obtained by pulverization of dried leaves and subsequent ethanol digestion. The replacement of the ethanol with ether or acetone changes the product of the reaction to "amorphous" chlorophyll. Half a century later Willstatter et al. [111] proved that the chlorophyll consists of two compounds chlorophyll-*a* and chlorophyll-*b*. The difference between the both types is the external chain: in chlorophyll-*a* it is -CH₃, while in chlorophyll-*b* it is CHO. The core structure of the chlorophyll molecule is a porphyrin ring (shown in red in figure 4.1) with a coordinated central atom.
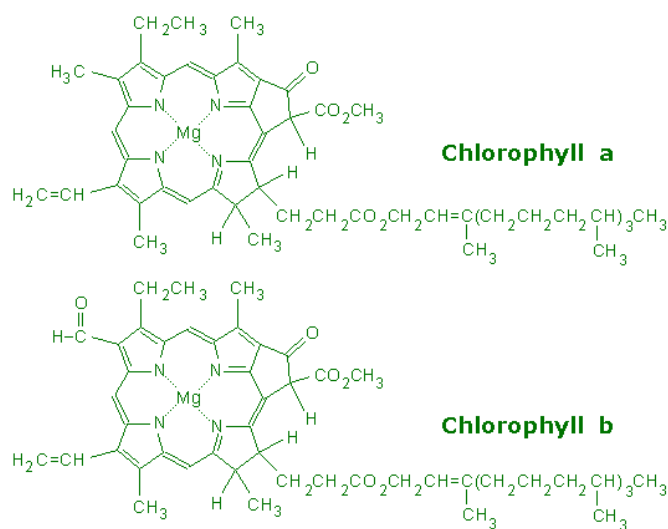
Figure 4.1 *Structural formula of chlorophyll-a and –b*

The structure gives rise to strong absorption bands in the visible regions of the spectrum, allowing the plant to absorb the energy from sunlight. The plants can absorb light from the blue and red part of the spectrum, however the light in the green region (between 500 and 600 nm) is almost completely reflected. When chlorophyll absorbs light, the molecule gets excited and an electron transition from the highest occupied molecular orbital to the lowest or second lowest unoccupied molecular orbital occurs [111]. The

energy of the red light corresponds to the transition of the electron from the ground state up to the first excited singlet state. The energy of the blue light is sufficient for the electron to reach higher excited singlet state. This state is not stable, it can fall off rapidly and loses energy. The result of that decay is the formation of the much more stable first exited state. Thus the energy available for photochemistry corresponds to that of the red photon (e.g. 680 nm = 1.82 eV). The energy of green light is not enough to promote a valence electron to an excited state. The photons with such energy cannot be absorbed but instead of that they are reflected or transmitted.

4.2. Porphyrin

Porphyrins and their derivates have attracted attention due to extraordinary physical, chemical and spectroscopic properties [112], [113] advanced for application in many fields. The porphyrin macrocycle is built from four pyrrole rings (see figure 4.2), bonded with methine bridges in an aromatic system. The molecule consists of 22 π electrons forming a planar structure.
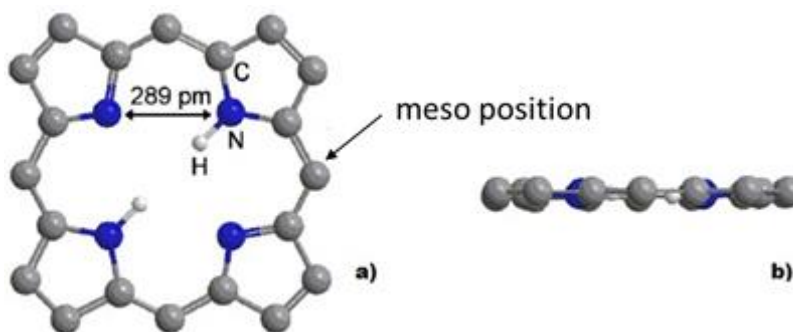
Figure 4.2 *a) Porphyrin skeleton structure; b) side view of the porphyrin molecule* [109]

Song [114] and Retsek [115], however, reported that the porphyrin molecule can be obtained also as a nonplanar structure. Due to the distortion of the ring, nonplanar molecules possess different physical and biological properties. Metalation, different side chains substitutions, alkylation of the pyrrolenine nitrogen atoms can be the reason for the deformation and change of the normal planar structure. The bonds are strong and the molecule stays stabile even under harsh conditions, e.g. in strong acids or bases. In the nature many plants and living organisms use porphyrins or some of their (metallo)-

derivates for essential processes. The peculiarity of the ring structure and the conjugated double bonds define the properties. For example, they determine the light harvesting mechanism in the photosynthesis, as they form blocks of chlorophylls and bacteriochlorophylls [116]. Metalloporphyrines can easily oxidize and help with the transport and/or storage processes. Another (meso) derivate - corrin with 3 carbon atoms bonding the pyrolle rings was observed in the vitamin B12 [117]. Porphyrines are called "pigments of life", because they are the indirect cause for the green color of the plants and the red of the blood [118].

The highly conjugated π-electrons effect the intensity and the color of the porphyrins. The transmission window of the porphyrin is spread in the near UV and the visible region of the spectrum (figure 4.3).
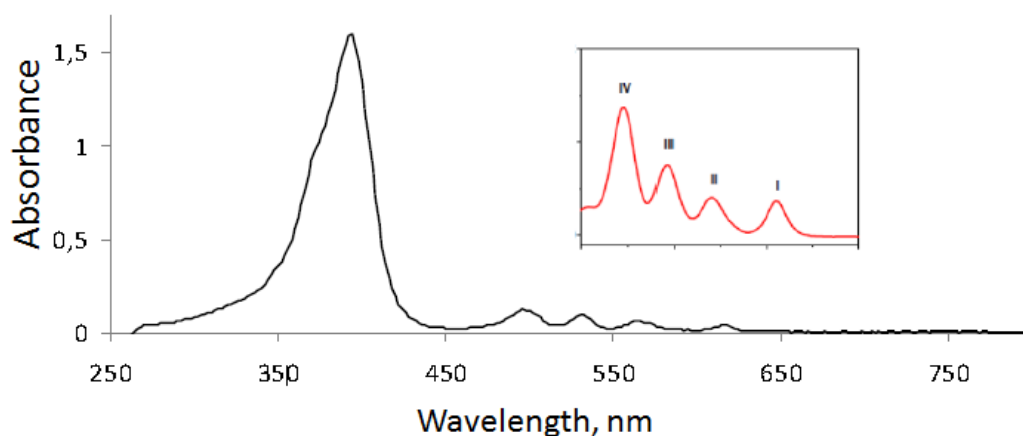
Figure 4.3 *UV visible spectrum of porphyrin (large print of Q band in the inset) [119]*

4.3. Phthalocyanine

Phthalocyanines (Pc) belong to the family of the cyclic tetrapyrroles, a large group of organic compounds possessing special photochemical and photophysical properties [120]. Tetrapyrroles are built from four pyrrole rings connected with a covalent bond or a C-C bridge. In the pyrrole ring four carbon and one nitrogen atoms are alternating, forming the ring structure (figure 4.4,a). The rings can be bonded linearly or micro cyclic to form the Pc molecule (figure 4.4,b). Pc was discovered by chance in the beginning of the 20th century by Braun ant Tcherniac. The structure was primarily studied by Linstead

[121] and Robertson [122] using X-ray diffraction analyses. Various atoms most common hydrogen and metal cations can be attached through coordinative bonds of nitrogen atoms from the pyrolle rings or ligands to the central atoms. The central cavity of the Pc ring can house various atoms: (i) metal atoms (more than 70 different elements are known to form metal-phthalocyanines MPc), (ii) complex oxides: common used are TiO and VO, (iii) hydrogen (metal-free phthalocyanine, H_2-Pc). Phthalocyanine molecule is flexible and the molecule geometry changes   depending on the size of the bounded central atom: from planar for small substituted atom to pyramidal for bigger one.
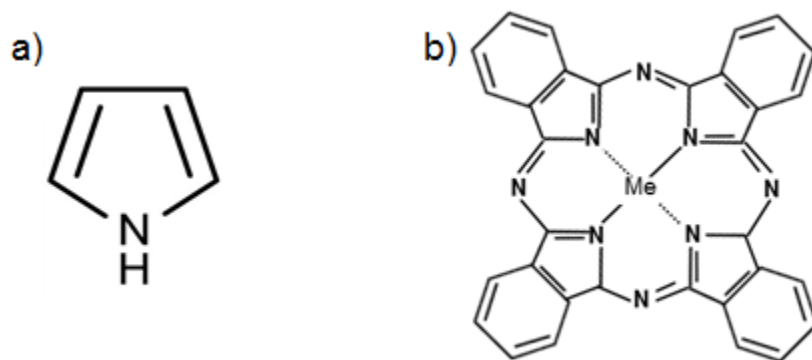
Figure 4.4 *Pyrolle a) and phthalocyanine b) structural formula*

The introduction of metal varies the properties of the Pc. For example, by the addition of d-orbitals the highest occupied molecular orbital (HOMO) and lowest unoccupied molecular orbital (LUMO) can be modified. The central metal atom can build a coordinative bond and form new complexes. The nature of the central metal, axial ligands, and solvents as well as that of substituents on the ring periphery determines the redox properties of a given complex. Electron-donating substituents such as alkylthio groups, increase the electron density of the ring and the central metal atom making it easier to oxidize and harder to reduce MPc complexes. Redox processes for MPc complexes occurring at the central metal or ring often result in color changes.

Phthalocyanines can be employed in optical logic display devices, electrophotography, security printing, gas detectors [123], solar cells [124], sensitizers and color filters [125] (see figure 4.5). The phthalocyanines are p-type semiconductors with a typical direct energy gap of about 1.8 eV, with low mobility and low carrier concentration. They commonly exist in two different crystalline phases: α-and β- forms.

The most stable form, the β-form is a monoclinic crystal, which consists of two phthalocyanine molecules per unit cell. The β-form may be thermally derived from the α-form [126].
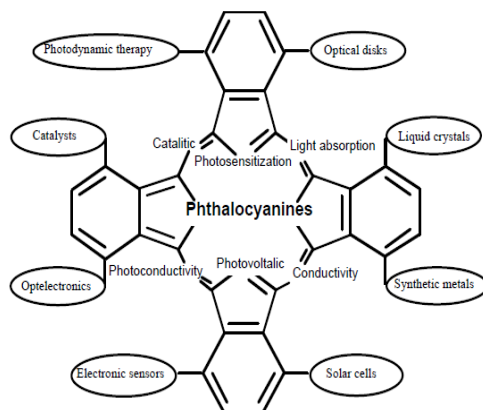
Figure 4.5 *Typical functions and applications of phthalocyanine derivatives [127]*

The remarkable and important physicochemical properties of Pc which define the areas of their applications are:

- Optical behaviors (UV-vis devices, nonlinear optics);
- Electronic conductivity (sensors, charge-transfer complexes);
- Photoconductivity, light harvesting/photovoltaic, electrochromism (Photovoltaic convertors and solar cells);
- Photooxidation and photoreduction (catalysts);
- Semiconductor behaviors (power dividers, radio frequency oscillators, photosensitization devices).

Phthalocyanies are frequently used in the dye industry as blue or green pigments. The high thermal (up to 500 °C) and chemical stability are the reason why Pc are attracting attention in developing organic based devices.

One of the most important advantages of the metal-Pc is the high hole mobility (μ_p). It can generate more photocurrent because of high photon absorption and wide spectral range of optical absorption in the visible and ultra-violet spectral range [128]. In comparison to porphyrins Pc-molecules possess longer excitation length. The main absorption region of Pc lies between 600 and 700 nm. The presence of a metal ion can

shift the absorption spectrum. In this work 3 types of metal-phtalocyanine, namely Mn-Pc, Ti-Pc and Cu-Pc, are used.

Manganese phthalocyanine complexes are attractive materials for electrochemical application because the manganese atoms exhibit variable oxidation states ranging from Mn^I to Mn^{IV}. This makes manganese phthalocyanine complexes potential electrocatalysts in many reactions. Substituted manganese phthalocyanine complexes are still relatively few, and their electrochemistry is not fully understood. The spectra of $Mn^{II}Pc$ and $Mn^{III}Pc$ complexes are well known, however, the spectra of $Mn^{IV}Pc$ complexes are reported only in few studies [129]. The formation of $Mn^{II}Pc$ by reduction of $Mn^{III}Pc$ derivatives occurs in the presence of mild reducing agents visualized by the change of color from red to green. Phthalocyanines with sulfur or nitrogen substituents generally absorb in the NIR region and therefore are suitable for devices working in this spectral region.

The **titanium phthalocyanine** is commonly used as organic photoconductor due to non-toxicity and good field-effect properties. Titanium *bis*-phthalocyanine "TiPc$_2$" is a sandwich-type phthalocyanine with a single metal atom coordinating two macrocycles. The neutral complex shows an unusual yelloworange colour because of the π delocalisation breaking by the two carbon σ bonds. It is easily sublimed and the thin films obtained are microcrystalline and stable in air. The conductivity at room temperature is very low and classifies TiPc$_2$ as an insulator, like other M(IV)Pc$_2$ sandwich complexes and MPc monomeric compounds. The electronic absorption of TiPc$_2$ film is in the region 800-400 nm.

Copper phthalocyanine is used in sensors for ionizing radiation. CuPc is known to be an air-stable, p-type organic semiconducting material avoiding any undesirable chemical interaction with other chemicals.

5. Diamond deposition

For the purpose of this work nanocrystaline diamond films were prepared by means of the hot filament chemical vapor deposition set-up at the Institute of Nanostructure Technologies and Analytics (INA), University of Kassel shown on figure 5.1. The sample was positioned on a substrate holder at a distance of about 10 mm from the filaments. The seven tungsten filaments (diameter 0.3 mm and length about 12 cm) were heated up to temperature of 2000-2100 °C. Due to disruption and vibration during the switching on and off of the used pyrometer causing the break of the filaments, the precise temperature was measured only for a limited number of experiments and in all cases it was over 2000 °C.
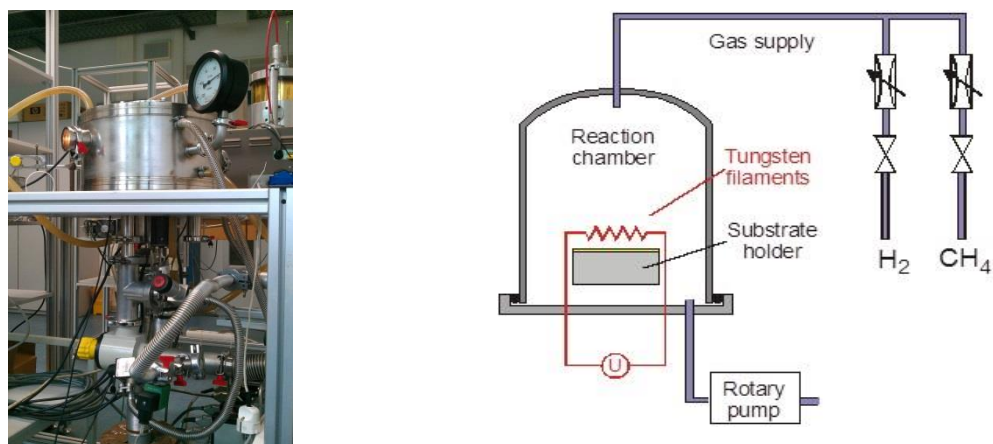
Figure 5.1 *Hot filament set up picture and schematic view*

The filaments were heated with a programmable DC Power Supply Genesys 3300W GEN30-110, which is capable of output voltage of 30 V and current of 110 A. For additional heating of the substrate a three-phase voltage transformer was used. It was connected to boron nitride heating plate, placed in the holder directly under the substrate. The reaction gases (hydrogen and methane) were introduced in ratio 100:1 into the chamber and homogeneously distributed above the substrate via a metal ring. The gas influx was controlled via mass flow controllers (MKS Instruments 247 with 4-channel).

The carburization is an important step in the diamond deposition before the real growth process, explained earlier in chapter 2. The procedure is desirable in order to minimize the risk of contamination of the films. The carbonized filaments possess higher resistance and higher voltage hardiness resulting in higher temperature in the reaction

chamber. The tungsten filaments are clamped over 2 copper blocks so that they are parallel to the sample holder. A coil spring handmade from the same wires was used in order to provide the needed tension. This is necessary because the filaments extend during the carburization. A rigid mounting of the tungsten would inevitably lead to a bending or even to the break of the filaments. For the first 30 minutes the chamber was heated slowly, using only the filaments in pure hydrogen ambient. A stepwise increase with a step of 5 A was used, until the maximal value of 70 A was reached (10 A for each filament). Then the methane was introduced into the chamber. Due to the different resistance of the non- and carburized W-filaments and the big difference in the thermal conductivity of the H_2 and CH_4 [130], the substrate temperature (respectively the heating voltage) was constantly decreasing. Therefore, every 30 min the heating current was controlled, i.e. put on 70.0 A. The process was carried out for at least 3 hour, or until the voltage was constant for more than 40 minutes. The process is carried out by a pressure of 25 mbar and gas flows of 500 sccm H_2 and 5 sccm CH_4. After that the transformer was shut down and dry nitrogen was used to purge and cool down the reaction chamber.

Before the diamond deposition a pretreatment procedure of the substrate is needed. The mechanical technique is chosen from the available techniques described in chapter 2.1.5 to obtain the necessary primary nucleation density. The pretreatment recipes are described in the next chapter.

5.1. Pretreatment recipes

High nucleation density is the requirement to start the diamond film growth on non-diamond substrates, like monocrystalline silicon wafers, which were used in the current work. To reach the desired density value a seeding process should be performed. We studied several diamond suspensions as seeding sources. The standard nucleation recipe included the following steps:

- 80 mg UDDP (ultradisperse diamond powder) and 50 mg NCD (D0.25) powder were measured with an analytical balance;
- 75 ml n-pentane was pipetted into an Erlenmeyer flask and mixed with the diamond powders;

- Etch solution (NH_4F+HF) was diluted with deionized water in 1:1 ratio;

- To remove the native silicon dioxide from the silicon substrate, it was submerged in the ammonium fluoride buffered etching solution for 35 seconds; afterwards it was cleaned in water and finally dried with nitrogen;

- Silicon substrate was placed in the diamond solution and treated in an ultrasonic bath for 60 minutes; also shorter pretreatment times were used of the ultrasonic bath in order to study the nucleation density;

- The temperature was monitored constantly, due to the low boiling point of n-pentane. The water in the ultrasonic bath was replaced every time when it was hotter than 34 °C;

- Afterwards the substrate was cleaned ultrasonically with acetone for 90 s, dried whit nitrogen, then cleaned again with isopropanol for 90 s and finally dried with nitrogen.

The described recipe will be called 'standard recipe' further in this work. The silicon substrates were pretreated only with diamond powder with grain size of 250 nm (so-called D 0.25 powder) and a slurry solution for better comparison between the different recipes. The slurry solution (Opal seed) is a commercially available product, which consists of nanodiamonds with average aggregate size of 20-30 nm and dimethyl sulfoxide (DMSO). The solvent provides advantages such as better resistance to sedimentation in colloidal suspensions, effective fractionation of a variety of DNDs including those that cannot be fractionated using DI water, thermal stability, etc [131].

The samples were measured after pretreatment with VEECO CPII atomic force microscope (AFM). Non-contact mode was chosen to reduce the interaction between the cantilever tip and the seeded diamond particles. The scan range was set at 2 μm to guarantee best overview. The conditions allowed the investigation of the seeded surface after the pretreatment and the determination of the nucleation density for the different recipes. The increase of the pretreatment time from 20 to 40 minutes does not affect significantly the nucleation density. Further pretreatment causes an increase of the number of the created nucleation sites (scratches or diamond particles) as shown on figure 5.2.
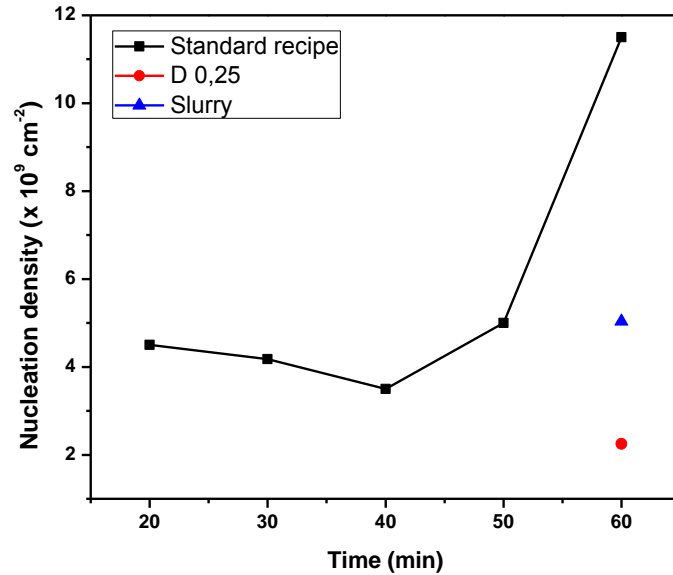
Figure 5.2 Determined nucleation density after different pretreatment recipes

During the ultrasonic bath treatment the diamond powder and the silicon substrate are interacting and particles from the diamond suspensions are sticking on the surface. This phenomenon can be observed on the AFM pictures (figure 5.3). The number of the nucleation sites (diamond particles and scratches) is in direct correlation with the time. The samples treated 20 minutes possess only 180 grains on area 2 x 2 μm while after one hour treatment this value increases almost 3 times (up to 460). The calculated nucleation density after 20 minutes is 4.5×10^9 cm^{-2}, it increases up to 1.5×10^{10} cm^{-2} after one hour of treatment. The increase is not linear and after the initial phase the density values slightly decrease. This can be attributed to the random nucleation distribution during the seeding process and the creation and destruction of nucleation sites.

a) b) c)

d) e)

Figure 5.3 *AFM images (2 x 2 µm) of standard pretreated samples after: a) 20 min; b) 30 min; c) 40 min; d) 50 min; e) 60 min*

For the slurry sample the determined nucleation density were 5.04 x 10^9 cm^{-2}. Large crystallites can be observed on the substrate surface, which can explain the high roughness. The pretreatment with slurry solution leads usually to higher growth rates and faster building of a homogeneous closed film /faster closing/ without any nodule structures and islands (figure 5.4)
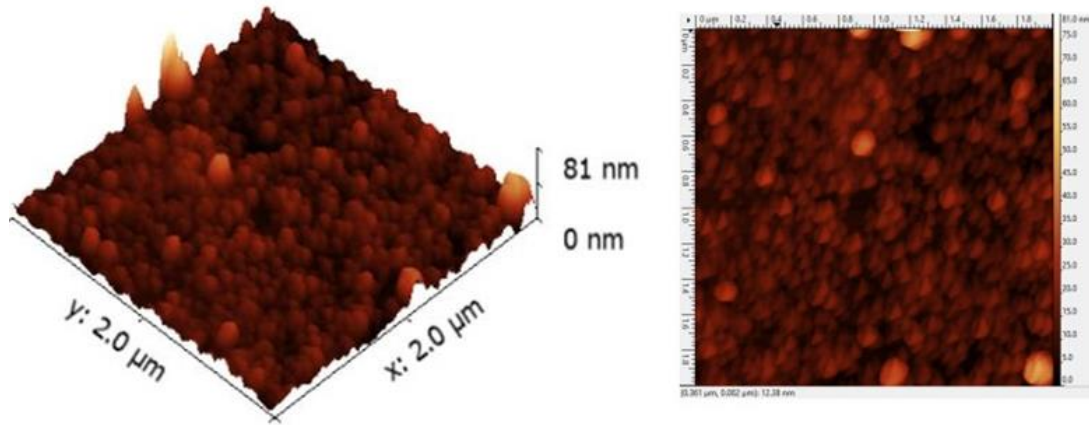
Figure 5.4 *3D and 2D views of a slurry pretreated sample*

As shown on figure 5.5 the presence of only large diamond powder (D 0.25 powder) in the pretreatment solution results in lower nucleation density. This pretreatment recipe can be used by pre-patterned growth or by growth of single diamond crystals.
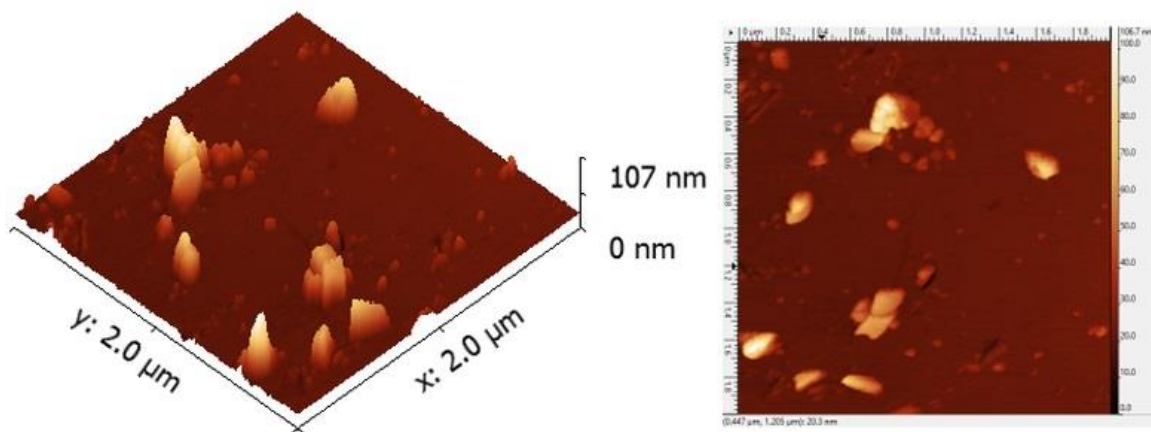
Figure 5.5 *3D and 2D views of a sample pretreated with D 0.25 powder*

5.2 Substrate temperature calibration

The substrate temperature is a decisive parameter which determines the quality and the properties of the diamond films: lowering of the temperature results in building of higher amount of sp^2 phase in the deposited film. Diamond films can be deposited at lower temperature, but this leads to increase of the amorphous carbon phase and to decrease of the diamond quality [132].

On figure 5.6 two samples grown at different temperatures are shown: DHF 8 was deposited at 870 °C and DHF 10 at nearly 600 °C. The temperature variance is responsible for the different morphology attained: the crystals obtained at higher temperature are well faceted with sizes of several hundred nanometers. With the temperature decrease the crystallite size decreases and the facets are less clear (see figure 5.6 right picture). Agglomerates of crystallites with different sizes can be also observed. The result at even lower growth temperature is disruption of the film homogeneity and transition to UNCD film.
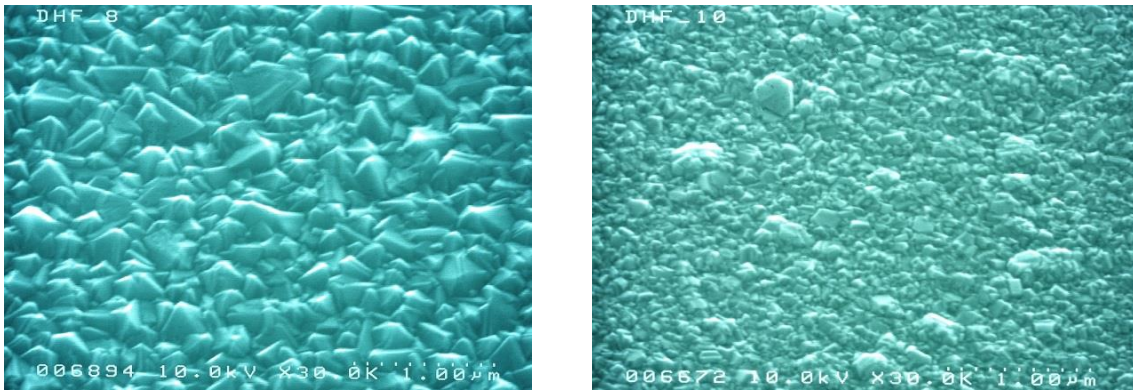
Figure 5.6 *Top view SEM pictures of sample DHF 8 (left) and DHF 10 (right)*

That is the reason why further study on the control of the substrate temperature was needed. Temperature calibration with additional substrate heating and only with filament heating was performed. The substrate holder was consequently heated with different currents applied on the filaments and respectively voltages applied on the substrate holder without wafer and the temperature was measured.

The dependences plotted on figures 5.7 and 5.8 reveal that the applied filament current and the substrate temperature are in direct relation. The increase of the applied current to the filaments leads to significant temperature rise (figure 5.7). With only 60.2 A applied to the filaments the substrate temperature is between 605 °C (with 40 V substrate voltage) and 718 °C (with 80 V substrate voltage). The maximum temperature that can be achieved is slightly higher than 700 °C without substrate heating.
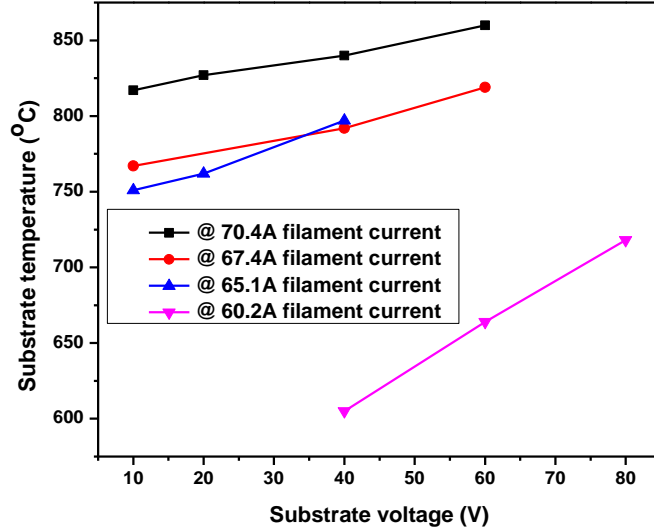
Figure 5.7 Dependence of substrate temperature on the heating plate bias and filament current
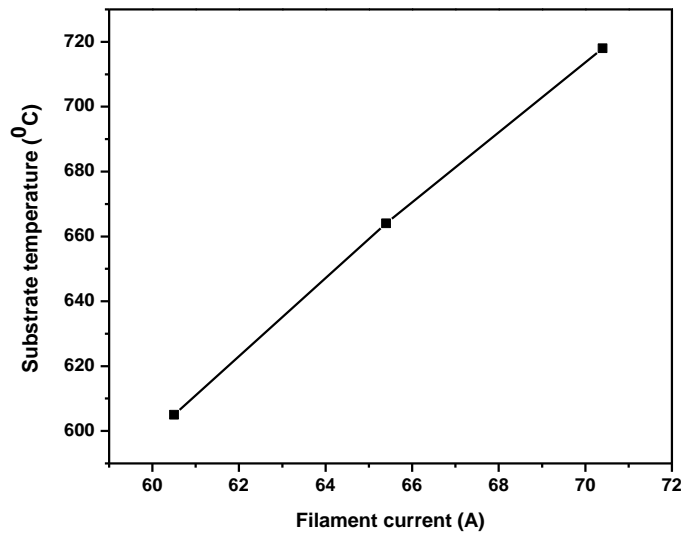
Figure 5.8 *Dependence of the substrate temperature on the filament current without substrate heating*

The relation as seen from the picture 5.8 is linear, however the maximum temperature is too low for high quality diamond film growth. Nevertheless the temperature is suitable for

diamond deposition on thermally sensitive materials (like III-V materials or glasses [133], [134]).

5.3 Deposition of NCD films

The self-assembled hot filament chemical vapor deposition set-up was used for the deposition of the non-doped NCD films used in this work. A standard pretreatment procedure was performed for each sample. The pretreated Si-wafer was placed on the substrate holder, the chamber was evacuated to a basic pressure of 10^{-3} mbar and after that filled with hydrogen with flow of 500 sccm. The pressure during the deposition was constantly held at 25 mbar. The needed substrate heating (120 V) and filament current (70 A) were applied in order that the desired deposition temperature was reached. After that 5 sccm methane (so that a 1:100 ratio between CH_4 and H_2 flux is preserved) were introduced into the chamber. Closed and homogeneous films can by deposit at substrate temperatures of 780-820 °C and deposition time of 360 minutes. These films were used for preliminary immobilization tests and for the surface characterization. For the photo-electrochemical investigations heavily doped NCD films were deposited at the University of Ulm by Dr. Alberto Pasquarreli. By the means of microwave plasma enhanced CVD (MPCVD) initially an undoped layer was grown. For this purpose a gas mixture of 4 sccm CH_4 and 400 sccm H_2, pressure of 20 mbar and deposition temperature of 700 °C was used. A high nucleation density (10^{10} cm^{-2}) was achieved with a bias enhanced nucleation. With the growth rate of more than 5 nm/min, a diamond film with a thickness of about 1 µm was deposited for 4 hours. After that the non-conducting layer was overgrown with boron-doped one. For this purpose a second MPCVD set-up, with 8 sccm CH_4 and 400 sccm H_2, 40 mbar pressure and deposition temperature of 800 °C, used. The layer was deposited with a thickness of ~200 nm. Boron filaments were used for the doping of the NCD film. The samples were characterized via diverse techniques. Transfer Length Measurements (TLM) in air has showed a sheet-resistance of ~500 Ω/□. In order to test if the samples are suitable for electrode applications, electrochemical capacitance-voltage measurements were performed. The estimated doping density was in the lower 10^{21} cm^{-3} range.
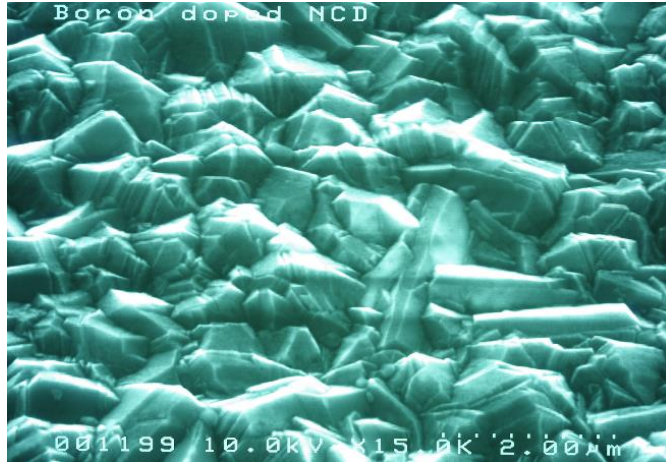
Figure 5.9 *Top view SEM picture of boron-doped NCD films*

Finally the samples were chipped into 1 x 1 cm pieces, so they can be glued to a cooper plate in the final step of the manufacture of the NCD electrode (see chapter 6). A typical SEM image of boron doped NCD film is shown on figure 5.9. The doping doesn't have any influence on the morphology of the sample. The same four-walled pyramidal facets as at the standard NCD samples (shown on figure 5.6) were observed.

6. Surface modifications of NCD films

6.1. Oxygen plasma

Oxygen plasma is used to replace the hydrogen atoms on the diamond surface with oxygen atoms. The oxygen plasma treatment was performed in TePla 200-G oxygen asher (figure 6.1) with a working pressure of 0.67 mbar and frequency of 2.45 GHz. These parameters are constant while the process time and the power of the asher were varied in order to investigate the surface termination and to optimize the process conditions. Two different discharge powers of 100 W and 200 W were applied and the modification time was increased stepwise from 1 to 10 minutes.

Figure 6.1 *TePla 200-G oxygen asher in INA, University of Kassel*

Initially the reactor was cleaned for 20 minutes at a full discharge power (250 W) before the modification process to minimize the risk of contamination. After that the samples were placed in a culture dish in the middle of the set-up for the modification step.

A set of experiments with different modification times was performed to study the efficiency of the process and to clarify the mechanism of the termination process. In order to investigate whether the modification is accompanied by etching of the diamond surface, the samples were studied with an atomic force microscope (AFM) Veeco CP-II. A non-contact mode was chosen for better picture quality and lower oscillation noise. The sample scan size was set to 1 μm x 1 μm, during all measurements 15 nN gain and scan speed of 1 Hz were applied. On figure 6.2 an AFM image of as-grown DHF 68 sample is

shown. Large diamond crystallites with a height up to 120 nm are visible on its surface. They are well facetted with rectangular shape. A rms surface roughness of 18.5 nm was evaluated with the freeware software Gwyddion.
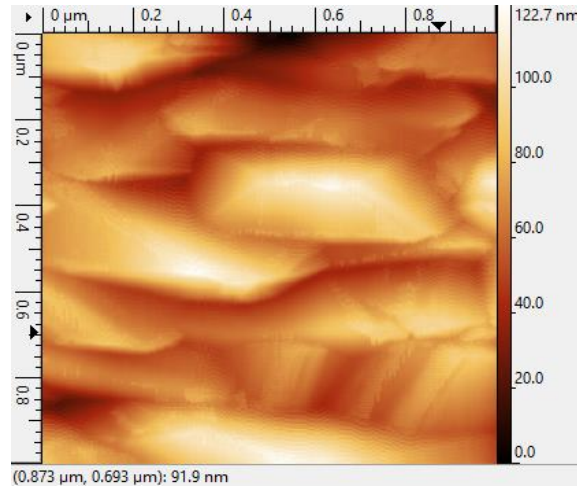
Figure 6.2 *AFM picture of DHF 68 directly after deposition (rms roughness 18.5 nm)*

Two sets of experiments were performed varying the modification time at 100 and 200 W plasma power. The results for the rms roughness and height (the difference between the highest and the lowest points) as evaluated from the AFM images (1 x 1 μm^2) are summarized in table 2. It should be pointed out that the samples were taken from different areas of one and the same NCD sample (DHF 68) which exhibit slightly different morphologies.

The AFM images of the samples modified at 100 W, shown on figure 6.3, reveal that the facets of the nanocrystals are preserved even after 10 minutes oxygen plasma. The values of rms roughness and height vary as seen in table 2, but this can be attributed to the non-uniform crystallinity of the NCD films. Following the van der Drift model of selection growth [135], the film texture results from different rates of growth between different crystal faces of the grains on the surface.
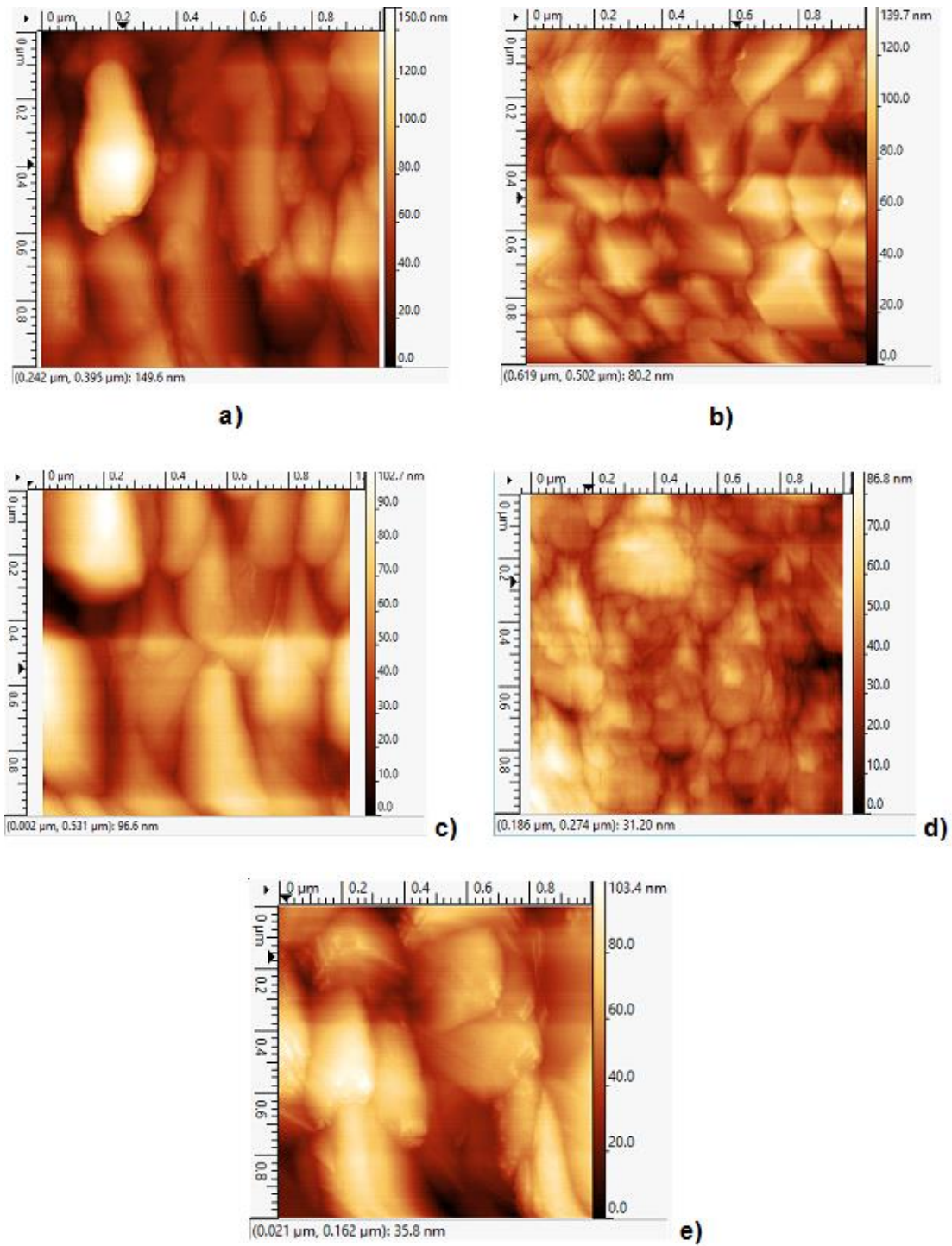
Figure 6.3 *AFM pictures of DHF 68 after: a) 2 min, b) 4 min, c) 6 min, d) 8 min and e) 10 min O$_2$ plasma modification at 100 W*

Table 2 *Rms roughness and heights of NCD film (DHF 68) after O$_2$ plasma modifications at 100 and 200 W*

Modification time, Min	100 W		200 W	
	rms, nm	height, nm	rms, nm	height, nm
as-grown	18.5	120.0	18.5	120.0
2 min	24.2	150.0	13.6	86.9
4 min	20.0	102.0	20.0	119.8
6 min	17.5	102.0	14.4	100.9
8 min	9.9	86.7	12.6	83.2
10 min	19.0	103.0	13.6	99.3

The grains with faster growing direction perpendicular to the surface are preserved while slower growing grains are terminated when they intersect the column walls of the "faster" crystallites. Furthermore, the rms roughness and height of the NCD films after growth and 10 minutes oxygen plasma at 100 W are rather similar which can exclude a strong etching effect during the modification process.

In the case of modification at 200 W plasma power, the roughness and heights of the samples decrease after O$_2$ plasma modification with different duration compared with the as-grown sample. In addition, a slight rounding of the sharp edges of the facetted crystallites, especially after 10 minutes modification, can be observed (see figure 6.4). As a conclusion, it can be stated that no strong etching effect were observed after oxygen plasma modification within the investigated ranges of process duration and plasma power.
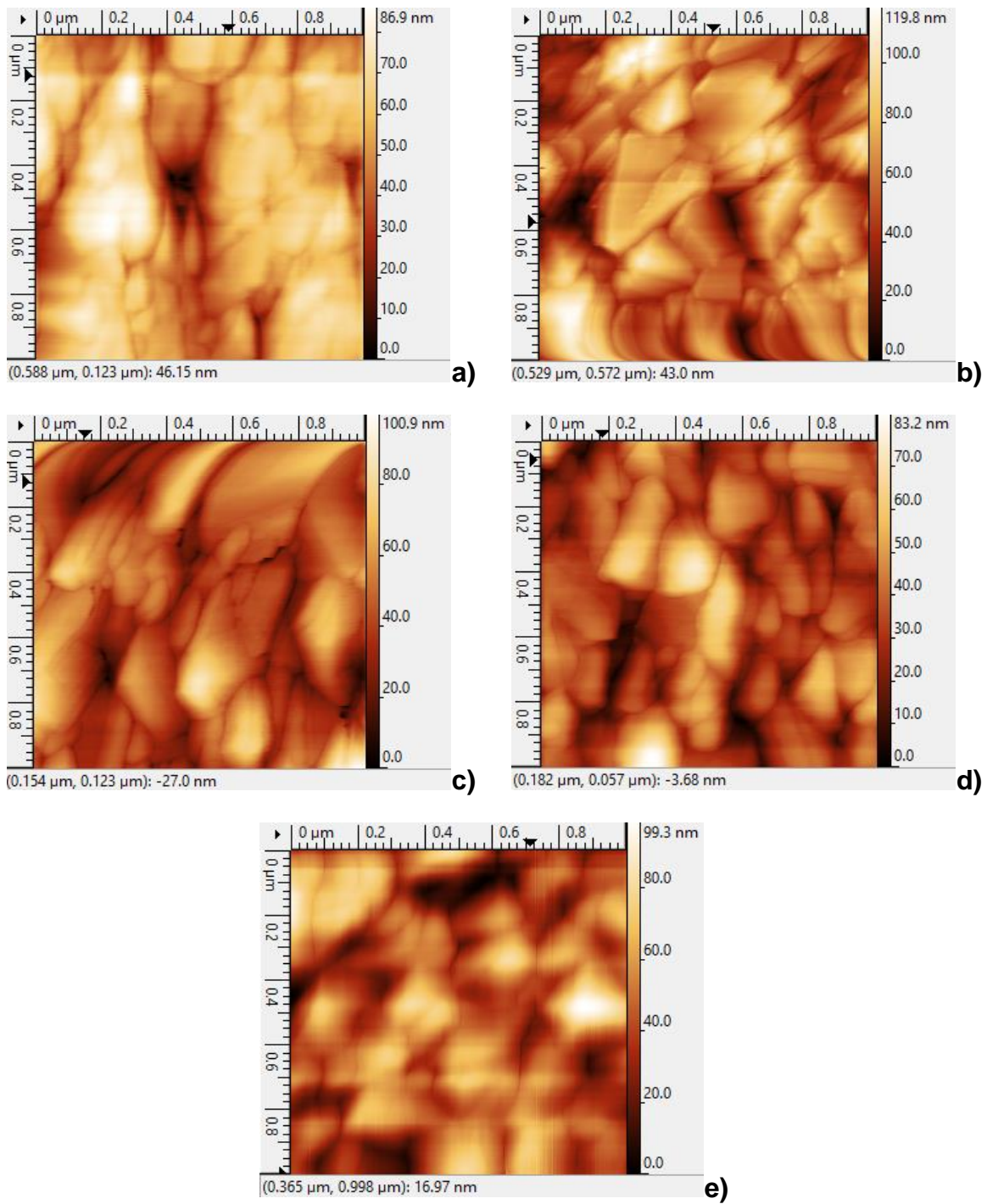
Figure 6.4 *AFM pictures of DHF 68 after: a) 2 min, b) 4min, c) 6 min, d) 8 min and e) 10 min O_2 plasma modification at 200 W*

6.1.1. Contact angles measurements

The wettability of the surface influences strongly its properties and can be measured using the contact angle measurement. The contact angle (CA) between a fluid and a solid surface is illustrated on figure 6.5. The angle (θ) is the mathematical expression of the interaction between the droplet and the solid surface. It depends on the topography of the sample and the chemical composition.
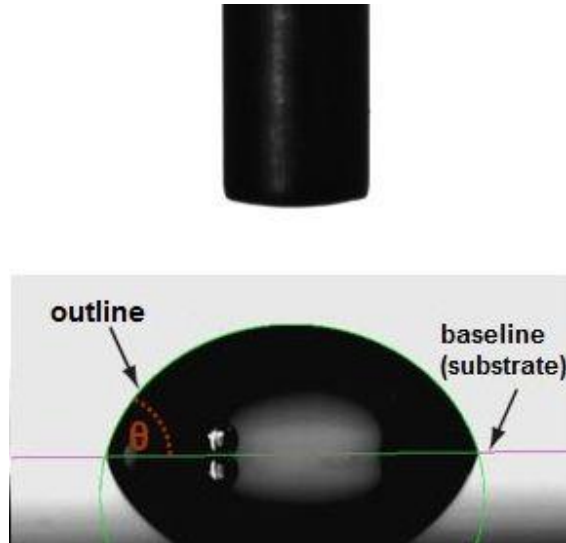
Figure 6.5 *Principle of the contact angle measurement*

The droplet can be characterized with Young-Laplace equation in the ideal situation based on the assumption, that the surface is chemically homogenous and topographically smooth:

$$\gamma_{lv} \cos \theta_Y = \gamma_{sv} - \gamma_{sl} \tag{6}$$

Whereby γ_{lv} is the liquid–vapor interfacial energy, the γ_{sv} solid–vapor interfacial energy and γ_{sl} solid-liquid interfacial energy represents. The equation is valid only under the consideration of a thermodynamic equilibrium of the three present phases.

In this work the sessile drop method was used for the contact angle measurements. A single droplet is dropped on the surface and it is illuminated and pictured nearly before and after reaching the sample. Thus the properties of a limited area of the solid surface are investigated. The angle between the baseline of the drop (purple line on picture 6.5) and the tangent at the drop boundary (outline marked in green) is

measured using a goniometer. The contact angle is measured close to the contact between the liquid and the solid phases. Due to the instability of the thermo dynamical equilibrium the camera was set to take pictures 200 ms after the interaction. The evaporation of part of the fluid and its interaction with the surface results in change of the size and shape of the droplet, which lead to different value of the contact angle.

A droplet of approximate 1 µl deionized water is dropped on the diamond surface by the means of a Hamilton-pipette. To reduce the error it is important that the droplet contains no air bubbles. The wettability of the sample was snapped with a CCD camera, and the obtained pictures were further analyzed with software CAM 100.
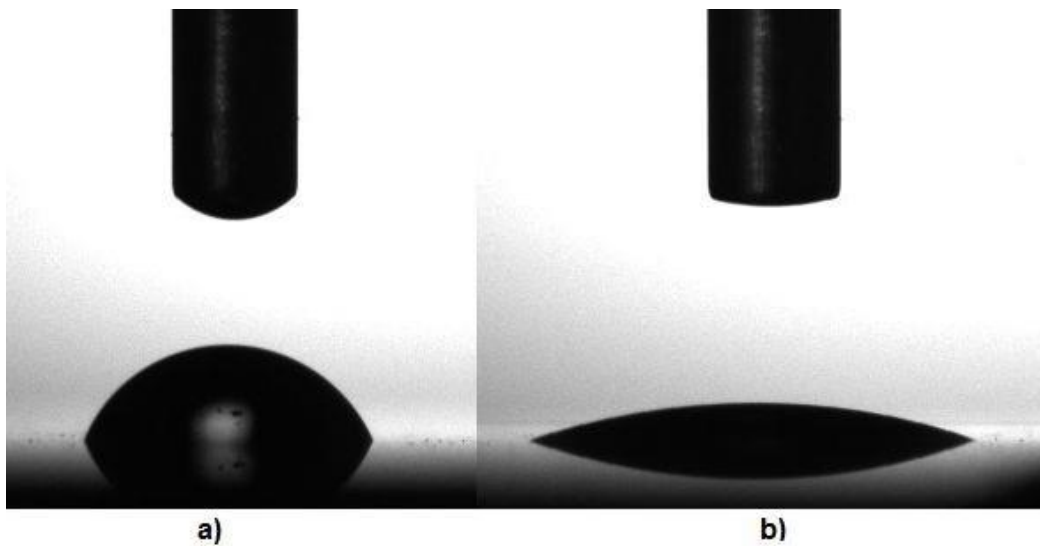
Figure 6.6 *Different contact angles of a water droplet on: a) hydrophobic surface - as-grown sample; b) hydrophilic surface - UV/O$_3$ modified NCD*

Pictures of two different diamond samples are shown on figure 6.6. Figure 6.6-a represents a NCD surface with hydrogen termination directly after the growth. The droplet is well formed and the sample shows hydrophobic properties. All measured as-grown samples have contact angle values between 70 and 80 degree. An UV/O$_3$ modified NCD is presented on the second picture. The sample has been modified for 10 minutes and has a contact angle close to 30 degree. The droplet is greatly deformed due to the strong hydrophilic character of the surface.

6.1.2. Contact angles measurements after oxygen plasma modification

The contact angle (CA) of all samples was measured after the modification using the as-grown sample as a reference. The average value of the CA from 5 measurements was calculated as $\theta= 73.3$ ° with a standard deviation of ± 1.9 °. After the exposure to oxygen plasma the NCD surface is modified and becomes hydrophilic with definitely smaller contact angles. The dependence between the contact angle and the modification time is shown on figure 6.7.
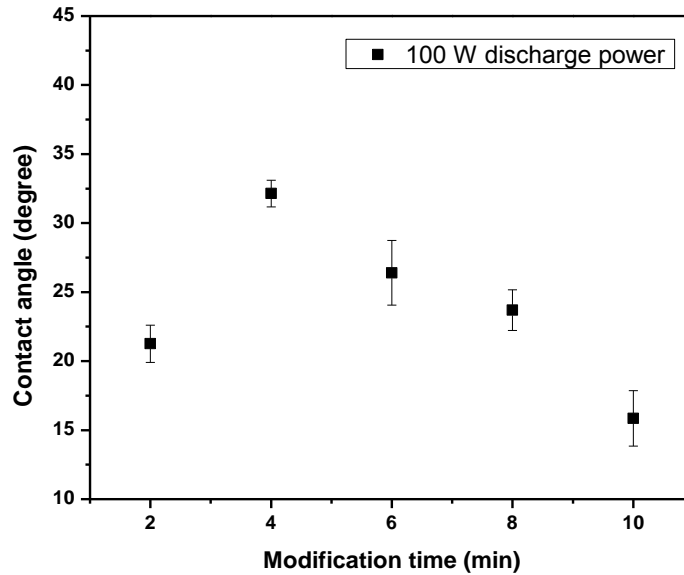
Figure 6.7 *Contact angles of NCD surfaces as a function of oxygen plasma modification time at 100 W power*

To reduce the standard deviation different areas of each sample were analyzed (applying 4 to 6 droplets). The surface changes rapidly from hydrophobic (of the as-grown sample) to hydrophilic (of the modified sample). After 2 minutes modification a contact angle of 21.3° was measured indicating a changed wettability. The contact angle after 4 minutes is higher, further exposure to the plasma causes only a decrease of the contact angle. The lowest value of $\theta= 15.9°$ with a standard deviation of ± 2.0°, is reached after 10 minutes.

Similar behavior was observed after modification with a higher discharge power. The contact angles for the 200 W series are higher and the values vary from 38 to 29

degree (see figure 6.8). Also in this case a change of wettability is demonstrated after 2 min modification, after 4 minutes only marginal variations of the contact angles are seen.
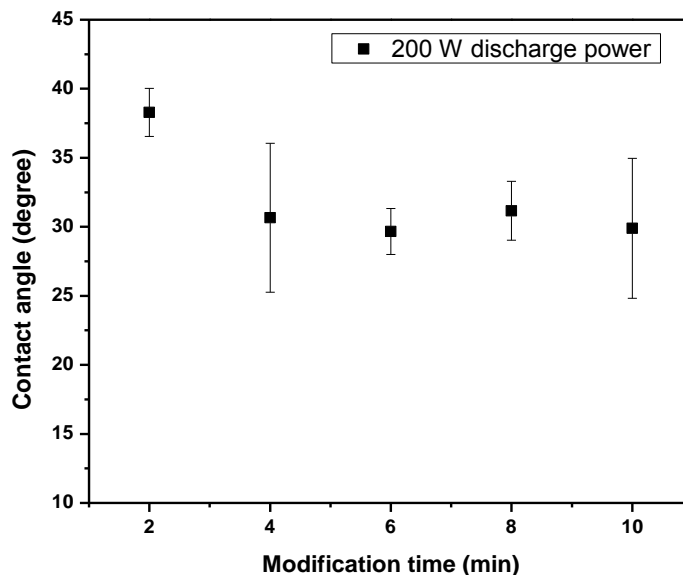
Figure 6.8 *Contact angles of NCD surfaces as a function of oxygen plasma modification time at 200 W power*

The large deviations from the average CA value by some samples can be related to the rough NCD surface as shown in the previous subchapter. As already mentioned, the roughness varies between different areas of the NCD film.

The conclusions derived from the AFM and contact angle measurement results were used to define the modification parameters of the samples for further investigations. Due to the successful modification and constant value of the contact angle of about 28 degree, discharge power of 200 W and modification time of 5 minutes were chosen and applied for further functionalization of the samples presented next in the work.

All initial CA measurements were performed immediately after the surface modifications, i.e. on 'fresh samples'. Some of the measurements of the samples (e.g. XPS) needed long transportation time, hence deeper knowledge about the stability of the termination was required. Therefore three different storage ways were used: (i) samples placed on a dust-free paper in a box. This series is marked as 'air' in figure 6.9; (ii) samples placed in a box and then in a vacuum sealed plastic bag in order to prevent the

interaction of the modified diamond surface with the air ('vacuum' samples); (iii) samples placed in a centrifuge tube and immersed in distilled water. These samples are marked as 'di H2O" on the graph below.
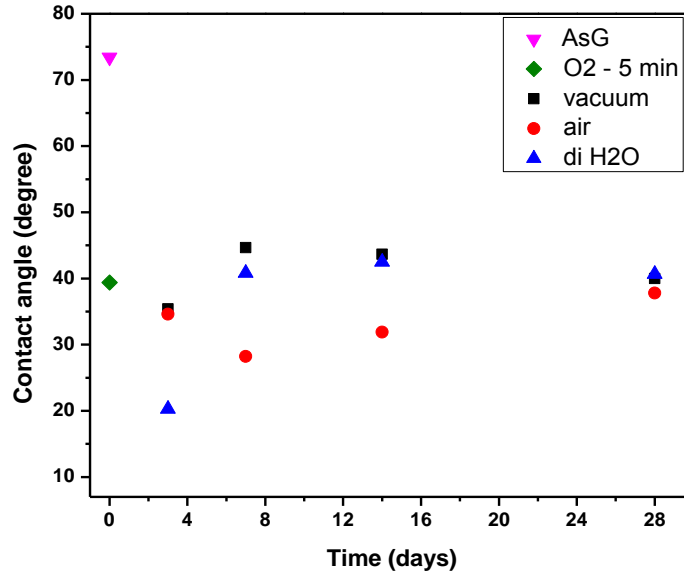
Figure 6.9 *Stability measurements of the contact angles of NCD samples modified for 5 min oxygen plasma at 200 W discharge power*

The CA of the samples were measured after 3, 7, 14 and 28 days. The data about the contact angle values presented on figure 6.9 reveal slight, almost not notable decrease for both 'air' and 'vacuum' samples after 3 days, while the CA of the immersed in water sample dropped to 20.3 degree due to further strong hydrophilization of the surface. The subsequent increase of the contact angles of all samples after longer storage can be expected, caused by the partial replacement of the oxygen containing groups on the diamond surface by contaminations from the ambient with time. As a result the CA increases and the diamond film becomes less hydrophilic. After 4 weeks the CA values of all samples packed are in the range between 38 and 40 degree, i.e. no significant difference is observed after the oxygen plasma modification. This fact indicates that this termination is relatively durable. After the oxygen plasma modification strong covalent bonds between the diamond surface and the activated oxygen are formed. They

cannot be dissociated easily with the time and the sample can hold its surface properties for longer period.

6.2. UV/ozone treatment and contact angle measurements

UV/ozone treatment, also called photomodification is another way for achieving of oxygen termination. Unlike the plasma processing, the photomodification has the advantage of easy operability as it allows processing under normal atmosphere. The high energy of a UV radiation derived from a low-pressure mercury lamp is used for the formation of oxygen-containing groups (like -OH, COO-, CO- and -COOH) on the diamond surface. For the modification of our NCD samples, a mercury lamp from BHK Inc., Claremont, California with a size of 125 x 125 mm and 600 W input power was applied. The radiation from low pressure mercury plasma is dominated by the two ground state resonance spectral lines at 253.7 nm and 185.0 nm. The irradiation of the atmospheric oxygen with ultraviolet light with a wavelength of 185 nm causes absorption of the ultraviolet rays and formation of O_3 under the reactions:

$$O_2 \rightarrow O + O \tag{7}$$

$$O + O_2 \rightarrow O_3 \tag{8}$$

Ozone illuminated with rays with a wavelength of 253.7 nm absorbs the ultraviolet light and decomposes. During the process of formation or decomposition of O_3, the generated atomic oxygen possesses strong oxidizing ability. Organic molecules attached to the surface of the sample can be cracked and oxidized by the UV light and the active oxygen forms CO_2 and H_2O, which desorb from the surface into the gas phase.

A homemade UV/O_3 setup (shown on figure 6.10) was used for the modification of the NCD films. Two samples (DHF 59 and DHF 60) with thickness of about 700 nm grown at 790 °C and 25 mbar pressure for 180 minutes are used for UV/O_3 treatment. The samples were exposed with UV low pressure mercury grid lamp in air. Prior to the modification the reaction chamber was purged for 5 minutes with nitrogen under 2.2 bar pressure. The distance between the lamp and the diamond film was 4 cm. The modification is performed in air to provide the necessary oxygen concentration. The diamond samples were terminated for 1, 2.5, 5, 7.5, 20, 30 and 40 minutes. Thereafter

the chamber was purged again with nitrogen and after 10 minutes the samples were taken out.
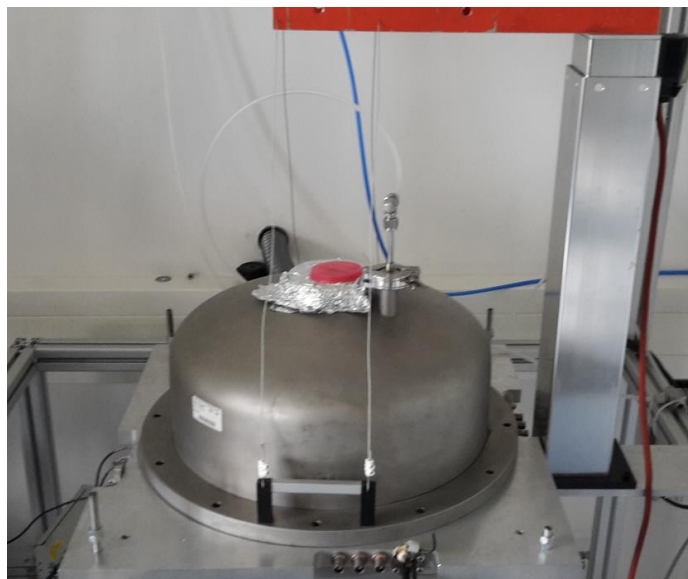
Figure 6.10 *UV/ozone modification set-up in INA, University of Kassel*

The contact angles were measured shortly after the surface modifications. Figure 6.11 demonstrates the dependence of the contact angles on the modification duration. The CA of 70.1±3 degree after one minute UV/O$_3$ treatment was close to that of as-grown sample (73.4°±1°) proving no substantial changes in the surface properties. Double exposure time led to a 10 degree sink of the CA. The first remarkable change appeared after 5 minutes modification. The contact angle decreased almost two times. With the increase of the exposure time, the CA dropped to 28.4°. This value is similar to the results obtained after the oxygen plasma, showing that the surface changed from hydrophobic to hydrophilic, i.e. the modification was successful. To test whether further enhancement of hydrophilicity is possible, the sample DHF 60, grown at the same conditions, was modified at the parameters of the previous sample but for longer treatment times (up to 50 minutes).
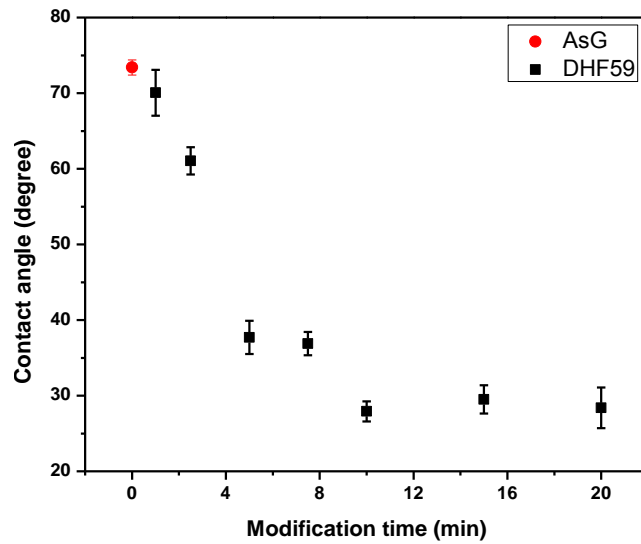
Figure 6.11 *Contact angles of NCD surfaces as a function of UV/O$_3$ treatment time, measured for sample DHF 59*

The diamond surface behaviors after the UV/O$_3$ treatment did not change, however the contact angles further decreased with the increase of the modification time, reaching a value of 7.9° after 30 minutes (figure 6.12).
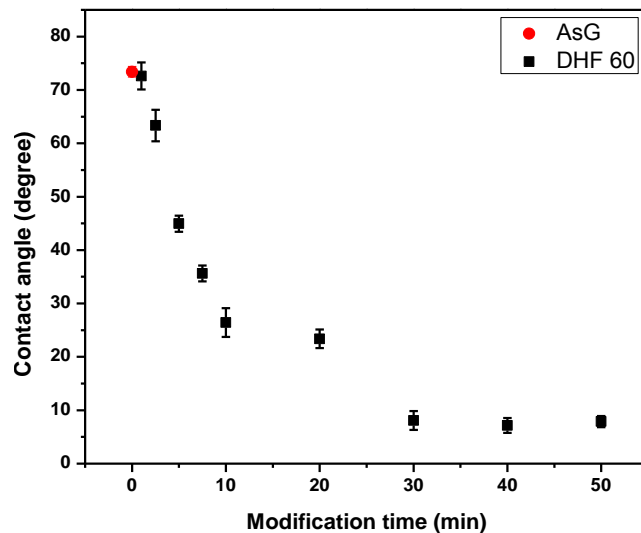
Figure 6.12 *Contact angles of NCD surfaces as a function of UV/O$_3$ treatment time, measured for sample DHF 60*

The difference in the CA values after 40 and 50 minutes was negligible. The conclusion is that 30 minutes are needed to complete the surface modification and to achieve highly hydrophylic surface.

The CA stability measurements of the three groups stored samples (in air, vacuum and distillated water) showed the results presented on figure 6.13. The samples modified by UV/O$_3$ treatment were less stable than the samples treated with oxygen plasma. The surface lost the hydrophilic properties after a couple of days and the contact angles raised constantly. After 3 days the contact angles jumped from 8 to 45-49 degree, irrespective of the storage method. The results for the 'air' and 'vacuum' samples were similar: the contact angles increased and after 4 weeks reached the value of 58-62 degree.
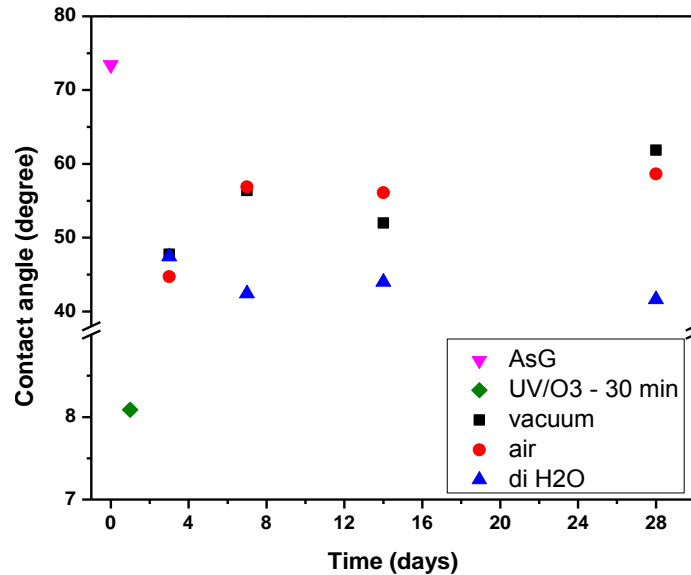
Figure 6.13 *Stability measurements after 30 min UV/O$_3$ treatment*

The immersed in water samples showed some slight differences. After the initial increase of the CA, the surface remained intact during the further storage in distillated water.

The results of the contact angle measurements exhibited that the termination after UV/O$_3$ treatment is not stable enough and the terminated surface lose to great extent its hydrophilic properties. Therefore this technique is not suitable for some of the further purposes of this work.

64

6.3. NH₃/N₂ plasma

The treatment with NH_3/N_2 plasma is the third modification method used in this work. The amination of the samples was performed in a homemade NH_3/N_2 set-up in the Institute of Nanostructure Technologies and Analytics, University of Kassel (figure 6.14). A commercial generator from Advanced Energy was applied to generate the RF signal (13.5 kHz). A copper coil (with a diameter of 6.5 cm, six times wounded and cooled with water) was used to couple the signal from the generator into the quartz chamber. A rotary vane pump and a turbo molecular pump from Pfeiffer were used to evacuate the chamber to the necessary pressure (5×10^{-3} mbar). The pressure was monitored with an Edwards penning gauge. The control of the chamber pressure during the process was carried out with a Baratron gauge (MKS) connected to a throttle valve (MKS). The used gases, nitrogen and ammonia, were introduced into the reaction chamber via thermal mass controllers (MKS). The precise gas flow was controlled by four channel readout (MKS).
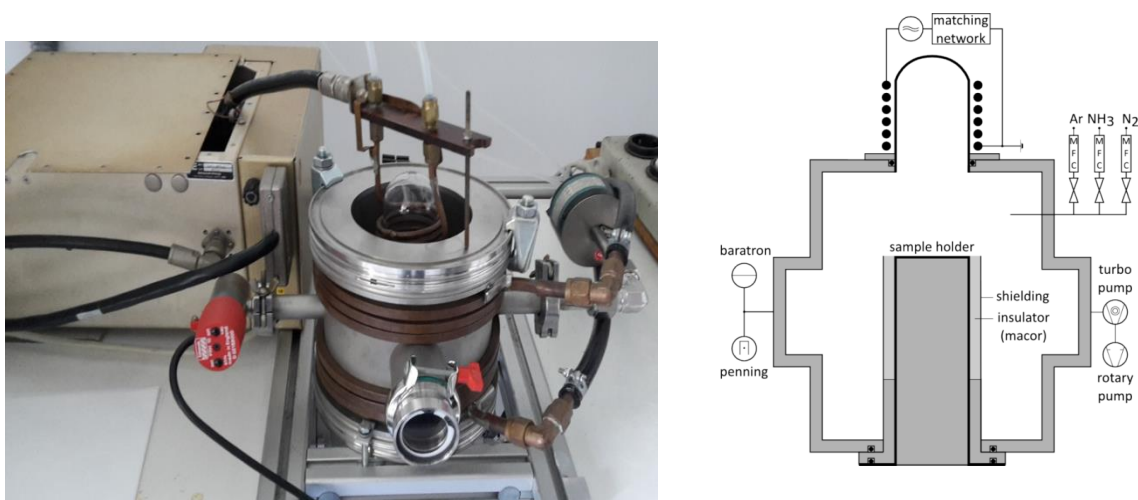
Figure 6.14 *Ammonia modification set-up in INA, University of Kassel: left: photo, right: schematic view*

The modification process was performed as follow:

i) The samples were placed in the middle of the chamber on the substrate holder;

ii) Evacuation for at least 30 minutes was applied to reach a residual gas pressure of approximately 5×10^{-3} mbar;

iii) Gas mixture was introduced into the chamber: 5 sccm NH_3 and 100 sccm N_2 flows at a working pressure of 1.8×10^{-2} mbar;

iv) The plasma was ignited and the reflecting power was manually adjusted. The samples were modified at 150 W for different durations;

v) To avoid contamination of the freshly modified surface, the reaction chamber was flushed with nitrogen for 10 minutes after the end of the process.

The contact angles were measured directly after the modification and the results are plotted in figure 6.15. The wettability of the surface changed significantly even after 1 minute and the CA decreased from 73.4 to 30.7 degrees. After that no remarkable differences were noticed and the contact angles stayed in the range of 18.1° - 6.2°. For the stability measurements a modification time of 5 minutes was chosen.
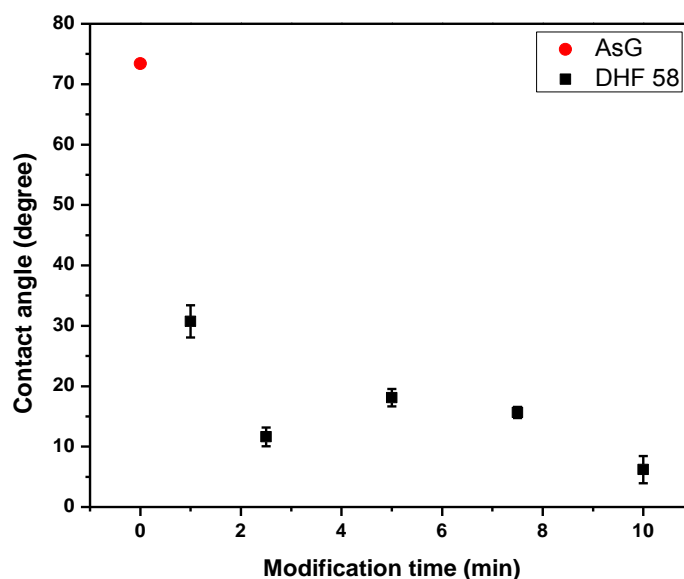
Figure 6.15 *Contact angles of NCD surfaces as a function of NH$_3$/N$_2$ plasma treatment time, measured for sample DHF 58*

The surface after modification was not so stable and loss of the hydrophilic properties was observed after a couple of days. After 4 weeks the contact angles increased from 20.0° to 35-39° depending on the storage media. The storage under 'vacuum' did not influence the stability of the termination and the CA changed as quickly as for the samples stored in simple boxes in air or immersed in water (see figure 6.16).
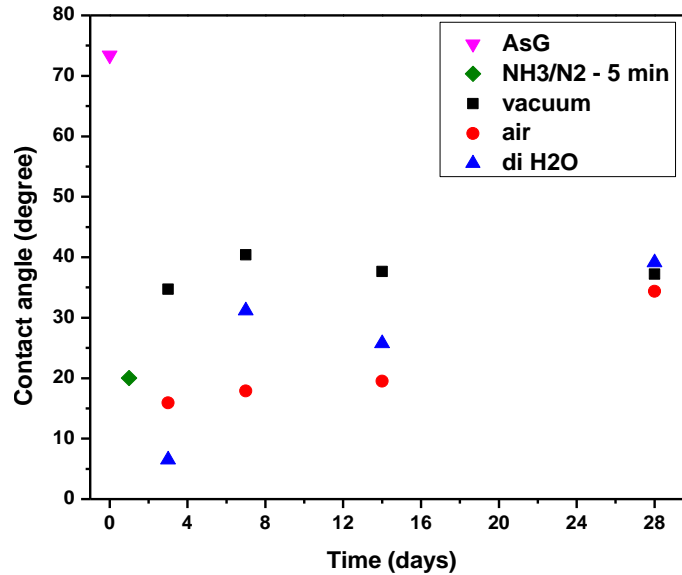
Figure 6.16 *Stability measurements after 5 min ammonia plasma modification*

6.4. Surface composition and chemical binding after modifications

X-ray photoelectron spectroscopy (XPS) was used to study the surface composition of the films after deposition and different modifications. For these measurements, an Axis Nova spectrometer (Kratos Analytical Ltd., UK) with a monochromatic Al Kα source was employed. An area from 400 x 700 mm^2 was analyzed with pass energy of 20 and 160 eV. Thereby survey and core level spectra were obtained. A filament (I = 1.9 A, V = 3.2 V) inserted in the magnetic lens system acted as neutralizer for surface charge compensation. All measurements were done by Dr.-Ing. Dr. Rolf Merz at the Institute for Surface and Thin Film Analysis (IFOS), University of Kaiserslautern.

Figure 6.17 shows the surface compositions of 4 different samples: as-grown (AsG) NCD; UV/ozone modified sample (UV/O$_3$), ammonia modified sample (NH$_3$/N$_2$) and sample after oxygen plasma modification (O$_2$). Directly after the deposition the diamond film has a very clean surface, which consists almost only of carbon atoms (98.5 ± 0.2 at%) and small oxygen contamination of 1.5 ± 0.2 at%. The oxygen content increased to 6.5± 0.1 at% after O$_2$ plasma treatment and to 5.4± 0.2 at% after UV/O$_3$ plasma treatment,

indicating an oxidation of the surface. The plasma treatment with NH_3 led to a surface nitrogen concentration of 3.6 ± 0.2 at%, but also to an oxygen content of 4.5 ± 0.2 at%. The detected oxygen is most likely due to the adsorption of air moisture and other impurities. An aminated NCD surface is well known for its hydroscopic properties to attract and to hold water [136]. The XPS results confirmed the successful modifications of the samples and the change of the surface termination after both plasma processes and UV/O_3 treatment.
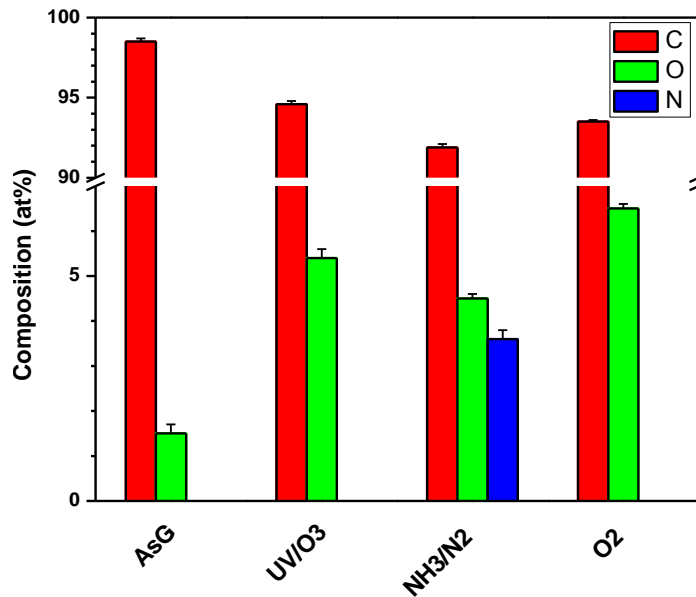
Figure 6.17 *Surface composition of NCD films after: depositon (AsG), UV treatment (UV/O_3), ammonia plasma (NH$_3$/N$_2$) and oxygen plasma (O$_2$)*

The C1s spectra of the samples plotted on figure 6.18 reveal the influence of the different modification techniques. The as-grown sample shows the narrowest peak, while the exposure to both ammonia plasma and UV treatment results in peak broadening on both sides. The broadening of the peaks after modification toward the higher bonding energy is due to the formation of new bonds (such as C-OH at 286 eV and 286.5-287 eV, C-O-C at 286 eV, C=O at 289 eV, O-C=O at 288.5 eV by the oxygen plasma modification [137] and C-N and C-OH at 286 eV and 286.5-287 eV, respectively by the ammonia plasma modification [138]) on the sample surface. Broadening into direction of the lower energy can be explained with the high sp^2 content und amorphous phase on the surface.
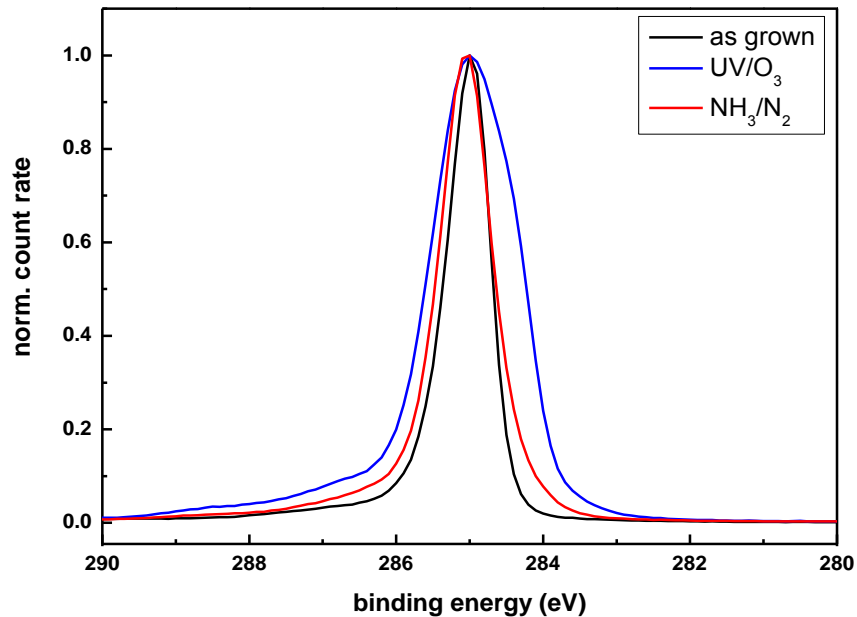
Figure 6.18 *C 1s core level spectra of NCD films after: deposition (AsG), UV treatment (UV/O$_3$) and ammonia plasma (NH$_3$/N$_2$)*

Raman spectroscopy measurements of the NCD films were performed with two different excitation wavelengths - 488 nm and 785 nm. The measurements were carried out with a Renishaw 1000 Raman spectrometer attached to a Leica DM/LM microscope. Diode laser with spot size of 1 µm, operating at 785 nm and the 488 nm line of an Ar-ion laser served as excitation sources. The laser power on the sample surface was ca. 5 mW for the first case and ca. 20 mW for the second one. The Raman measurements were done by Dr. Miklos Veres at the Wigner Research Centre for Physics, Hungarian Academy of Sciences, Budapest, Hungary.

Raman spectra of the NCD films before and after the modifications taken with 785 nm excitation wavelength are presented in figure 6.19. The characteristic diamond peak is observed at 1332 cm^{-1} together with a broad peak around 1500 cm^1 originating from a non-diamond phase (G-band). The broad peak at 946 cm^{-1} can be attributed to the silicon from the substrate. The exposure to diverse plasmas or UV/O$_3$ does not influence the quality of the diamonds films.
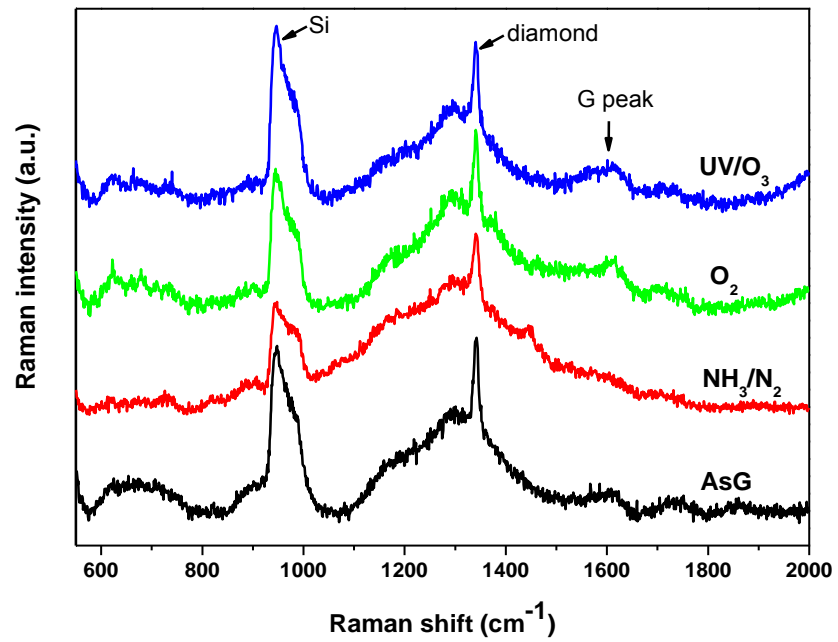
Figure 6.19 *Raman spectra (785 nm excitation wavelength) of NCD films after:*
deposition (AsG), UV treatment (UV/O₃) and ammonia plasma (NH₃/N₂)

7. Grafting of phthalocyanines on NCD surface

7.1. Synthesis of with different central atoms and side chains

All phthalocyanine compounds used in the current work have been synthesized in the Institute of Chemistry in the workgroup of Prof. Dr. U. Siemeling (University of Kassel, Dept. of Metalorganic Chemistry) by Philipp M. Reintanz and co-workers [139]. The synthetic procedures are described shortly below.

Synthesis of chlorido-[2,3,9,10,16,17,23,24-octakis(n-dodecylthio)phthalocyaninato] manganese(III), [MnClPc(S(n-C$_{12}$H$_{25}$))$_8$] or MnSPc

The synthesis follows a well-established approach by Siemeling *et al.* [140]: 987 mg (1.87 mmol) 4,5-bis(*n*-dodecylthio)phthalodinitrile, 103 mg (0.52 mmol) manganese(II) chloride tetrahydrate and 15 mL 1-pentanole were mixed in a Schlenk pressure tube under nitrogen atmosphere. 0.35 mL 1,8-diazabicyclo[5.4.0]undec-7-ene was added and the resulting mixture was heated for 3 hours at 170 °C with stirring.
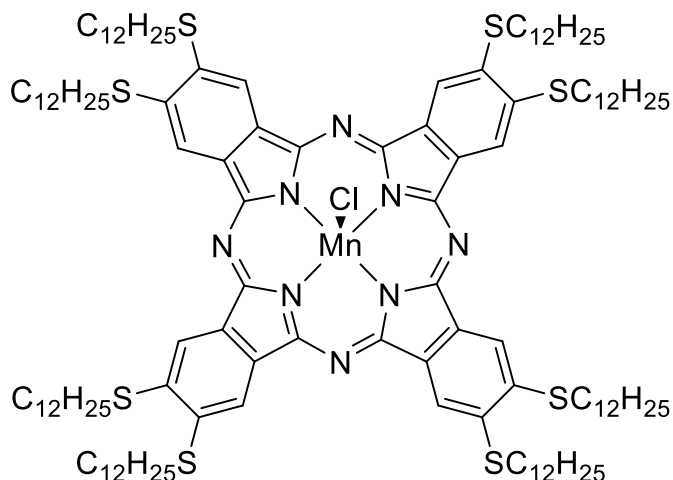
Figure 7.1 *Structural formula of [MnClPc(S(n-C$_{12}$H$_{25}$))$_8$]*

Afterwards, the resulting solution was cooled down to room temperature. 30 mL dichloromethane was added, the solution was moved to a round-flask and 30 mL of methanol was added. Dichloromethane was removed under reduced pressure (50 °C bath temperature, 400 mbar) to afford a red-brown crude product. The residue was

filtered off and washed with 60 mL methanol. The product (shown on figure 7.1) was purified with column chromatography (silica gel, chloroform/methanol 20:1). Yield 742 mg (0.34 mmol, 72%).

Synthesis of chlorido-[2,3,9,10,16,17,23,24-octakis(n-pentoxycarbonyl)phthalo-cyaninato]- manganese(III) ([MnClPc(COOC$_5$H$_{11}$)$_8$] or MnPc)

The precursor compound 4,5-bis(pentoxycarbonyl)phthalodinitrile has been synthesized according to Opris *et al*. [141]. The new manganese phthalocyanine has been first described by Anna Degenhardt in her diploma thesis (2014): 128 mg (0.39 mmol) 4,5-bis(pentoxycarbonyl)phthalodinitrile, 26 mg (0.14 mmol) manganese(II) chloride tetrahydrate, 10 mL 1-pentanole and 84.5 µL 1,8-diazabicyclo[5.4.0]undec-7-ene were mixed in a Schlenk pressure tube. The resulting mixture was heated at 170 °C for 4 hours. The blue solution was cooled down to room temperature, 30 mL dichloromethane was added and the solution was moved to a round-bottomed flask. After addition of 30 mL methanol, dichloromethane was removed under reduced pressure (50 °C bath temperature, 400 mbar). The dark-blue precipitate was filtered off, washed with 60 mL methanol and dried under reduced pressure. Yield 25%. The structural formula of the phthalocyanine molecule is presented on figure 7.2 below.
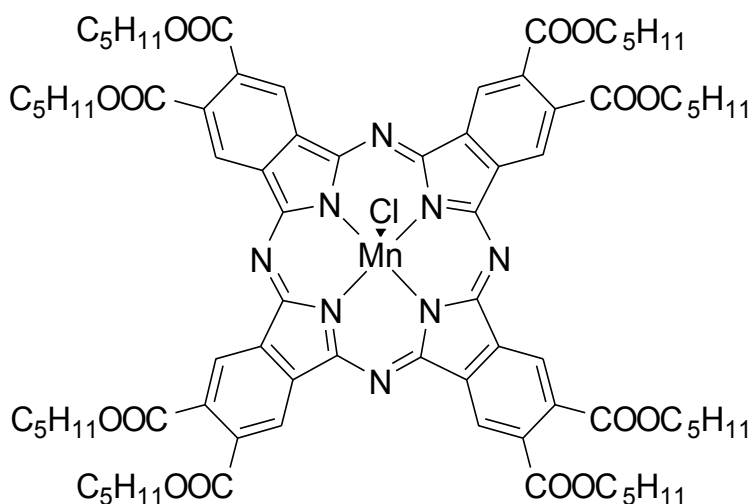
Figure 7.2 *Structural formula of [MnClPc(COOC$_5$H$_{11}$)$_8$]*

Synthesis of [2,3,9,10,16,17,23,24-octakis(n- pentoxycarbonyl)phthalocyaninato] copper(II),([CuPc(COOC5H11)8] or CuPc)

The product was achieved as side-product during the synthesis of 4,5-bis(*pentoxycarbonyl*)phthalodinitrile according to Opris et al. [141]: 2.154 g (4.64 mmol) 4,5-dibromophthalobispentylester, 900 mg (9.9 mmol) copper(I) cyanide, 20 mg (0.12 mmol) potassium iodide and 30 mL abs. *N,N*-dimethylformamide were mixed under nitrogen atmosphere in a Schlenk flask. The resulting mixture was refluxed for 3.5 hours. After cooling down to room temperature, 40 mL dest. water was added and the solution was filtered. The green-blue solid was dried on air and diluted in 60 mL dichloromethane-methanol (1:1). Dichloromethane was removed under reduced pressure (50 °C bath temperature, 400 mbar), the precipitate was filtered off and washed with 60 mL methanol to yield 176 mg (0.11 mmol, 10 %) copper phthalocyanine. The obtained phtalocyanine is shown on figure 7.3.
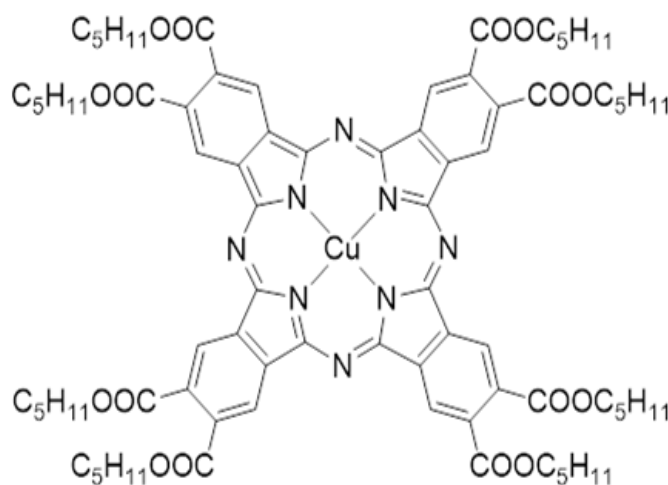
Figure 7.3 *Structural formula of [CuPc(COOC5H11)8]*

Synthesis of oxo[2,3,9,10,16,17,23,24-octakis(nodecylthio)phthalo-cyaninato] titanium (IV), ([TiOPc(S(n-C12H25))8] or TiPc) [139]

695 mg (1.31 mmol) 4,5-bis(*n*-dodecylthio)phthalodinitrile and 45 mg (0.75 mmol) urea were heated in a Schlenk pressure tube at 70 °C. 216 mg (0.65 mmol) tetrachlorobis(tetrahydrofuran)titanium(IV) was added under nitrogen and the resulting mixture was heated at 150 °C for 17 hours. Tetrahydrofuran was removed under reduced pressure and the black-brown crude product was diluted in 30 mL dichloromethane. The

solution was moved to a round flask and 30 mL of methanol was added. Dichloromethane was removed under reduced pressure (50 °C bath temperature, 400 mbar), the precipitate was filtered off, washed with 60 mL methanol and dried on air. The crude product (see picture 7.4) was purified with column chromatography (silica gel, *n*-hexane/ethyl acetate 1:1) to yield 400 mg (0.18 mmol, 45 %) of a brown product.
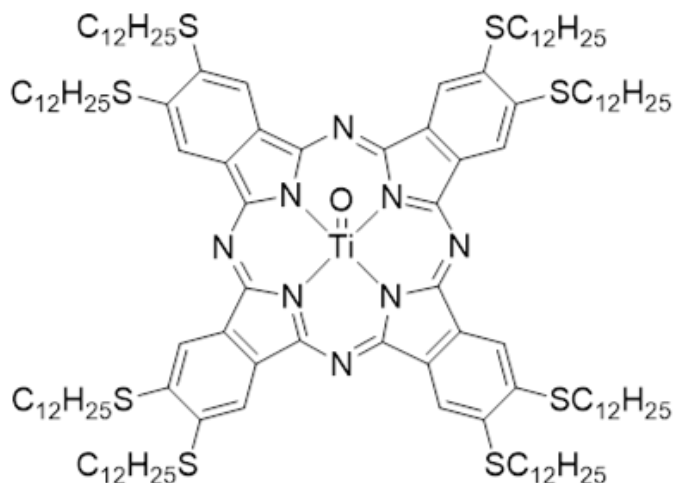
Figure 7.4 *Structural formula of [TiOPc(S(n-C$_{12}$H$_{25}$))$_8$]*

7.2. Raman spectra

NCD films were exposed directly after growth or after surface modification by oxygen or NH$_3$/N$_2$ plasma to the phtalocyanines. The samples were immersed in a solution of the Pc molecules (1 µM) in dichloromethane for approximate 12 h. Afterwards the films were ultrasonically cleaned in CH$_2$Cl$_2$ and dried with N$_2$ flow

Initially, Raman spectra with two different excitation wavelengths of 488 and 785 nm were taken from the Pc molecules. For this purpose, droplets of Pc were placed on silicon and the solvent was evaporated.

According to Tackley et al. [142] there is a band in the Raman spectra of phthalocyanines which is highly sensitive to the central metal atom, more specifically to the ion radius of the metal and the influence it has on the structure of the inner ring of the phthalocyanines. This most intensive bond is assigned to B$_1$ mode related to the C-N-C ring displacement due to the central metal ion. The movements of the atoms in the Pc molecule are presented on figure 7.5.
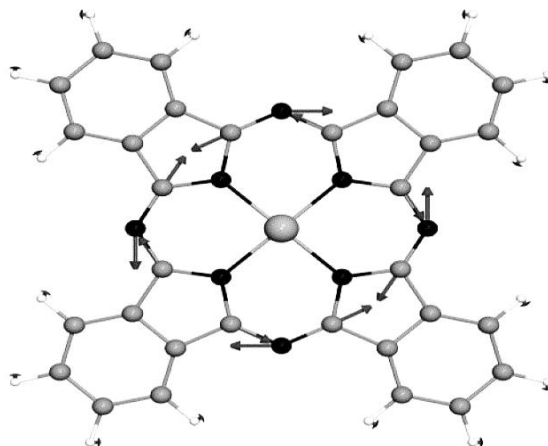
Figure 7.5 *Atomic movements responsible for the B_1 vibration of Pc molecules*

Large metal ions can deform the ring structure by taking a position out of the ring plane, which causes shifts of the Raman peaks related to the ring. The B_1 band is located between 1495 and 1545 cm^{-1}, depending on the size of the metal ion [142]. Additional intensive bands due to the ring deformation appear in the region between 650 and 770 cm^{-1}. Their positions also depend on the metal ion and they can be shifted to higher or lower energies by metal substitution.

The Raman spectra of the phthalocyanines of this study on Si taken with an excitation wavelength of 488 nm are shown on figure 7.6. They exhibit series of defined, relatively narrow peaks, part of them related to the central ring, the others to the periphery chains.
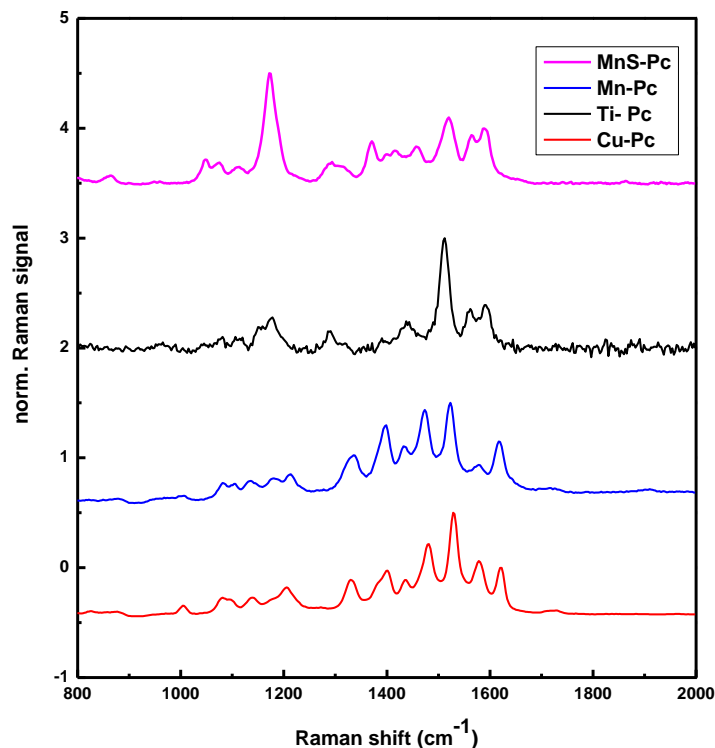
Figure 7.6 *Compression between the Raman spectra of the used phthalocyanines at 488 nm excitation wavelength*

From section 7 describing the syntheses of different Pc and showing their structural formulas it can be expected that the B_1 bands are shifted depending on the central metal ion. This is indeed the case and the positions of B_1 bands are given in table 3. On the other hand, the same peripheral chains of MnS-Pc and Ti-Pc, and Mn-Pc and Cu-Pc, respectively, give rise to peaks with same position in the Raman spectra.

Table 3 *Positions of the B_1 band for Ti-Pc, Cu-Pc, MnS-Pc and Mn-Pc detected from the Raman spectra*

Excitation wavelength	MnS-Pc	Mn-Pc	Ti-Pc	Cu-Pc
488 nm	1523.2	1520.1	1512.1	1528.7
785 nm	1525.1	1533.5	1517.3	1536.9

The Raman spectra of the four phthalocyanines taken with excitation wavelength of 785 nm are plotted on figure 7.7. The spectra exhibit similar peaks with the exception of Ti-Pc. In this case the peaks are rather brood resembling more those of a solid than of an assembly of molecules. According to Tackley et al. [142] the phthalocyanines are prone to fluorescence by excitation with wavelengths of 785 nm. In the case of Ti-Pc, this could lead to heating and subsequent reactions of the Pc molecules, which is responsible for the observed spectrum.
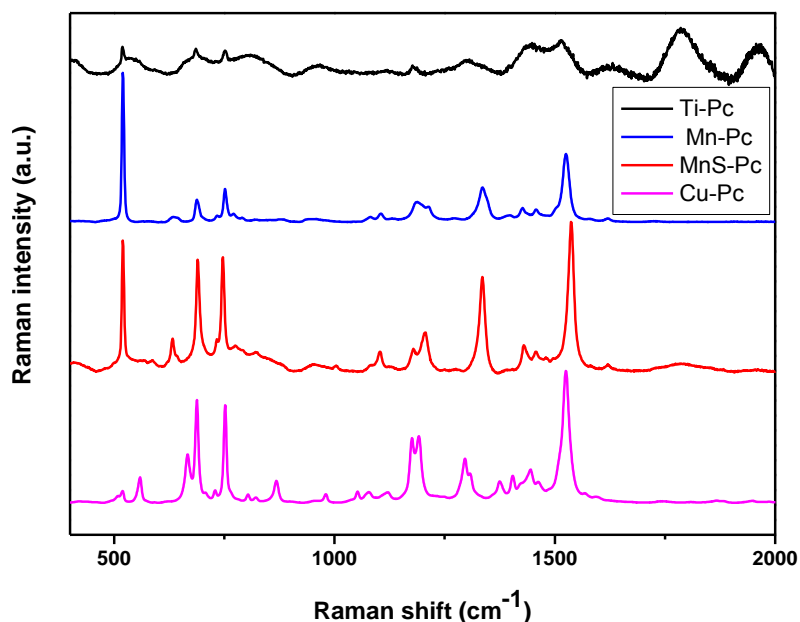
Figure 7.7 *Compression between the Raman spectra of the used phthalocyanines at 785 nm excitation wavelength*

The positions of the B_1 bands in the 785 nm spectra are also summarized in table 3. As in the case of 488 nm spectra, the observed shifts in the peak position are attributed to the influence of the different metal ions on the C-N-C ring deformation. For both excitation wavelengths the highest Raman shifts are observed for Cu-Pc and the lowest for Ti-Pc.

The direct comparison between the two different excitation wavelengths, e.g. for the MnS-Pc, has shown that the intensity of the peaks in the spectrum recorded at 785

nm wavelength is approximately 2 orders of magnitude higher as compared to the spectrum taken at lower excitation wavelength (figure 7.8).
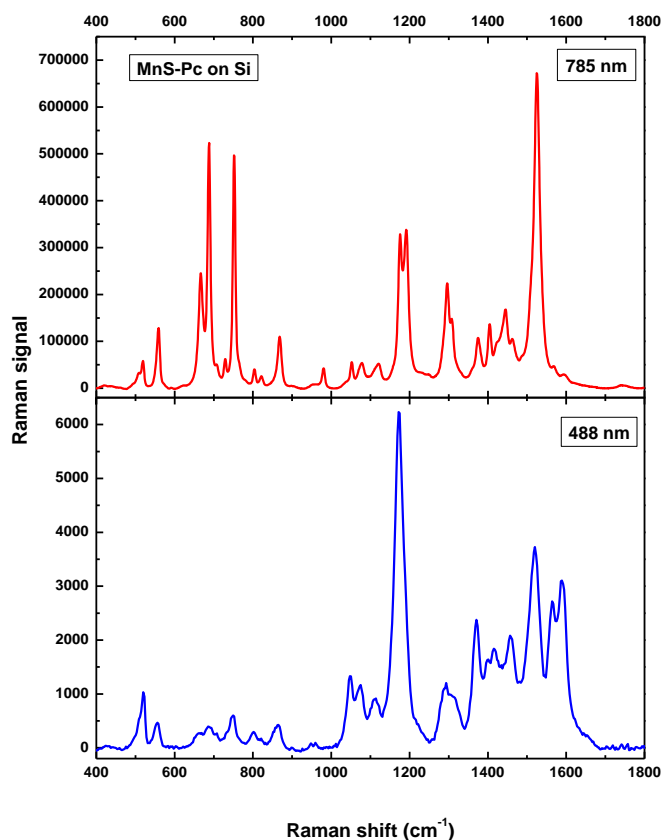
Figure 7.8 *Raman spectra of MnS-Pc at 488 and 785 nm excitation wavelength*

This can be attributed to the absorption maximum which is about 767 nm as determined by UV-Vis spectroscopy. The most intensive band in the spectrum (at 1525 cm^{-1}) can be assigned to a B_1 mode due to a C-N-C ring modification. The modification depends strongly on the metal ion in the complex as discussed above and reported for various phthalocyanines [143]. The observed B_1 band of the Mn-Pc is between those of Pb-Pc (1498 cm^{-1}) and Ni-Pc (1545 cm^{-1}) [144] corresponding very well to the data from the literature. Two additional intensive peaks attributed to the ring deformation were observed at 688 and 752 cm^{-1}. Figure 7.8 can be considered as a finger print of the MnS-Pc and will be used as a reference for further investigation. On the contrary, the spectrum at lower excitation level does not reveal additional information about the phthalocyanines; the

majority of the peaks visible at 785 nm excitation are also presented at 488 with much lower intensity (note the intensity of the Raman signals).

On figure 7.9 is plotted the Raman spectrum of MnS-Pc immobilized on a boron doped diamond film taken with 488 excitation wavelength. It exhibits the characteristic diamond peak at 1332 cm^{-1}, the peaks at 1180 und 1480 cm^1 can be attributed to the nanocrystalline nature of the diamond film, while no peaks associated to the phthalocyanine molecules are detected. Therefore, the lower excitation wavelength is not appropriate for the detection of photosensitive molecules.
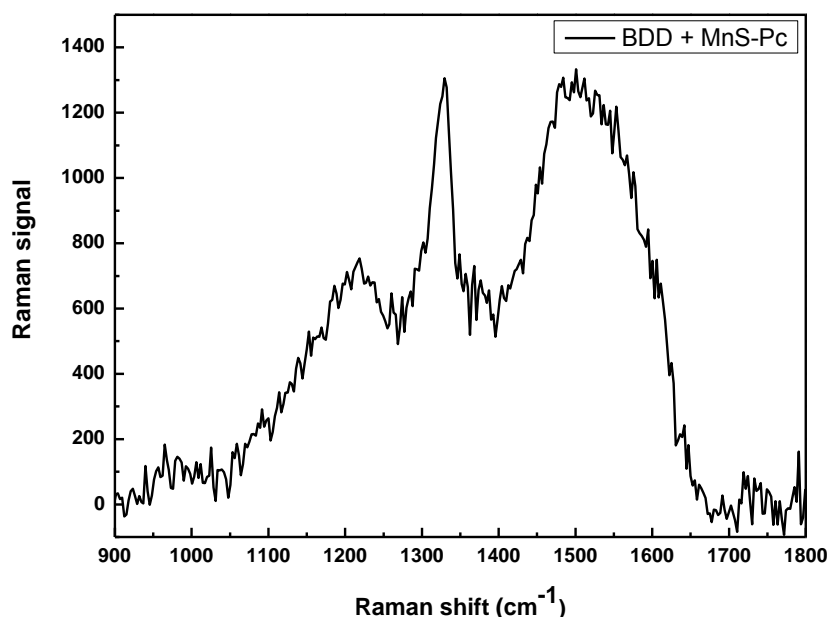
Figure 7.9 *Raman spectrum of a BDD film with grafted MnS-Pc at 488 nm excitation wavelength*

In the contrary, the Raman investigation of the same sample with higher excitation wavelength (plotted on figure 7.10) showed peaks originating from the phthalocyanine molecule. First of all, the B_1 peak of the Pc at 1525 cm^{-1} is presented in the spectrum of BDD with grafted MnS-Pc. Two additional peaks attributed to the ring deformation were observed at 688 and 750 cm^{-1} both in the spectra of the reference sample (fingerprint of MnS-Pc) and of the diamond sample, indicating a successful immobilization of the molecules.
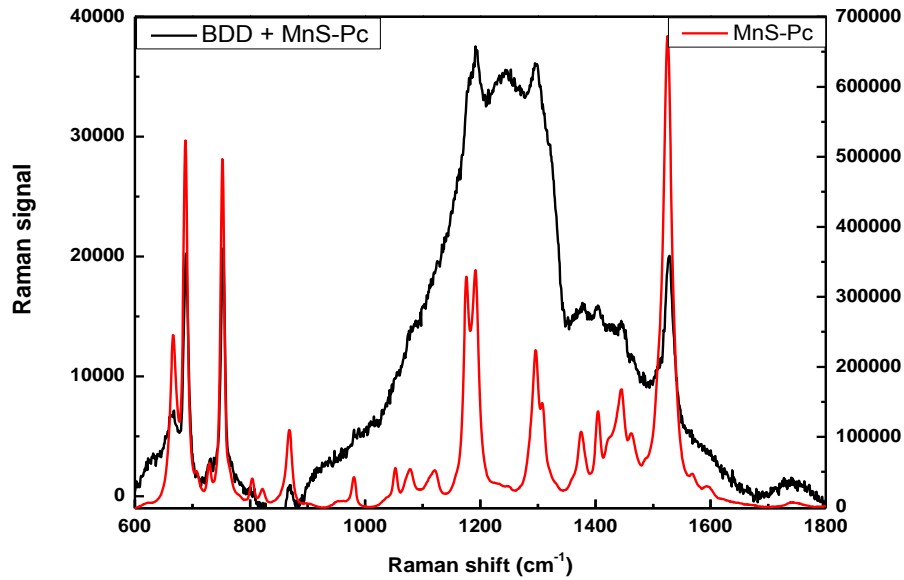
Figure 7.10 *Raman spectra of MnS-Pc on Si (as reference) and immobilized on a BDD-film at 785 nm excitation wavelength*

An oxygen terminated sample immersed in phthalocyanine, was also subjected to Raman investigation at 785 excitation wavelength (see figure 7.11).
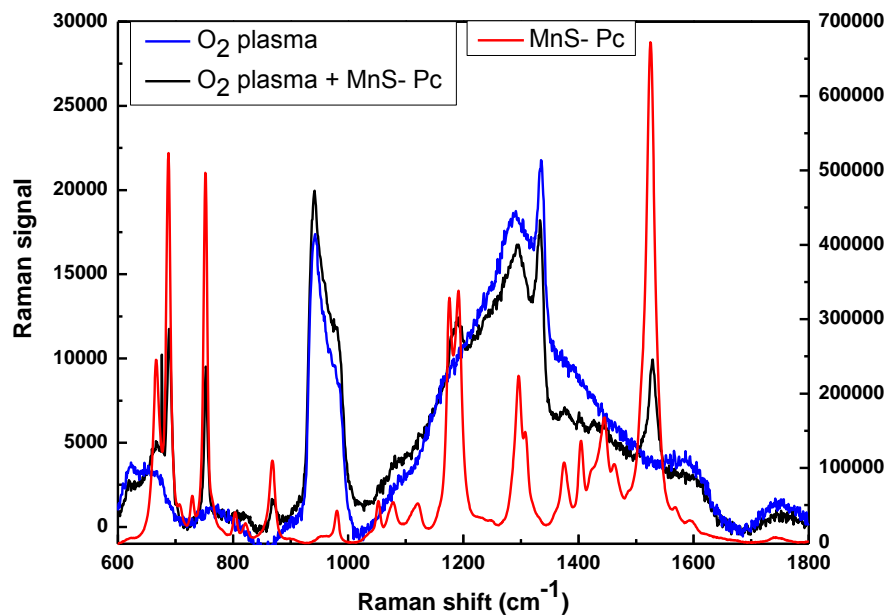
Figure 7.11 *Raman spectra of NCD (785 nm excitation wavelength) after oxygen plasma modification and grafting of MnS-Pc (the spectrum of MnS-Pc is given as reference)*

7.3. XPS spectra

The surface composition of the nanocrystalline diamond films after different plasma treatments and after grafting of different Pc molecules was investigated by XPS in two series. In the first series the attachment of the manganese (III) phthalocyaninato complex ($C_{96}H_{144}ClMnN_8S_8$) was studied (Fig.7.12). The as-grown NCD surface is very clean, having only 1.9 ± 0.1 at% oxygen impurities. This content increases to 7.1 ± 0.1 at% after the O-termination by oxygen plasma treatment. The exposure to NH_3 plasma leads to a surface nitrogen concentration of 3.2 ± 0.3 at% but also an oxygen content of 7.9 ± 0.2 at%. As already explained in the previous chapter this increase is due to the hydroscopic nature of the aminated surface [136].
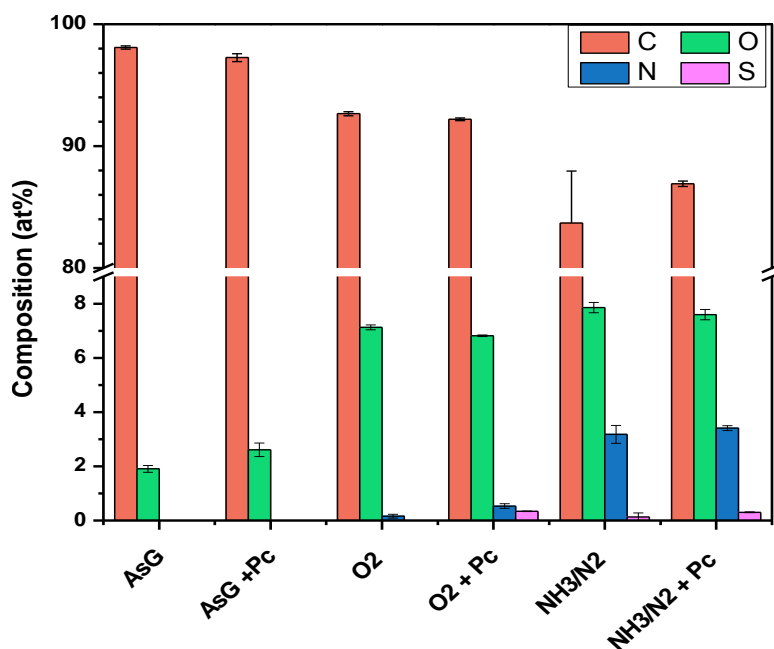
Figure 7.12 *Surface composition of as-grown and modified NCD surfaces with and without MnS-Pc*

The oxygen content is a possible result also of the oxygen presence in the reaction chamber during the treatment. Oxygen-containing species from the residual gas are established even after evacuation of the plasma chamber. The nitrogen- (from the NH_3 molecules) and oxygen-containing species are in competition to replace the terminating

hydrogen atoms. This phenomenon has been observed also by other authors after NH$_3$ plasma or UV treatments of diamond surfaces [145], [146].

Figure 7.12 shows the changes in the surface composition after both plasma processes and exposure to Pc. The grafting of the phthalocyanine leads to minor changes of the oxygen content: slight increase (by 0.7 at%) on the as-grown surface and a slight decrease (by 0.3 at%) on the plasma treated diamond surface, respectively.

The nitrogen content of the oxygen terminated sample shows an increase to approximately 0.5 at% after exposure to Pc, which is due to the nitrogen atoms from the Pc molecule ($C_{96}H_{144}ClMnN_8S_8$). The N content increases also on the NH$_2$-terminated surface after the grafting of the phtalocyanine from 3.2 to 3.4 at%. In addition, sulphur with concentrations of 0.3 - 0.4 at% is also detected on both plasma modified samples after exposure to Pc.

The bonding environment of the samples has been further investigated with the XPS core level spectra. O1s spectra of the samples before and after modification and grafting of the photosensitive molecules plotted on figure 7.13 show a marginal difference between the spectra. On the other hand modification and immobilization of MnS-Pc result in a slight broadening on both sides of the spectra.
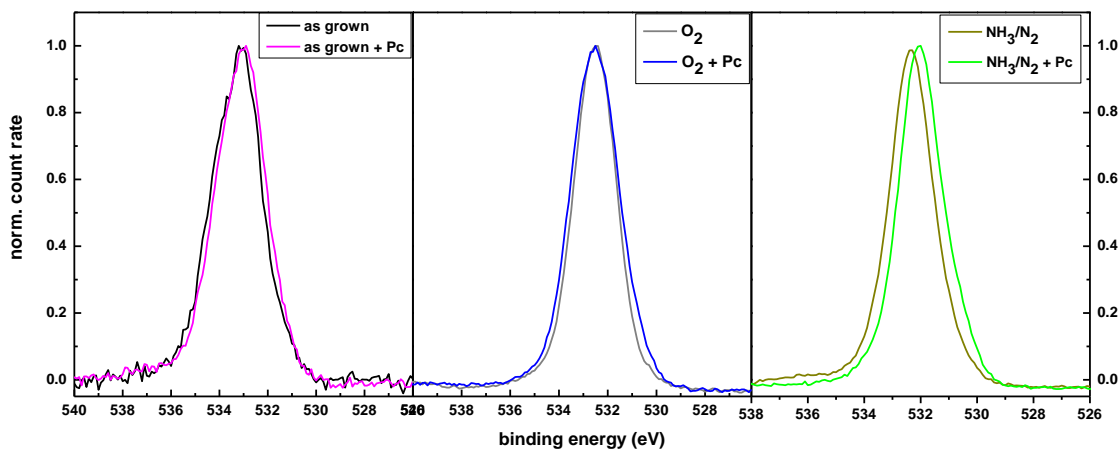
Figure 7.13 *O1s core spectra of as-grown and plasma modified NCD surfaces without and with MnS-Pc as determined by XPS*

N1s core spectra reveal several differences in the six studied samples. As expected no traces of nitrogen are detected on the as-grown diamond surface with and without phthalocyanine (figure 7.14,a). The XPS spectra of oxygen terminated sample

does not show nitrogen content on the surface. However, oxygen terminated sample functionalized with MnS-Pc reveals a nitrogen peak at 400 eV (figure 7.14,b). After NH_3 plasma exposure (figure 7.14,c) a new signal due to N1s at 399 eV is detected. This can be attributed to the amination of the diamond surface.
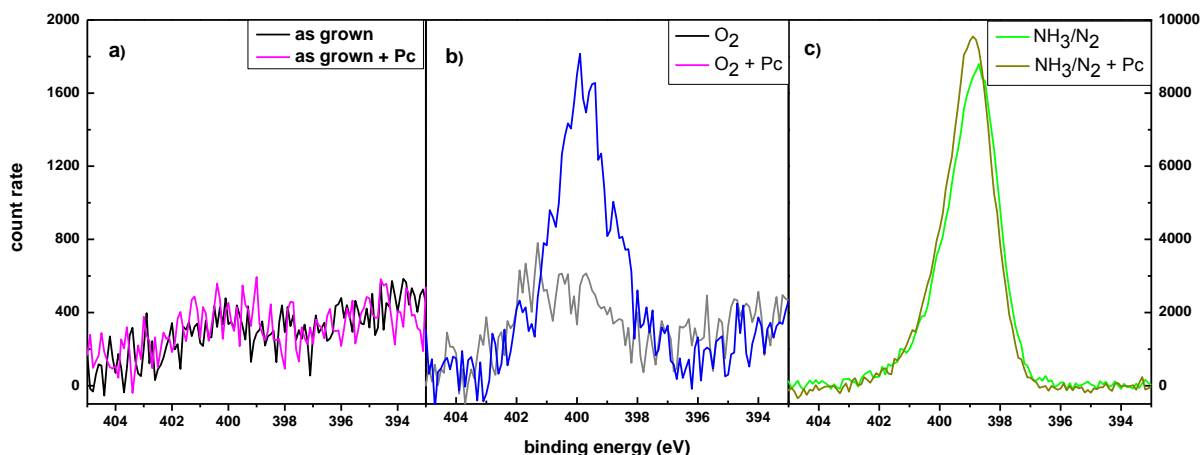
Figure 7.14 *N1s core spectra of as-grown and plasma modified NCD surfaces without and with MnS-Pc as determined by XPS*

Grafting of the phthalocyaninato complex leads to higher intensity and broadening of the N1s signal toward the higher bonding energy. It should be noticed that the intensity of these spectra is almost one order of magnitude higher in comparison with the previous ones (as-grown and O_2 plasma modified).

The S2p core level spectra are of interest due to the presence of sulphur in the phthalocyaninato complex. The S2p spectra of four samples with and without grafted molecules after background subtraction and without normalization are presented in figure 7.15.

Doublets with a $2p_{3/2}$ binding energy of 163.3 and 164.3 eV (present at the both samples with phtalocyanine) can be attributed to the grafted MnS-Pc molecules. The immersing of the modified diamond samples in a solution of MnS-Pc leads to a chemisorption on the diamond surface. As a result the formation of complexes between the NCD surface and the phtalocyanines ($C_{diamond}$-N-Mn or $C_{diamond}$-O-Mn units) and the release of an apical chlorido ligand can be supposed. Furthermore, because of contamination in the modification chamber, peaks between 168 and 169 eV after the NH_3 treatment are observed (the green line in figure 7.15).
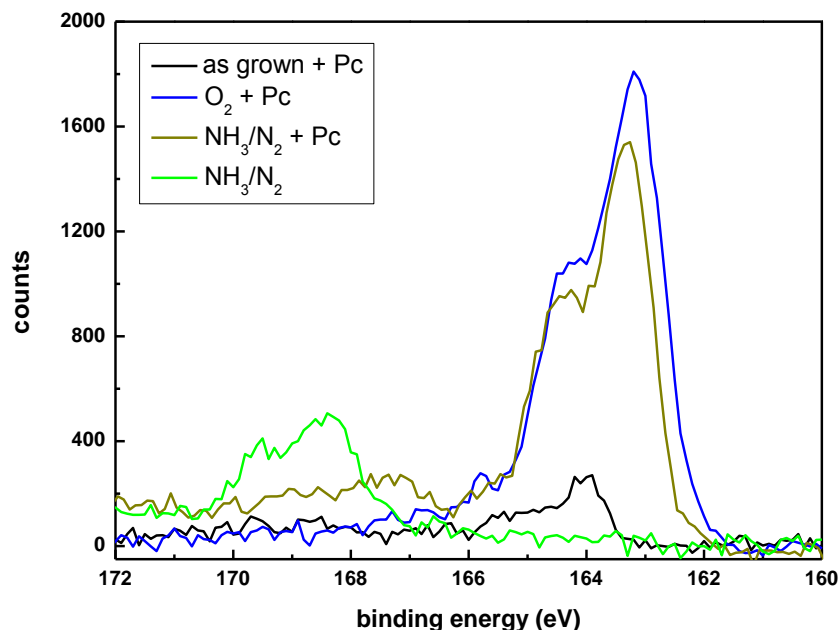
Figure 7.15 *S2p core spectra of as-grown and plasma modified NCD surfaces without and with Mn-Pc as determined by XPS*

In a second series of experiments, NCD samples have been modified in an oxygen plasma for 5 minutes at 200 W. Afterwards three different Pc molecules have been grafted on the NCD surface, as-grown and O-terminated: Mn-Pc ($C_{80}H_{96}ClMnN_8O_{16}$), Cu-Pc ($C_{80}H_{96}CuN_8O_{16}$), Ti-Pc ($C_{128}H_{208}N_8OS_8Ti$) and the surface composition is presented on the figure 7.16. The carbon content, which is in the range of 98-99 at% for as-grown and 89-91 at% for oxygen-terminated samples, is deliberately not presented, because of unimportance of the information with regard to the immobilization process.

The diamond samples after growth possess also in this case relatively clean surface with no contamination with undesirable elements. As a result of grafting the Pc molecules on the as-grown surface all three metals were detected - Ti and Cu in similar concentrations on the order of 0.02 – 0.06 at%, Mn with a much higher content (0.26 at%).

All three phthalocyanines contain eight nitrogen atoms per each metal atom. Since the as-grown NCD surface is free of nitrogen, any nitrogen detected after the functionalization should be due to the grafted Pc molecules. This was indeed the case for all exposed samples for which N concentrations up to 0.47 at% were registered. The

nitrogen content was eight times the metal concentration, e.g. for Ti-Pc on as-grown NCD and for Cu-Pc on O-terminated NCD. In the other cases there were discrepancies, which are most pronounced for Mn-Pc [147].
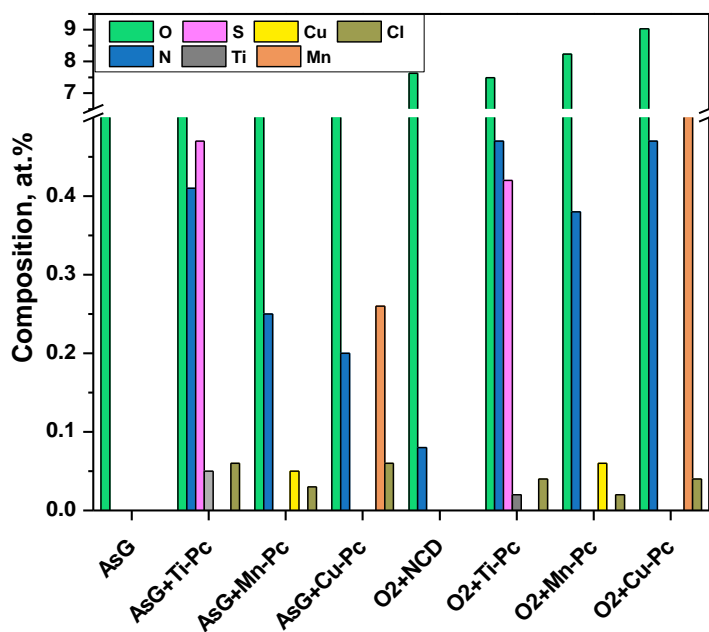
Figure 7.16 *Surface composition of as-grown and oxygen-terminated NCD surfaces before and after grafting of different Pc molecules*

The oxygen concentration increased after the grafting of Cu-Pc and Mn-Pc due to the presence of 16 oxygen atoms in each molecule. No increase is observed for the Ti-Pc which contains only 1 O atom.

Traces of sulfur were detected only in the sample grafted with Ti-Pc with concentrations close to those of N which has to be expected having in mind the composition of Ti-Pc. These results prove that the side chains of the phthalocyanine molecules were still present after grafting.

Chlorine contamination with content of up to 0.06 at.% was observed in all samples and can be attributed to the dichloromethane used as a solvent of the Pcs and for the final cleaning after grafting.

After the oxygen plasma modification an increase of the oxygen concentration was observed to 7.63 at% and it increased even further up to 9.03 at%, depending on the

immobilized Pc-molecule. This is can be explained with the presence of O with higher content in the Mn-Pc ($C_{80}H_{96}ClMnN_8O_{16}$) in contrast to Ti-Pc ($C_{128}H_{208}N_8OS_8Ti$). The values are similar to the previous obtained after the grafting of the manganese phtalocyanine complex (MnS-Pc), shown on figure 7.12. The low content of nitrogen (between 0.38 at% and 0.47 at%) in all three samples is due to the nitrogen from the grafted Pc molecules. As already presented earlier, the oxygen terminated diamond surface without immobilized molecules has no nitrogen contamination. More important, traces of copper, manganese or titanium are detected only on the samples grafted with the corresponding Pc. The contents of titanium, sulfur and nitrogen, detected by the XPS measurements, are in the ratio 1:8:8, which corresponds to the element concentration in the Pc molecule $C_{128}H_{208}N_8OS_8Ti$. A ratio 1:8 is determined between Cu and N for the sample Cu-Pc. The sample with Mn-Pc has the highest content of nitrogen and also traces of manganese (ca. 0.62 at%) are detected.

Summarizing the results of the surface composition, it can be stated that all three phthalocyanines have attached to the as-grown and O-terminated NCD surfaces. The content of Mn was much higher than that expected with respect to the detected N and O concentrations. A possible reason could be a partial decomposition of the Pc macrocycle and release of oxidized manganese. The large difference in the Mn content between as-grown and O-terminated NCD may be a hint that a possible Pc decomposition is enhanced by the O-terminated surface. As a result, manganese-oxygen species should be detected on the surface. It can be assumed that the peripheral ester group of Cu- and Mn-Pc interact with the O-terminated surface. They provide a better binding of the Pc molecules to the surface. In contrast, the titanium content is remarkably low on the O-terminated NCD.

The O1s core level spectra of the samples (as-grown and grafted with the 3 Pc molecules) are illustrated on figure 7.17. The spectra taken from the as-grown NCD surfaces are much more complex than those from the O-terminated surfaces. This is due to the fact that the oxygen content of the as-grown samples is rather low, thus, additional features from the grafted Pc molecules are far better discernable. More interesting are the spectra after grafting of Mn-Pc and Cu-Pc. These phthalocyanines contain 16 oxygen atoms each on exactly the same positions and with the same bonding configuration.
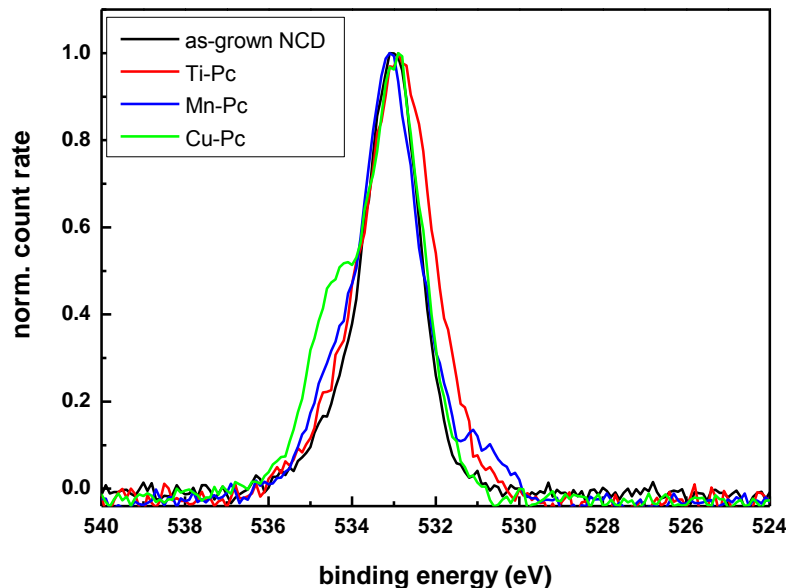
Figure 7.17 *O1s core spectra of as-grown NCD surfaces with different Pc molecules determined by XPS*

From figure 7.17 it can be seen that the spectra of Mn-Pc and Cu-Pc clearly show a substantial sub-peak on the high binding energy side of the main sub-peak. In addition, the Mn-Pc possesses also a clearly discernable sub-peak on the low energy side with, however, with a substantially lower intensity. The binding energies are 533.0 eV for the main peak, 534.5 eV for the higher energy sub-peak, and ca. 530.5 eV for the small lower energy sub-peak. The main peak can be assigned to the standard oxygen contamination of our NCD films after deposition and the oxygen atoms from the periphery ester groups of the Pcs. These ester groups are very hygroscopic and thus an intrinsic water source. Possible hydrogen bonds between the ester groups from the Pc molecules and the oxygen from the NCD surface may cause a slightly higher peak energy. Consequently, the peak is observed for both Cu- and Mn-Pc which bear periphery ester groups, but not for Ti-Pc. The low energy sub-peak is only observed for Mn-Pc and it can be assumed that the signal originates from MnO_2 impurities.

Figure 7.18 shows the O1s core level spectra of the samples after oxygen modification. The spectrum of the NCD sample after O_2 plasma modification is narrow while the spectra of the Pc grafted samples are broadened indicating the surface changes

appearing after grafting. The intense signal at 533 eV can be attributed to carbon double bond with oxygen (C=O) [148].
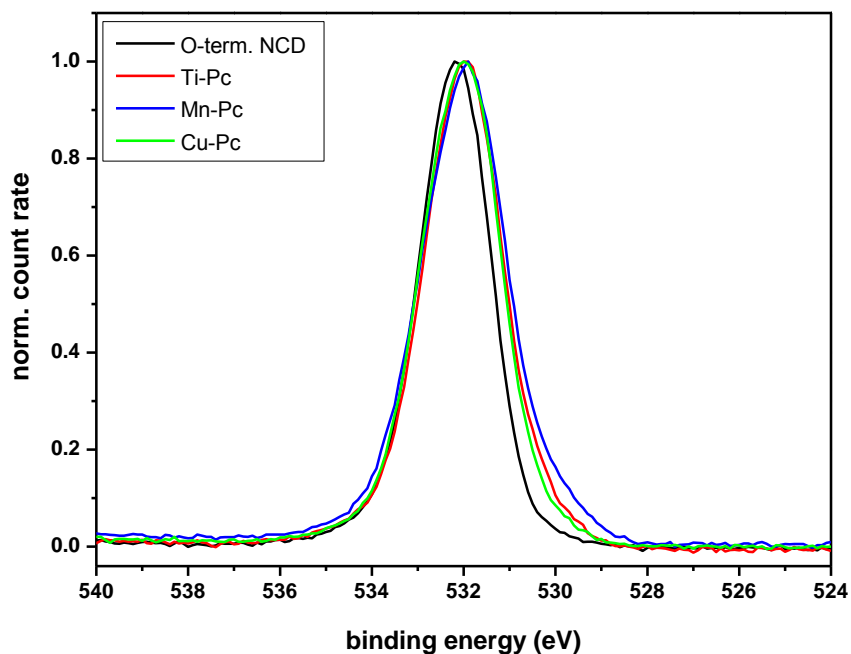
Figure 7.18 *O1s core spectra of NCD surfaces after O2 plasma modification with different Pc molecules as determined by XPS*

Seredych et al. reported that the peaks at 531 eV, 532 eV, and 535 eV originate from C=O groups, C–O–C groups, C–OH groups and chemisorbed oxygen [149]. The interaction with Ti-Pc leads to a broadening of the peak toward lower binding energies. The reason for that is probably the coordinate bond between the oxygen atom and the central metal atom. The signal between 534 eV and 535 eV in O1s peak of the Cu-Pc can be ascribed to the bonds with copper atom. Schmidt and coworkers reported that signals at around 534 eV appear due to the presence of tetra carboxylic di-anhydride/copper ($C_{24}H_8O_6$/Cu) [150].

The N1s spectra of the as-grown NCD samples before and after functionalization with Pc are shown in figure 7.19. They are shifted along the y-axis for clarity. The sample without photosensitive molecules shows no signal attributed to nitrogen, which indicates that the diamond surface have no contaminations. In all cases of phthalocyanine exposure there is a nitrogen peak discernable. This is a clear evedance of attachment of the Pc molecules to the NCD surface.
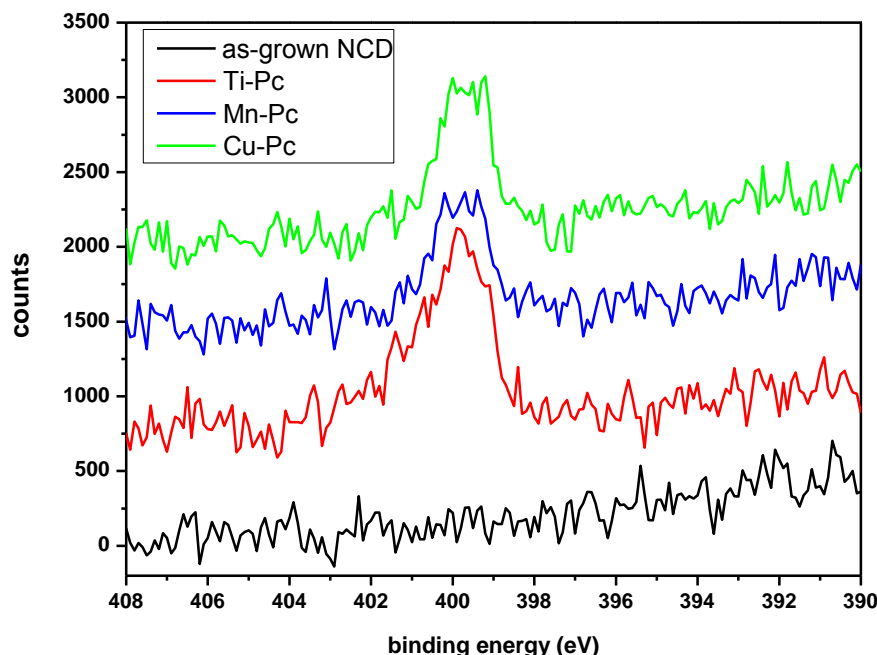
Figure 7.19 *N1s core spectra of as-grown NCD surfaces with different Pc molecules as determined by XPS*

As the number of nitrogen atoms is eight for all three phthalocyanines a rough estimation about the number of the attached molecules can be made from the peak intensities. The N1s peaks possess roughly the same heights, although that for Ti-Pc on as-grown NCD is a little bit higher, suggesting a better attachment. Furthermore, all peaks are rather broad and a closer observation reveals that they may well consist of two contributions with almost equal strength. The phthalocyanine macrocycle bears two types of nitrogen atoms: four in the outer ring system, four in the inner ring.

The successfully anchoring of Pc molecules on NCD changes the electronic structure of the nitrogen atoms, thus providing a recognizable energy shift. Based on literature data, we suggest that the feature at ca. 399.8 eV originates from the outer nitrogen atoms (–N=), whereas the feature at lower energies depends on the metal-coordinating nitrogen atoms (–N–M, ca. 398 eV) [151]

N1s core level of the oxygen terminated NCD surface clearly shows the presence of nitrogen in the spectra of all three samples grafted with phthalocyanines (figure 7.20). The broad signal between 399 eV and 400 eV arises from the nitrogen atoms in the Pc molecules.
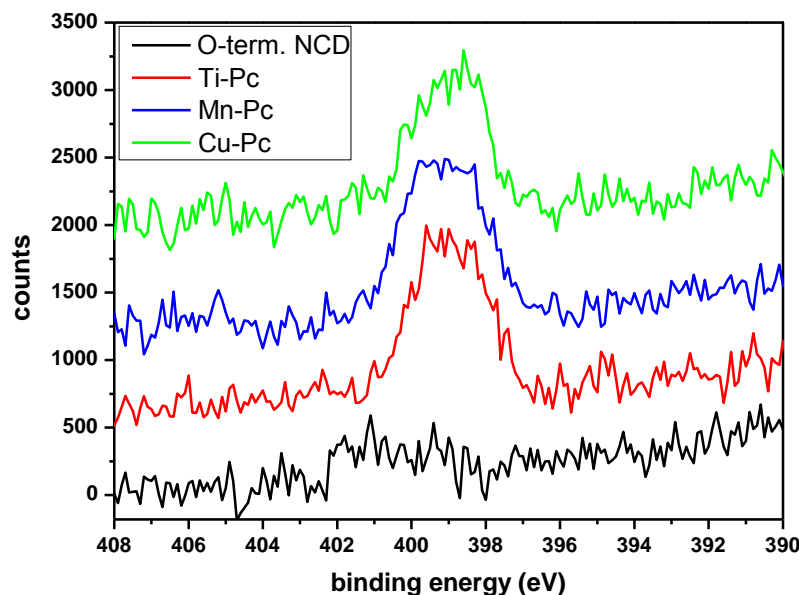
Figure 7.20 *N1s core spectra of NCD surfaces after O_2 plasma modification with different Pc molecules as determined by XPS*

The S2p spectra of all as-grown and grafted samples are presented in figure 7.21. A clear peak can be observed only for the NCD surfaces exposed to Ti-Pc, in agreement with figure 7.16 and also with the composition of the molecules shown in figures 7.1-7.4.

The peak at 164.4 eV dominates the spectrum of the as-grown NCD and can be assigned to neutral sulfur stemming from the thioether groups in the Ti-Pc molecule. A weak double peak at 166/167 eV which is due to oxidized sulfur from some contaminations can be observed on the high binding energy side of the main peak in both spectra.
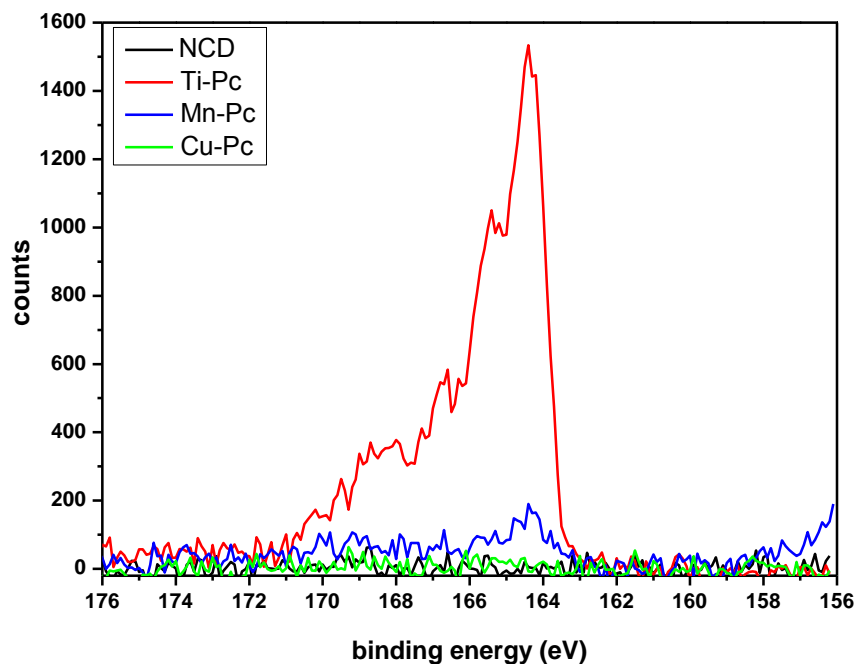
Figure 7.21 *S2p core spectra of as-grown NCD surfaces with different Pc molecules as determined by XPS*

Figure 7.22 presents the S2p core level spectra of four samples: one after O_2 plasma modification and other three oxygen terminated samples grafted with different Pc molecules. The broad signal between 163 eV and 167 eV in the spectrum of the sample exposed to Ti-Pc is attributed to the grafted photosensitive molecules on the diamond surface. This Pc is the only one from the tested in this series, which contains sulfur. As a result of its grafting on O-terminated NCD surface a S2p doublet is observed like in the case of MnS-Pc from the first series (figure 7.12).
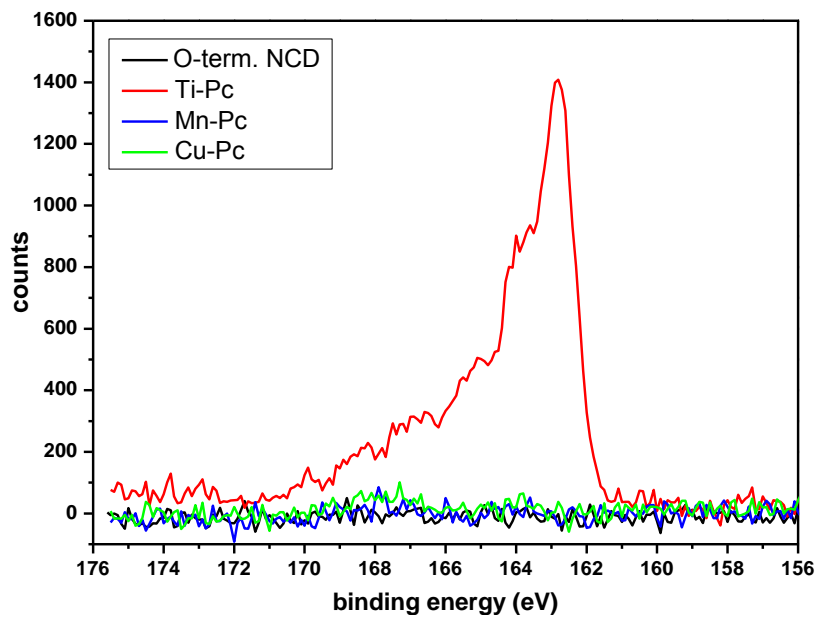
Figure 7.22 *S2p core spectra of NCD surfaces after O$_2$ plasma modification with different Pc molecules as determined by XPS*

8. Photoelectrochemical measurements

The diamond samples grafted with all four different phthalocyanines were further subjected to photo electrochemical measurements. The aim was to investigate the response to illumination with light wavelength near to the absorption maximum of the Pc molecules. All experiments were performed at the Institute of Electron Devices and Circuits, University of Ulm under the supervision of Dr. Alberto Pasquarelli.

Diamond electrodes were prepared as follows: the sample with size 1x1 cm was glued to a copper plate by means of silver paste to provide good electrical contact between the conductive BDD layer and the plate. The as-prepared BDD electrode was tightly encapsulated in teflon tape with a hole with diameter of 3 mm, determining the working area for the electrode (figure 8.1 on the left).
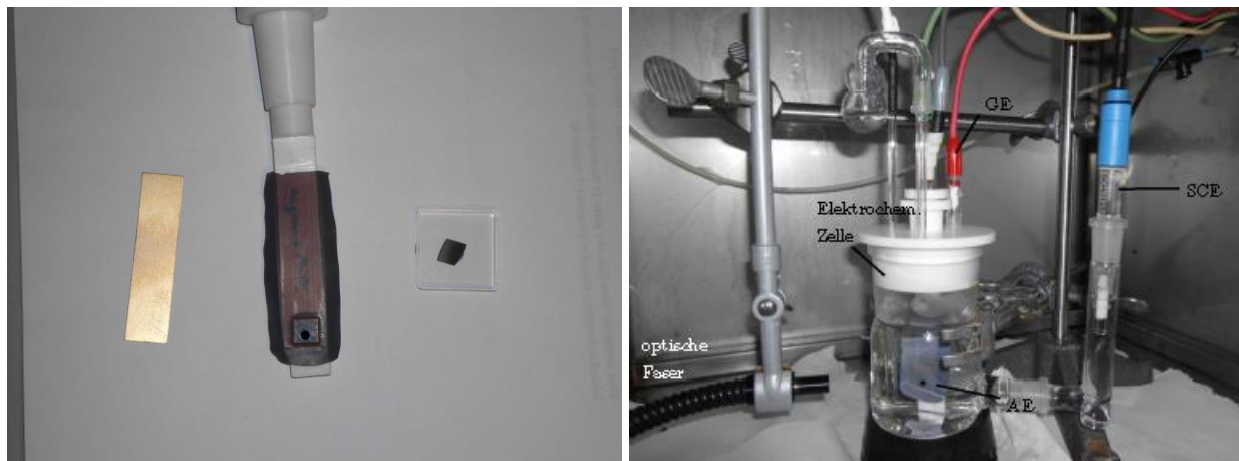
Figure 8.1 *Photos of an assembled BDD electrode (left) and the three-electrode glass cell (right)*

Two different light sources were used: a xenon lamp and a light emitted diode (LED). Further test has revealed that the LED lamp from OSA Opto Light with a wavelength of 770 nm was more appropriate light source. The irradiation wavelength of this LED is close to the absorption maxima of the phtalocyanines. The position of the copper plated diode was settled 2 mm apart from the working diamond electrode at the same altitude as the BDD working area. Both copper plates were provided with wires for electrical contacts and positioned into a teflon holder. The complete assembly was introduced into the electrochemical cell.

All photoelectrochemical measurements were performed in three-electrode glass cell controlled by a potentiostat (Princeton Applied Research PARSTAT 2273). The three-electrode cell contains: BDD electrode as a working electrode, Pt counter electrode and Ag/AgCl reference electrode. The measurements were performed in a dark Faraday cage in order to eliminate the influence of environment light (figure 8.1 right). Phosphate buffered saline (PBS) with pH = 7.4, 1 mM $Ru(NH_3)_6Cl_3$ in 0.1 M KCl or 1 mM $K_4Fe(CN)_6$ in 0.1 M KCl were used as electrolytes. The characteristics of the electrodes were determined by cyclic voltammetry and open circuit potential measurements in dark and under illumination at ambient temperature.

8.1 Cyclic voltammetry measurements

Cyclic voltammetry is a standard electrochemical method for investigation of the adsorption processes or charge transfers on the electrodes. All voltammetry measurements were performed in aqueous electrolytes with the purpose to investigate the electrochemical behaviors of the boron doped diamond electrodes with different surface modifications and grafted with Pc molecules: potential window, background current and oxygen/hydrogen evolution reactions. Several scans with the electrodes in PBS were performed at the beginning of the investigations in order to reach a steady state. All measurements were performed with a scan rate of 50 mV/s. A typical cyclic voltammetry curve of an oxygen terminated diamond electrode in PBS solution is shown on figure 8.2. A wide potential window of ca. 3 V between the hydrogen and oxygen evolution reactions is clearly visible on the graph confirming the literature data [152]. The metal electrodes mostly used in the industry, like Pt, possess an electrochemical window of approximately 1.2-1.5 V width. The observed peak on figure 8.2 prior to the onset of the hydrogen evolution occurs due to surface phenomena like adsorption or desorption of accumulated ions. This occurrence is typical for the BDD electrodes in both hydrogen and oxygen evolution region. The repeated cycles showed no difference in the voltagramms, i.e. the electrode has reached a steady state.
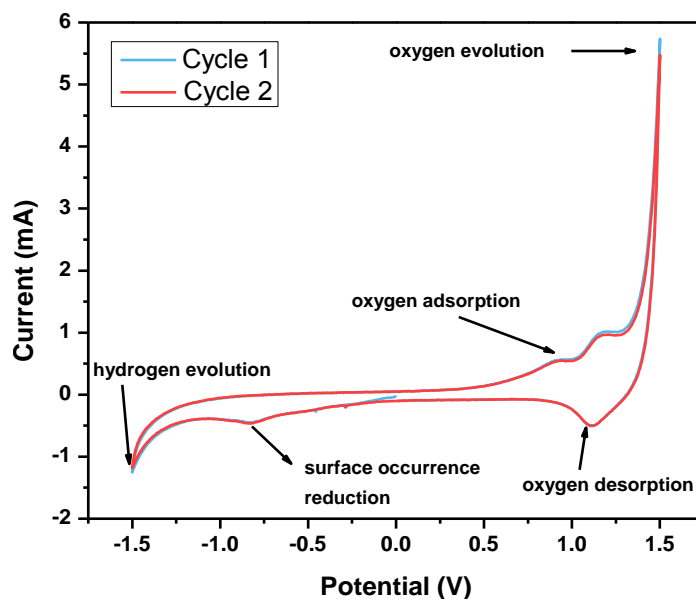
Figure 8.2 *Cyclic voltammogram of oxygen terminated BDD film with MnS-Pc*

The diamond electrodes were further investigated with respect to the response to illumination. The as-grown and plasma modified samples with different surface terminations without or with MnS-Pc were studied. The recorded cyclic voltammograms of the tested electrodes with and without illumination are presented on figure 8.3.

The as-grown sample possesses the narrowest curve on figure 8.3. The hydrogen evolution region was very small with a slightly defined peak of the curve recorded in dark. In the region of the oxygen evolution reaction the curves in dark and with light were nearly identical. The voltammograms of the amino terminated BDD film were overlapped and only a small broadening for the sample without light in the hydrogen evolution region was detected. The oxygen terminated electrodes showed an extended oxygen evolution region due to the surface termination and additional oxidation of the sample. The major difference could be observed in the hydrogen evolution region of the same sample, namely its resulting in substantial extension for the sample measured in dark.
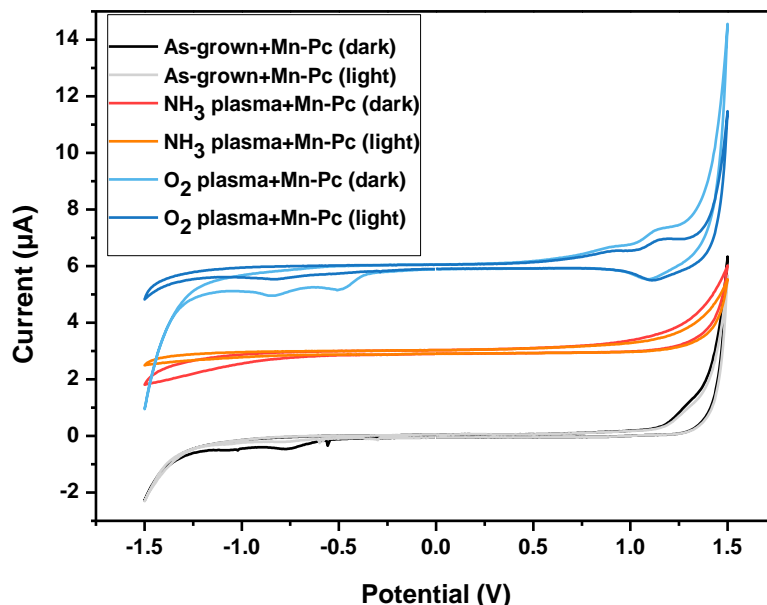
Figure 8.3 *Cyclic voltammograms of diamond electrodes with different surface terminations (grafted with [MnClPc(S(n-C$_{12}$H$_{25}$))$_8$])*

The stability of the semiconductor BDD films /electrodes/ is a critical issue. The surface modification, i.e. the existing surface bonds, determines both the sensing ability and the electron transfer sites (electronic surface state distribution). Hydrogen- and oxygen-termination are commonly used for the manufacturing of electrochemical electrodes [153] and for ion-sensitive field-effect transistors (ISFETs) [154]. However, high anodic overpotential can convert the H-terminated surface to an O-terminated one [155]. Oxygen termination is the more stable one and cannot be affected by overpotential, oxidizing media or anodic polarization [156]. Carbon-oxygen surface bonds (C–O–C bridges, C–O ketone, C–OH hydroxyl groups, CO–O–CO polycarbonate groups) determines the pH sensitivity of O-terminated diamond in electrolytes [157].

The stability of the electrodes was studied after several cycles of measurements. The results of amino terminated sample with and without illumination with the LED are presented on figure 8.4. After the first switching ON/ OFF of the light source the steady state of the electrode was reached and only marginal difference in the curves could be observed both in darkness and under illumination.
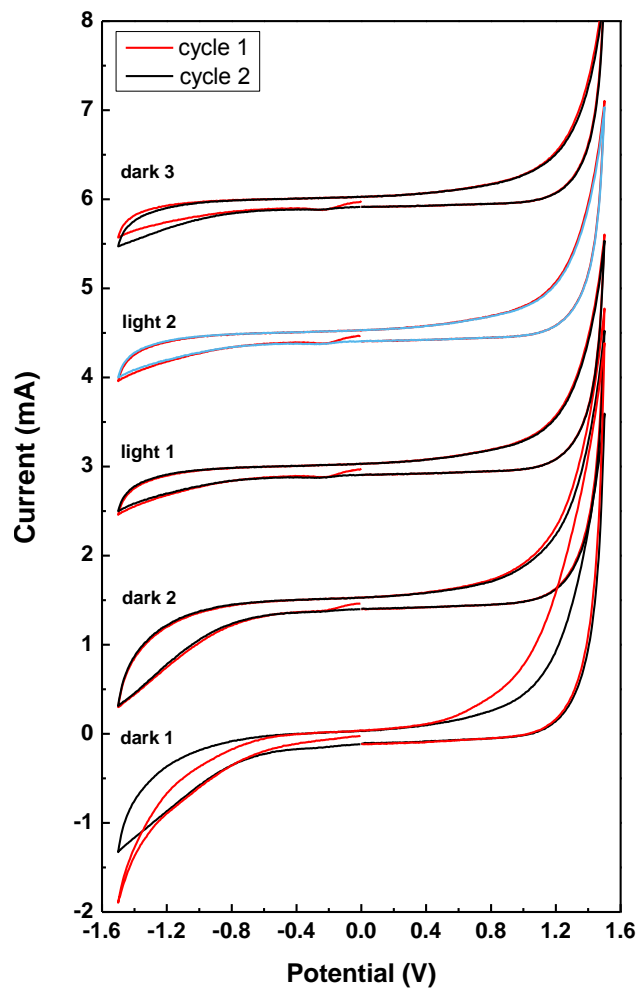
Figure 8.4 *Cyclic voltammograms of diamond electrodes with amino-termination and grafted with [MnClPc(S(n-C$_{12}$H$_{25}$))$_8$] after several light/dark cycles*

8.2 Open circuit potential of diamond electrodes

The open circuit potential (OCP) represents the potential of the working diamond electrode versus the reference electrode. The photoresponse of the working electrode was investigated without applying any potential or current to the cell. To measure the OCP characteristics a potentiostat with a voltmeter with a high internal resistance was

used. In addition to the effect of the light on the current and potential, also the influence of the different electrolytes was studied

An amino-terminated sample grafted with MnS-Pc will be shown as an example. It was immersed in PBS and left in the glass cell for 15 minutes to reach a saturation level before the OCP measurements. The OCP investigations were conducted after the voltammogram cycles to ensure the establishment of an equilibrium (figure 8.5). The sample was measured for about 2000 s switching on/off the light source manually for 100 seconds at the beginning and later illuminated for a longer period.

A swift raise of the photocurrent directly after applying the illumination was observed (figure 8.5). The peak to valley distance in the recorded curves for the amino terminated sample corresponded to a photocurrent value of about 1.1 nA. The value was negative due to the p-type conductivity of the boron-doped diamond film, as reported in literature [158]. The generated photopotential measured straight after switching on the light showed a value of 0.03 V. It should be mentioned that the slopes of the curves were quite different: the curves were much steeper before the illumination as after that. This is most probably due to the longer time for relaxation in comparison to the excitation one.
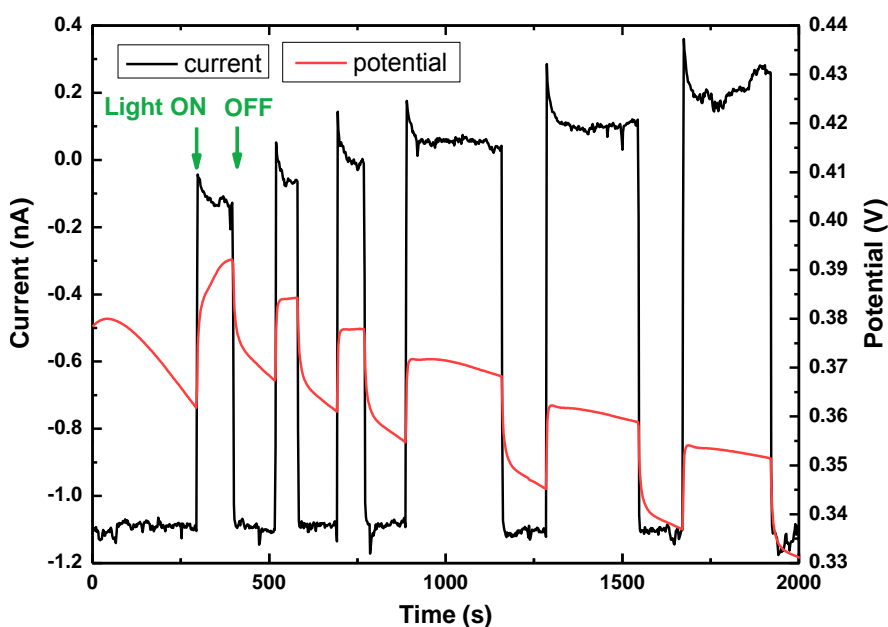
Figure 8.5 *Photocurrent and photopotential of NH$_2$-terminated diamond electrode grafted with MnS-Pc under illumination with 770 nm wavelength*

The influence of the electrolyte on the photocurrent was also studied. Figure 8.6 shows the results for two electrolytes - phosphate buffered saline (pH 7.4) and $K_4[Fe(CN)_6]$. The photocurrent was higher when freshly prepared PBS solution was used and the difference between a fresh and used PBS was more than two orders of magnitude, 0.002 µA vs. 0.26 µA, respectively as seen from figure 8.6. The highest values of the photocurrent were measured using $K_4[Fe(CN)_6]$ as electrolyte (1.97 µA).
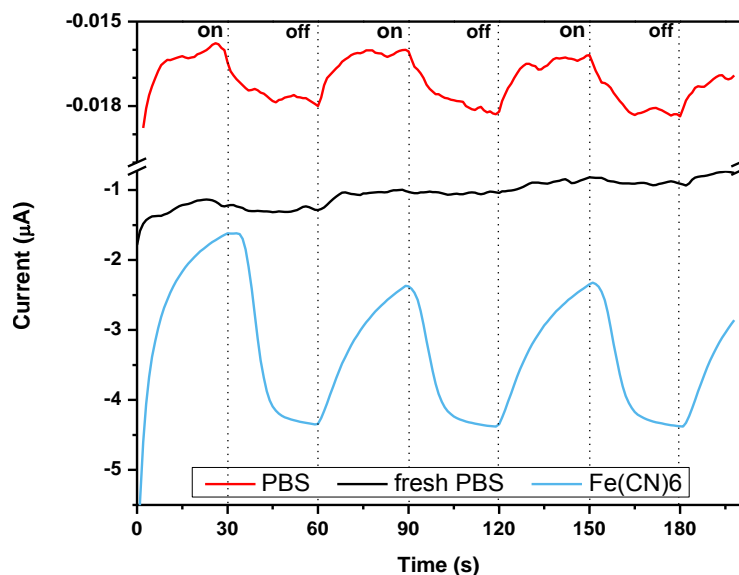
Figure 8.6 *Compararision between the chronoamperometric measurements of NH₂-terminated diamond electrode grafted with Mn-Pc different electrolytes*

These initial results confirmed the importance of the electrolyte selection to obtain high photocurrent values. Our observation showed that further investigations will be needed in order to find the most suitable electrolyte.

Figure 8.7 represents a hypothesis regarding the processes taking place in the (photo) electrochemical cell with BDD electrode sensitized wit Pc. The light causes the excitation of electrons from the dye (Pc) followed by electron transition from the dye into the electrolyte. The vacancy in the dye migrates as a hole in the depletion region of the semiconductor (BDD), whereby the dye returns to its ground state. The holes as charge carriers in the semiconductor contribute to a current flow. The ejected into the electrolyte

electrons are emitted to the counter electrode. As a result, the electrolyte also returns to the initial state. The information obtained during our initial investigations has led to the proposed photogeneration and the charge-transfer mechanisms. Additional investigations regarding the electron affinity, the band bending of NH$_2$-terminated diamond and the position of the energy levels of Mn-Pc respectively of the valence band of diamond are needed.
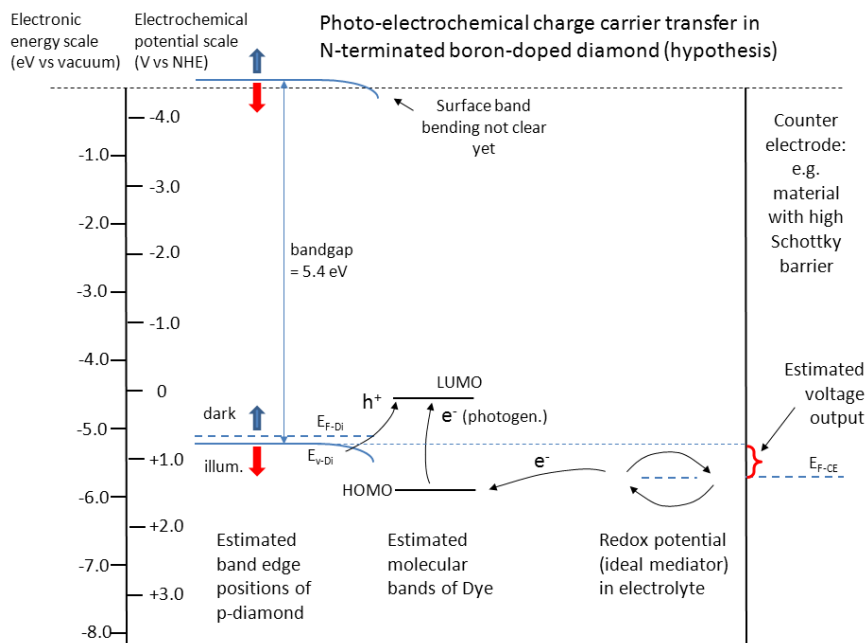
Figure 8.7 *Hypothetical photoelectrochemical charge transfer in NH$_2$-terminated boron doped NCD grafted with MnS-Pc*

9. Summary

The purpose of the present work is to investigate the topography, morphology and the surface properties of nanocrystalline diamond films.

The goal is to characterize various diamond films: undoped and boron doped with a number of techniques like atomic force microscope (AFM), scanning electron microscope (SEM), X-Ray photoelectron spectroscopy (XPS), Raman spectroscopy, cyclic voltammetry and Open Circuit Potential (OCP) technique.

Thus, the first three chapters of the thesis are theoretical and they consider the methods of the diamond films preparation, the diamond growth mechanism, and the basic diamond films properties in relation to the surface modification.

The forth chapter presents the experimental diamond growth process. The starting carburization process is thoroughly studied. The process conditions are optimized using recipes with different diamond powder mixture and pretreatment time to achieve different nucleation density and vary the deposition parameters: growth temperature, filament current and substrate voltage.

All samples are investigated straight after nucleation and after the growth process with AFM to define the nucleation density, the topography and the surface roughness of samples. The dependence between the surface roughness and crystalyte height as a function of the deposition time is determined from SEM and AFM measurements. The most appropriate parameters: pretreatment recipe and growth rate have been selected for the purpose of further experimental work.

In the fifth chapter the results from the diamond surface modification and termination are summarized. The hydrogen atoms on the surface are substituted with oxygen atoms from oxygen plasma asher and by photo modification with UV-lamp. Plasma discharge power and modification time are varied in order to find the optimal process parameters. Diamond samples surface were aminated via NH_3/N_2 plasma. The surface of the NCD layers is more hydrophilic and can easier graft molecules.

The successful modification of the diamond surface of the as grown and the freshly modified samples is proven from measured contact angles values and the change of the surface behavior from hydrophobic to hydrophilic of the treated samples.

Summary

In the chapter 6 are presented experiments focused on surface composition of as grown and modified samples investigated with XPS instrument at the University of Kaiserslautern. Core spectra has been shown as a proof of the successful surface termination. Four different photosensitive molecules (Phtalocyanines) were synthesized in the group of professor Siemeling at the University of Kassel, grafted on the NCD-films was also proved with the XPS core spectra. Diamond samples grafted with phtalocyanine were submerged to Raman investigation. Two different wavelengths has been applied and Pc fingerprint has been obtained to confirm the successful grafting of Pc. The increased oxygen, nitrogen, sulfur, manganese, cupper or titanium content in the samples can be explained with the presence of the phtalocyanine molecule.

In the last chapter the results from the photoelectrochemical measurements of diamond electrodes conducted at the University of Ulm under the supervision of Dr. Alberto Pasquarelli are described. Two different light sources: Xenon lamp and light emitted diode are used as an illumination source. The LED lamp proved to be more appropriate due to the irradiation wavelength which is close to the Pc absorption maxima. Cyclic voltammetry measurements have shown both oxygen and hydrogen evolution. Samples remain stable after several cycle of switching on and off of the light source. The open circuit potential (OCP) have shown a quick response of the electrode to the illumination resulting in photo current registration. The influence of the electrolyte on the photo current has been studied.

Bibliography

[1]   R. Robertson, J. Fox, A. Martin, "Two types of diamond," *Philosophical Transactions of the Royal Society A,* vol. 232, p. 463, 1934.

[2]   R. Robertson, J. Fox, A. Martin, "Further work on two types of diamond," *Proceedings of the Royal Society A,* vol. 157, p. 579, 1936.

[3]   C. Breeding, J. Shigley, "The 'type' classification system of diamonds and its importance in gemology," *Gems & Gemology,* vol. 45, p. 96, 2009.

[4]   W. Kaiser, W. Bond, "Nitrogen, A Major Impurity in Common Type I Diamond," *Physycal Review,* vol. 115, p. 857, 1959.

[5]   P. Nayar, "Luminescence, absorption and scattering of light in diamonds: Part I. Fluorescence," *Proceedings of the Indian Academy of Science, Series A,* vol. 14, p. 483, 1941.

[6]   P. Nayar, "Luminescence, absorption and scattering of light in diamonds: Part III. Absorption," *Proceedings of the Indian Academy of Science, Series A,* vol. 14, p. 1, 1941.

[7]   C. Raman, "The nature and origin of the luminescence of diamond," *Proceedings of the Indian Academy of Science, Series A,* vol. 19, p. 199, 1944.

[8]   W. Kaiser, W. Bond, "Nitrogen, A Major Impurity in Common Type I Diamond," *Physal Review,* vol. 115, p. 857, 1959.

[9]   C. Breeding, J. Shigley, "The 'type' classification system of diamonds and its importance in gemology," *Gems & Gemology,* vol. 45, p. 96, 2009.

[10]   H. Dyer, F. Raal, L. Du Preez, J. Loubser, "Optical absorption features associated with paramagnetic nitrogen in diamond," *Philosophical Magazine ,* vol. 11, p. 763, 1965.

[11]   J. Custers, "Unusual phosphorescence of a diamond," *Physica,* vol. 18, p. 489, 1952.

[12]   J. Custerc, "Type IIb diamonds," *Physica,* vol. 20, p. 183, 1954.

[13]   R. Wentorf Jr.,H. Bovenkirk, "Preparation of semiconducting diamond," *Journal of Chemical Physics,* vol. 36, p. 1987, 1962.

[14]   [Online]. Available: http://dao.mit.edu/8.231/CarbonPhaseDia.html. [Accessed 3 2015].

[15] O. I. Leipunskii, *Usp. Khim.,* vol. 8, p. 1520, 1939.

[16] R. D. Vies, "Synthesis of diamond under metastable conditions," *Annual Review of Materials Research,* vol. 17, p. 161, 1987.

[17] A. Malave, "Sensoren für die Rastersondemikroskopie auf Basis von polykristallinem Diamant”," *PhD thesis, University of Kassel ,* 2003.

[18] T. Huang, W. Tang, F. Lu, J. Gracio, N. Ali, "Argon to hydrogen ratio in plasma jet chemical vapor," *Surface and Coating Technology,* vol. 190, p. 48, 2005.

[19] J.W. Zimmer, G. Ghandler, T. Sharda, "Wide area deposition and stress control by sp3 hot filament CVD reactor," *Thin Solid Films,* vol. 516, p. 696, 2008.

[20] J. Butler, R. Woodin, "Thin film diamond growth mechanisms," in *Thin film diamond ,* Springer, 1994, p. 209.

[21] M. Amaral, A. Fernandes, M. Vil, F. Oliveira, R. Silva, "Growth rate improvements in the hot-filament CVD deposition of nanocrystalline diamond," *Diamond and Related Materials,* vol. 15, p. 1822, 2006.

[22] M. Dipalo, "Nanocrystalline Diamond Growth and Device Applications," *PhD thesis, Ulm University,* 2008.

[23] M. Kamo, Y. Sato., S. Matsumoto, N. Setaka, "Diamond synthesis from gas phase in microwave plasma," *Journal of Crystal Growth,* vol. 62, p. 642, 1983.

[24] P. May, "Diamond thin films: a 21st-century material," *Philosophical Transactions of the Royal Society A,* vol. 358, p. 473, 2000.

[25] M. Hiramatsu, M. Hori, , Carbon Nanowalls, Synthesis and Emerging Applications, Springer, 2010.

[26] P. Bachmann, W. Drawl, D. Knight, R. Weimer, R. Messier, G. Johnson, A. Badzian, M. Geis, "Diamond and diamond-like materials synthesis," *MRS Symposium Proceedings, Materials Research Society,* vol. 15, p. 99, 1988.

[27] G. Goodwin, J. E. Butler, Handbook of industrial diamonds and diamond films, Marcel Dekker INC, edited by M. Prelas, G. Popovici, L. K. Bigelow, 1997.

[28] P. Bachmann, H. Hagemann, H. Lade, D. Leers, F. Picht, D. Weichert, H. Wilson, "Diamond chemical vapor deposition: gas compositon and film properties," *Diamond, SiC and Nitride Wide Bandgap Semiconductors,* p. 267, 1994.

[29] P. John, D. Milne, W. Vijayarajah, M. Jubber, J. Wilson, "The growth of (100) oriented diamond films," *Diamond and Related Materials,* vol. 4, p. 388, 1994.

[30] M. McMaster, W. Hsu, M. Coltrin, D. Dandy, J. Wilson, "Dependence of the gas composition in a microwave plasma-assisted diamond chemical vapor deposition reactor on the inlet carbon source: CH4 versus C2H2," *Diamond and Related Materials,* vol. 4, p. 1000, 1995.

[31] G. Pastor-Moreno, "Electrochemical Applications of CVD Diamond," *PhD Thesis, University of Bristol,* 2002.

[32] B. Derjaguin, D. Fedoseev, "The synthesis of diamond at low pressures," *Scientific American ,* vol. 233, p. 102, 1975.

[33] M. Frenklach, R. Kematick, D. Huang, W. Howard, K. E. Spear, A. Phelps, R. Koba, "Homogeneous nucleation of diamond powder in the gas phase," *Journal of Applied Physics,* vol. 66, p. 395, 1989.

[34] D. Fedoseev, V. Vamin, B. Deryagin, "D. Fedoseev, V. Vamin, B. Deryagin:"Synthesis of Diamond in Its Thermodynamic Metastability Region," *Russian Chemical Reviews,* vol. 53, p. 435, 1984.

[35] S. Matsumoto, Y. Matsui, "Electron microscopic observation of diamond particles grown from the vapour phase," *Journal of Materials Science,* vol. 1785, p. 18, 1983.

[36] [Online].   Available: http://www.just.edu.jo/~aobeidat/PDF/research/Nucleation/Diamond_Nucleation.pdf. [Accessed 4 2015].

[37] S. Godleski, P. Schleyer, E. Osawa, W. Wipke, "The Systematic Prediction of the Most Stable Neutral Hydrocarbon Isomer," *Progress in Physical Organic Chemistry,* vol. 13, p. 63, 1981.

[38] S. Stein, "Diamond and graphite precursors," *Nature,* vol. 346, p. 517, 1990.

[39] B. Lux, R. Haubner, in *Diamond and Diamond-like Films and Coatings*, New York, Plenum Press, edited by R. Clausing, L. Horton, J. Angus, P. Koidl, 1991, p. 579.

[40] M. Schreck, "Heteroepitaxial Growth," in *CVD diamond for electronic devices and sensors*, John Wiley & Sons, Ltd, 2009, p. 125.

[41] R. Haubner, A. Lindlbauer, B. Lux, "Diamond nucleation and growth on refractory metals using microwave plasma deposition," *International Journal of Refractory Metals and Hard Materials,* vol. 14, p. 119, 1996.

[42] J. Yang, X. Su, Q. Chen, Z.Lin, "Si implantation: A pretreatment method for diamond nucleation on a Si wafer," *Applied Physics Letters,* vol. 24, p. 3284, 1995.

[43] J. Yang, Z. Lin, L. Wang, S. Jin, Z. Zhang, "Structural study of diamond film formed on silicon wafer by hot-filament chemical vapor deposition method," *Applied Physics Letters,* vol. 65, p. 3203, 1994.

[44] O. Williams, O. Douhéret, M. Daenen, K. Haenen, E. Osawa, M. Takahashi, "Enhanced diamond nucleation on monodispersed nanocrystalline diamond," *Chemical Physics ,* vol. 445, p. 255, 2007.

[45] C. Chang, Y. Liao, G. Wang, Y. Ma, R. Fang, "CVD Diamond Growth," in *Crystal Growth Technology*, Springer, 2003, p. 93.

[46] V. Srikanth, X. Jiang, "Synthesis of diamond films," in *Synthetic Diamond Films: Preparation, Electrochemistry, Characterization and Applications*, John Wiley and Sons, 2010, p. 21.

[47] S. Yugo, T. Kanai, T. Kimura, T. Muto, "Generation of diamond nuclei by electricfield in plasma chemical vapor deposition," *Applied Physics Letters,* vol. 58, p. 1036, 1991.

[48] B. Stoner, G. Tessmer, D. Dreifuss, "Bias assisted etching of diamond in a conventional chemical vapor deposition reactor," *Applied Physics Letters,* vol. 62, p. 1803, 1993.

[49] X. Jing, C-P. Klages, "Epitaxial diamond thin film on (001) silicon substrates," *Applied Physics Letters,* vol. 62, p. 3438, 1993.

[50] S. Yugo, T. Kimura, T. Kanai, "A new method for the generation of diamond nuclei by plasma CVD," *Diamond and Related Materials,* vol. 2, p. 388, 1992.

[51] E. Vietzke, V. Philipps, K. Flaskamp, P. Koidl, C. Wild, "The reaction of atomic hydrogen with a-C:H and diamond films," *Surface and Coating Technology,* vol. 47, p. 156, 1991.

[52] W.. Zhang, X. Jiang, Y. Xia, "The selective etching with H + ions and its effect on the oriented growth of diamond," *Journal of Applied Physics,* vol. 82, p. 1896, 1997.

[53] [Online]. Available: http://www.britannica.com/EBchecked/topic/387714/Mohs-hardness. [Accessed 12 2014].

[54] F. Knoop, C. Peters, W. Emerson, "A sensitive pyramidal diamond tool for indentation measurements," *Journal of Research of the National Bureau of Standards,* vol. 23, p. 39, 1939.

[55] M. Grrimsditch, A. Ramdas, "Brillouin scattering in diamond," *Physical Review B,* vol. 11, p. 3139, 1975.

[56] M. Quiroz, E. Bandala, "Types of conducting diamond materials and their properties," in *Synthetic Diamond Films: Preparation, Electrochemistry, Characterization and Application*, Willey, 2011, p. 57.

[57] H. Kato, T. Makino, S. Yamasaki, H. Okushi, "n-type diamond growth by phosphorus doping on (0 0 1)-oriented surface," *Journal of Physics D: Applied Physics,* vol. 40, p. 6189, 2007.

[58] S. Koizumi, K.Watanabe, M. Hasegawa and H. Kanda, "Ultraviolet emission from a diamond pn junction," *Science,* vol. 292, p. 1899, 2001.

[59] H. Kato, D. Takeuchi, N. Tokuda, H. Umezawa, S. Yamasaki, H. Okushi, "Electrical activity of doped phosphorus atoms in (001) n-type diamond," *Physica Status Solidi (a),* vol. 205, p. 2195, 2008.

[60] M. Gabrysch, S.Majdi, D. Twitchen, J.Isberg, "Electron and hole drift velocity in chemical vapor deposition diamond," *Journal of Applied Physics,* vol. 109, p. 63719, 2011.

[61] A. Azevedo, M. Baldan, N. Ferreira, "Doping level influence on chemical surface of diamond electrodes," *Journal of Physics and Chemistry of Solids,* vol. 74, p. 599, 2013.

[62] J. Wei, Ch. Li, X. Gao, L. Hei, F. Lvun:, "The influence of boron doping level on quality and stability of diamond film on Ti substrate," *Applied Surface Science,* vol. 258, p. 6909, 2012.

[63] Y.Pleskov, A. Sakkharova, M. Krotova, L. Bouilov, B. Spitsyn, "Photoelectrochemical properties of semiconductor diamond," *Journal of Electroanalytical Chemistry,* vol. 228, p. 19, 1987.

[64] M. Granger, M. Witek, J. Xu, J. Wang, M. Hupert, A. Hanks, M. Koppang, J. Butler, G. Lucazeau, M. Mermoux, J. Strojek, G. Swain, "Standard Electrochemical Behavior of High-Quality, Boron-Doped Polycrystalline Diamond Thin-Film Electrodes," *Analytical Chemistry,* vol. 72, p. 3793, 2000.

[65] M. Krotova, Y. Pleskov, A. Khomich, V. Ralchenko, D. Sovyk, V. Kazakov, "Semiconductor Properties of Nanocrystalline Diamond Electrodes," *Russian Journal of Electrochemistry ,* vol. 50, p. 101, 2014.

[66] C. Pietzka, "Characterization of Oxygen-terminated Diamond Electrodes for Electrochemical Applications," *PhD thesis, Ulm university,* 2011.

[67] C. Hamann, A, Hamnett, W. Vielstich, Electrochemistry, Willey VCH, 2007.

[68] G. Sutherland, D.Blackwell, W. Simeral, "G. Sutherland, D.Blackwell, W. SimeralThe Problem of the Two Types of Diamond," *Nature,* vol. 174, p. 901, 1954.

[69] J. Carlisle, "Diamond films: Precious biosensors," *Nature,* vol. 3, p. 668, 2004.

[70] A. Fischer, Y. Show, G. Swain, "Electrochemical Performance of Diamond Thin-Film Electrodes from Different Commercial Sources," *Analytical Chemistry,* vol. 76, p. 2553, 2004.

[71] P. Lim, F. Lin, H. Shih, V. Ralchenko, V. Varnin, Y. Pleskov, S. Hsu, S. Chou, P. Hsu, "Improved stability of titanium based boron-doped chemical vapor deposited diamond thin-film electrode by modifying titanium substrate surface," *Thin Solid Films,* vol. 516, p. 6125, 2008.

[72] S. Pehlivanova, Ch. Petkov, C. Popov, P. Petkov, V. Boev, T. Petkova, "Nanostructured Diamond Electrodes for Energy Conversion Applications," in *Nanoscience Advances in CBRN Agents Detection, Information and Energy Security*, Springer, 2014, p. 479.

[73] C. Martinez-Huitle , S. Ferro, "Electrochemical oxidation of organic pollutants for the wastewater treatment: direct and indirect processes," *Chemical Society Reviews,* vol. 35, p. 1324, 2006.

[74] C. Terashima, T. Rao, B. Sarada, D. Tryk, A. Fujishima, "Electrochemical oxidation of chlorophenols at a boron-doped diamond electrode and their determination by high-performance liquid chromatography with amperometric detection," *Analytical Chemistry,* vol. 74, p. 895, 2002.

[75] K. Van Hege, M. Verhaege, W. Verstraete, "Indirect electrochemical oxidation of reverse osmosis membrane concentrates at boron-doped diamond electrodes," *Electrochemistry Communications,* vol. 4, p. 296, 2002.

[76] R. Compton, J. Foord, F. Marken:, "Electroanalysis at Diamond-Like and Doped-Diamond Electrode," in *Electroanalysis*, vol. 15, WILEY-VCH, 2003, p. 1349.

[77] J. Strojek, M. Granger, G. Swain, "Enhanced Signal-to-Background Ratios in Voltammetric Measurements Made at Diamond Thin-Film Electrochemical Interfaces," *Analytical Chemistry,* vol. 68, p. 2031, 1996,.

[78] J. Saterlay, D. Tibbettus, R .Compton, "Comparative study to evaluate the feasibility of sono-anodic and sono-cathodic stripping voltammetry for the determination of Pb in a Cu-Pb alloy," *Analytical Science,* vol. 16, p. 1055, 2000.

[79] J. Foord, K. Eaton, W. Hao, A. Crossley, "Interaction between co-deposited metals during stripping voltammetry at boron-doped diamond electrodes," *Physical Chemistry Chemical Physics,* vol. 7, p. 2787, 2005.

[80] J. Saterlay, J. Foord, R .Compton, "Sono-cathodic stripping voltammetry of manganese at a polished boron-doped diamond electrode: application to the determination of manganese in instant tea," *Analyst,* vol. 124, p. 1791, 1999.

[81] J. Xu, G. Swain, "Oxidation of Azide Anion at Boron-Doped Diamond Thin-Film Electrodes," *Analytical Chemistry,* vol. 70, p. 1502, 1998.

[82] Y. Zhou, J. Zhi, "Development of an amperometric biosensor based on covalent immobilization of tyrosinase on a boron-doped diamond electrode," *Electrochemistry Communications,* vol. 8, p. 1811, 2006.

[83] A. Chatterjee, R. Wiltshire, K. Holt, R. Compton, J.Foord, F. Marken, "Abrasive stripping voltammetry of silver and tin at boron-doped diamond electrodes," *Diamond and Related Materials ,* vol. 22, p. 646, 2002.

[84] L. Codognoto, S. Machado, L. Avaca, "Square wave voltammetry on boron-doped diamond electrodes for analytical determinations," *Diamond and Related Materials ,* vol. 11, p. 1670, 2002.

[85] K. Honda, T. Rao, D. Tryk, A. Fujishima, M. Watanabe, K. Yasui, H. Masuda, "Electrochemical Characterization of the Nanoporous Honeycomb Diamond Electrode as an Electrical Double-Layer Capacitor," *Journal of The Electrochemical Society,* vol. 147, p. 659, 2000.

[86] K. Honda, T. Rao, D. Tryk, A. Fujishima, M. Watanabe, K. Yasui, H. Masuda, "Impedance Characteristics of the Nanoporous Honeycomb Diamond Electrodes for Electrical Double-Layer Capacitor Applications," *Journal of The Electrochemical Society,* vol. 668, p. 148, 2001.

[87] E. Almeidaa, V. Trava-Airoldia, N. Ferreiraa, J. Rosolen, "Electrochemical insertion of lithium into a doped diamond film grown on carbon felt substrates," *Diamond and Related Materials ,* vol. 14, p. 1673, 2005.

[88] "http://www.cvd-diamond.com/properties_en.htm," [Online]. Available: http://www.cvd-diamond.com/properties_en.htm. [Accessed 10 2015].

[89] V. Vorlick, J. Rosa, M. Vanacek, M. Nesladek, L.M. Stals, "Proceedings of the 7th European conference on Diamond and Diamond-Like and Related Materials," *Diamond and Related Materials ,* vol. 2, p. 704, 1996.

[90] B. Dischler, C. Wild, Low-Pressure Synthetic Diamond Manufacturing and Applications, Springer, 1998.

[91] F. Maier, J. Ristein, L. Ley, "Electron affinity of plasma-hydrogenated and chemically oxidized diamond (100) surfaces," *Physical Review B,* vol. 64, p. 165411, 2001.

[92] R. Sussmann, CVD Diamond for Electronic Devices and Sensors, Wiley, 2009.

[93] M. Wang, N.Simon, C. Decorse-Pascanut, M. Bouttemy, A. Etcheberry, M. Li, R. Boukherroub, S. Szunerits, "Comparison of the chemical composition of boron-doped diamond surfaces upon different oxidation processes," *Electrochimica Acta,* vol. 54, p. 5818, 2009.

[94] A. Lafosse, M. Bertin, Sh. Michaelson, R. Azria, R. Akhvlediani, A. Hoffman, "Surface defects induced by in-situ annealing of hydrogenated polycrystalline diamond studied by high resolution electron energy loss spectroscopy," *Diamond and Related Materials,* vol. 17, p. 949, 2008.

[95] V. Seshan, D. Ullien, A. Castellanos-Gomez, S. Sachdeva, D. Murthy, T. Savenije, H. Ahmad, T. Nunney, S. Janssens, K. Haenen, M. Nesládek, H. van der Zant, E. Sudhölter, L. de Smet, "Hydrogen termination of CVD diamond films by high-temperature annealing at atmospheric pressure," *Journal of Chemical Physics,* vol. 138, p. 234707, 2013.

[96] M. Kasu, K. Ueda, H. Ye, Y. Yamauchi, S. Sasaki, T. Makimoto, "High RF output power for H-terminated diamond FETs," *Diamond and Related Materials,* vol. 18, p. 783, 2006.

[97] M. Wang, N. Simon, G. Charrier, M. Bouttemy, A. Etcheberry, M. Li, R. Boukherroub, S. Szunerits, "Distinction between surface hydroxyl and ether groups on boron-doped diamond electrodes using a chemical approach," *Electrochemistry Communications ,* vol. 12, p. 351, 2010.

[98] H.El-Haji, A. Denisenko, A. Kaiser, R. Balmer, E. Kohn, "Diamond MISFET based on boron delta-doped chanel," *Diamond and Related Materials,* vol. 17, p. 1259, 2008.

[99] M. Wang, N. Simon, C. Decorse-Pascanut, M. Bouttemy, A. Etcheberry, M.Li, R. Boukherroub, S. Szunerits, "Comparison of the chemical composition of boron-doped diamond surfaces upon different oxidation processes," *Electrochimica Acta,* vol. 54, p. 5818, 2009.

[100] N. Simon, H. Girard, D. Ballutaud, S. Ghodbane, A. Deneuville, M. Herlem, A. Etcheberry, "Effect of H and O termination on the charge transfer of moderately boron doped diamond electrodes," *Diamond and Related Materials,* vol. 14, p. 1179, 2005.

[101] S. Ghodbane, T. Haensel, Y. Coffinier, S.Szunerits, D.Steinmüller-Nethl, R. Boukherroub, S. Ahmed, J. Schaefer, "HREELS Investigation of the Surfaces of Nanocrystalline Diamond Films Oxidized by Different Processes," *Langmuir,* vol. 26, p. 18798, 2010.

[102] X. Wang, M. Hasegawa, K. Tsugawa , A. Ruslinda , H. Kawarada, "Controllable oxidization of boron doped nanodiamond covered with different solution via UV/ozone treatment," *Diamond and Related Materials,* vol. 24, p. 146, 2012.

[103] T. Sakaia, K.-S. Song, H. Kanazawa, Y. Nakamura, H. Umezawa, M. Tachiki, H. Kawarada, "Ozone-treated channel diamond field-effect transistors," *Diamond and Related Materials,* vol. 12, p. 1971, 2003.

[104] A. Voss, M. Mozafari, C. Popov, G. Ceccone, W. Kulisch, J. Reithmaier, "Stability of the surface termination of differently modified ultrananocrystalline diamond/ amorphous carbon composite films," *Surface and Coatings Technology,* vol. 209, p. 184, 2012.

[105] J. Miller, D. Brown, "Photochemical Modification of Diamond Surfaces," *Langmuir,* vol. 12, p. 5809, 1996.

[106] G. Zhang, K. Song, Y. Nakamura, T. Ueno, T. Funatsu, I. Ohdomari, H. Kawarada, "DNA Micropatterning on Polycrystalline Diamond via One-Step Direct Amination," *Langmuir ,* vol. 22, p. 3728, 2006.

[107] P. Actis, A. Denoyelle, R. Boukherroub, S. Szunerits, "Influence of the surface termination on the electrochemical properties of boron-doped diamond (BDD) interfaces," *Electrochemistry Communications ,* vol. 10, p. 402, 2008.

[108] F. Arefi-Khonsari, J Kurdi, M Tatoulian, J Amouroux, "On plasma processing of polymers and the stability of the surface properties for enhanced adhesion to metals," *Surface and Coatings Technology,* vol. 142–144, p. 437, 142–144.

[109] J. Melomedov, "Novel porphyrin amino acids as building blocks for artificial photosynthetic Reaction Centers: photoinduced energy and electron transfer," *PhD-thesis, Johannes Gutenberg university, Mainz,* 2014.

[110] S. Szunerits , C. Jama, Y. Coffinier, B. Marcus, D. Delabouglise, R. Boukherrou, "Direct amination of hydrogen-terminated boron doped diamond surfaces," *Electrochemistry Communications,* vol. 8, p. 1185, 2006.

[111] R. Willstater, "Investigations on Chlorophyll: Methods and Results," *Science Press,* 1928.

[112] K. Smith, "Porphyrins and Metalloporphyrins," *Elsevier,* p. 381, 1975.

[113] K. Kadish, K. Smith, R. Guilard, "The Porphyrin Handbook," in *Applications: Past, Present, Future ,* Academic Press, 2000.

[114] Y. Song, R. Haddad, S.-L. Jia, "Energetics and Structural Consequences of Axial Ligand Coordination in Nonplanar Nickel Porphyrins," *Journal of the American Chemical Society,* vol. 127, p. 1179, 2005.

[115] J. Retsek, C. Drain, C. Kirmaier, D. Nurco, C. Medforth, "Photoinduced Axial Ligation and Deligation Dynamics of Nonplanar Nickel Dodecaarylporphyrins," *Journal of the American Chemical Society,* vol. 125, p. 9787, 2003.

[116] P. Lanciano, B. Khalfaoui-Hassani, N. Selamoglu, F. Daldal, "Intermonomer Electron Transfer between the b Hemes of Heterodimeric Cytochrome bc1," *Biochemistry,* vol. 52, p. 7196, 2013.

[117] H. Horton,L. A. Moran, K. Scrimgeour, M. Perry, J. Rawn, Biochemie, 4th ed., Pearson Education, Inc., 2006.

[118] A. Battersby, C. Fookes. G. Matcham, E. McDonald, "Biosynthesis of the pigments of life: formation of the macrocycle," *Nature,* vol. 285, p. 17, 1980.

[119] R. Giovannetti, "The Use of Spectrophotometry UV-Vis for the Study of Porphyrins," *INTECH Open Access Publisher,* 2012.

[120] X. Wanga, H. Tamiaki, "Cyclic tetrapyrrole based molecules for dye-sensitized solar cells," *Energy & Environmental Science,* vol. 3, p. 94, 2010.

[121] R. Linstead, "Phthalocyanines. Part I. A new type of synthetic colouring matters," *Journal of the Chemical Society,* p. 1016, 1934.

[122] J. .Robertson, "An X-ray study of the structure of the phthalocyanines. Part I. The metal-free, nickel, copper, and platinum compounds," *Journal of the Chemical Society,* p. 615, 1935.

[123] J. Byrne, P.Kurz, *U.S.Patent,* p. 3, [121967.

[124] I. Muzikante, V. Parra, R. Dobulans, E. Fonavs, J. Latvels, M. Bouvet, "A Novel Gas Sensor Transducer Based on Phthalocyanine Heterojunction Devices," *Sensor,* vol. 7, p. 2984, 2007.

[125] A. Hains, Z. Liang, M. Woodhouse, B. Gregg, "Molecular semiconductors in organic photovoltaic cells," *Chemical Reviews,* vol. 110, p. 6689, 2010.

[126] L. Li, Q. Tang, H. Li, X. Yang, W. Hu, Y. Song, Z. Shuai, W. Xu, Y. Liu, D. Zhu, "An Ultra Closely p-Stacked Organic Semiconductor for High Performance Field-Effect Transistors," *Advanced Materials,* vol. 19, p. 2613, 2007.

[127] H. T. Y. Mizukawa, "Metal phtalocyanine dye mixture, curable composition, color filter, and method for producing color filter". US Patent US 8,445,167 B2, 2013.

[128] K. Sakamoto, E. Ohno-Okumura, "Synthesis and Functional Properties of Phthalocyanines," *Materials,* vol. 2, p. 1127, 2009.

[129] Y. Harima, S. Furusho, K. Okazaki, Y. Kunugi, K. Yamashita, "Charge transport in vacuum-sublimed films of metal-free tetraphenylporphyrin and its relation to capacitance and photocurrent measurements," *Thin Solid Films,* vol. 300, p. 213, 1997.

[130] "engineersedge.com," [Online]. Available: https://www.engineersedge.com/heat_transfer/thermal-conductivity-gases.htm. [Accessed 9 2015].

[131] O. Shenderova, S. Hens, G. McGuire, "Seeding slurries based on detonation nanodiamond in DMSO," *Diamond and Related Materials,* vol. 19, p. 260, 2010.

[132] W. Kulisch, C. Petkov, E. Petkov, C. Popov, P. Gibson, M. Veres, R. Merz, B. Merz, J.Reithmaier, "Low temperature growth of nanocrystalline and ultrananocrystalline diamond films: A comparison," *Physica Status Solidi (a),* vol. 9, p. 1664, 2012.

[133] K. Tsugawa, M. Ishihara, J. Kim, Y. Koga, M. Hasegawa, "Nucleation Enhancement of Nanocrystalline Diamond Growth at Low Substrate Temperatures by Adamantane Seeding," *Journal of Physical Chemistry C ,* vol. 114, p. 3822, 2010.

[134] W. Yang, F. Lu, Z. Cao, "Growth of nanocrystalline diamond protective coatings on quartz glass," *Journal of Applied Physics,* vol. 19, p. 10068, 2002.

[135] A. V. d. Drift, "Evolutionary selection, a principle governing growth orientation in vapour-deposited layers," *Philips Research Reports,* vol. 22, p. 267, 1967.

[136] Q. Wang, A. Kromka, J.Houdkova, O. Babchenko, B.Rezek, M.Li, R.Boukherroub, S.Szunerits, "Nanomolar Hydrogen Peroxide Detection Using Horseradish Peroxidase Covalently Linked to Undoped Nanocrystalline Diamond Surfaces," *Langmuir,* vol. 28, p. 587, 2012.

Bibliography

[137] "http://xpssimplified.com/elements/carbon.php," [Online]. Available: http://xpssimplified.com/elements/carbon.php. [Accessed 10 2015].

[138] T. Ramanathan, F. Fisher, R. Ruoff, L. Brinson, "Amino-Functionalized Carbon Nanotubes for Binding to Polymers," *Chemistry of Materials,* vol. 17, p. 1290, 2005.

[139] P. Reintanz, "Dissertation, Uneversity of Kassel," 2015.

[140] U. Siemeling, C. Schirrmacher, U. Glebe, C. Bruhn, J. E. Baio, L. Árnadóttir, D. G. Castner, T. Weidner, "Phthalocyaninato complexes with peripheral alkylthio chains: disk-like adsorbate species for the vertical anchoring of ligands onto gold surfaces," *Inorganica Chimica Acta,* vol. 374, p. 302, 2011.

[141] D. Opris, F. Nüesch, C. Löwe, M. Molberg, M. Nagel, "Synthesis, characterization, and dielectric properties of phthalocyanines with ester and carboxylic acid functionalities," *Chemistry of Materials,* vol. 20, p. 6889, 2008.

[142] D. Tackley, G. Dent, W. Smith, "Phthalocyanines: structure and vibrations,," *Physical Chemistry Chemical Physics,* vol. 3, p. 1419, 2001.

[143] Y. Coffinier, S. Szunerits, B. Marcus, R. Desmet, O. Melnyk, L. Gengembre, E. Payen, D. Delabouglise, R. Boukherroub, "Covalent linking of peptides onto oxygen-terminated boron-doped diamond surfaces," *Diamond and Related Materials,* vol. 16, p. 892, 2007.

[144] Z. Xu, A. Kumar, A. Kumar, "Amperometric Detection of Glucose Using a Modified Nitrogen-Doped Nanocrystalline Diamond Electrode," *Journal of Biomedical Nanotechnology,* vol. 1, p. 416, 2005.

[145] J. Yang, K. Chong, G. Zhang, K.-S. Chong, M. Degawa, Y. Sasaki, I. Ohdomari, H. Kawarada, "Characterization of DNA Hybridization on Partially Aminated Diamond by Aromatic Compounds," *Langmuir,* vol. 22, p. 11245, 2006.

[146] G. Zhang, K. Chong, Y. Nakamura, T. Ueno, T. Funa-tsu, I. Ohdomari, H. Kawarada, "DNA Micropatterning on Polycrystalline Diamond via One-Step Direct Amination," *Langmuir,* vol. 22, p. 3728, 2006.

[147] Ch.Petkov, P. Reintanz, W. Kulisch, A. Degenhardt, T. Weidner, J. Baio, R. Merz, M. Kopnarski, U. Siemeling, J.P. Reithmaier, C. Popov , "Functionalization of nanocrystalline diamond films with phthalocyanines," *Applied Surface Science,* 2016.

[148] [Online]. Available: http://xpssimplified.com/elements/oxygen.php. [Accessed 10 2015].

[149] M. Seredych, D, Hulicova-Jurcakova, G. Lu, T. Bandosz, "Surface functional groups of carbons and the effects of their chemical character, density and accessibility to ions on electrochemical performance," *Carbon,* vol. 46, p. 1475, 2008.

[150] A. Schmidt, T. Schuerlein, G. Collins, N. Armstrong, "Ordered Ultrathin Films of Perylenetetracarboxylic Dianhydride (PTCDA) and Dimethylperylenebis(dicarboximide) (Me-PTCDI) on Cu(100): Characterization of Structure and Surface Stoichiometry by LEED, TDMS, and XPS," *Journal of Physical Chemistry,* vol. 30, p. 11770, 1995.

[151] L. Lozzi, L. Ottaviano, S. Santucci, "High resolution XPS studies on hexadecafluoro-copper-phthalocyanine deposited onto Si(111)7×7 surface," *Surface Science,* vol. 470, p. 265, 2001.

[152] E. Kohn, A. Denisenko, "Doped Diamond Electron Devices," in *CVD diamond for electronic devices and sensors*, John Wiley & Sons, 2009, p. 313.

[153] H. Kawarada, V. Araki, H. Umezawa, "Electrolyte-solution-gate FETs using diamond surface," *Physica Status Solidi (a),* vol. 185, p. 79, 2001.

[154] A. Denisenko, G. Jamornman, H. El Hajj, E. Kohn, "pH sensor on O-terminated diamond using boron-doped channel," *Diamond and Related Materials,* vol. 16, p. 905, 2007.

[155] T. Kondo, K. Honda, D. Tryk, A. Fujishima, "Covalent Modification of Single-Crystal Diamond Electrode Surfaces," *Journal of The Electrochemical Society,* vol. 2005, p. E18, 2005.

[156] H. Notsu, I. Yagi, T. Tatsuma, D. Tryk, A. Fujishima;, "ntroduction of oxygen–containing functional groups onto diamond electrode surface by oxygen plasma and anodic polarisation," *Electrochemical and Solid-State Letters,* vol. 2, p. 522, 1999.

[157] T. Rao, D. Tryk, K. Hashimoto and A. Fujishima, "Band-edge movements of semiconducting diamond in aqueous electrolyte induced by anodic surface treatment," *Journal of The Electrochemical Society,* vol. 146, p. 680, 1999.

[158] J. Bechter, C. Pietzka, C. Petkov, P. Reintanz, U. Siemeling, C. Popov, A. Pasquarelli, "Investigation of diamond electrodes for photo-electrochemistry," *Physica Status Solidi (a),* vol. 211, p. 2333, 2014.

[159] H. T. X.F. Wanga, "Cyclic tetrapyrrole based molecules for dye-sensitized solar cells," *Energy Environ. Sci., vol. 3,* p. 93, 2010.

[160] O. Shenderova, S. Hens, I.Vlasov, V. Borjanovic, G. McGuire, "Nanodiamond Particles in Electronic and Optical Applications," *Mater. Res. Soc. Symp. Proc. ,* vol. 1203, p. 1203, 2010.

[161] M. Schreck, "Heteroepitaxial Growth," in *CVD diamond for electronic devices and sensors*, John Wiley & Sons, Ltd, 2009, p. 125.

Publications of the author

1. Ali B. Alamin Dow, Lu Hanlei, M. Schneider, **Ch. Petkov**, A.Bittner, C. Popov, U. Schmid, Nazir P. Kherani, "Ultra-nanocrystalline diamond based high velocity SAW davice fabricated by electron beam lithography", *IEEE Transaction on Nanotechnology*, vol. 11, p. 979, 2012

2. W. Kulisch, **Ch. Petkov**, E. Petkov, C. Popov, P.N. Gibson, M. Veres, R. Merz, B. Merz, J.P. Reithmaier, "Low temperature growth of nanocrystalline and ultrananocrystalline diamond films: A comparison", *Physica Status Solidi (a)*, vol. 209, p. 1664, 2012

3. **Ch. Petkov**, L. Himics, U. Glebe, R. Merz, E. Petkov, W. Kulisch, A. Pasquarelli, U. Siemeling, C. Pietzka, J.P. Reithmaier, M. Veres, C. Popov: "Grafting of manganese phthalocyanine on nanocrystalline diamondfilms", *Physica Status Solidi (a)*, vol. 210, p. 2048, 2013

4. J.Evtimova, W.Kulish, **Ch.Petkov**, E. Petkov, F. Schnabel, J.P. Reithmajer, C. Popov: "Reactive ion etching of nanocrystalline diamond for the fabrication of one-dimensional nanopillars", *Diamond and Related Material*, vol. 36, p. 58, 2013

5. E. Petkov, C. Popov, T. Rendler**, Ch. Petkov**, F. Schnabel, H. Fedder, S.-Y, Lee, W. Kulisch, J.P. Reithmaier and J. Wrachtrup, "Investigation of NV centers in diamond nanocrystallites and nanopillars", *Physica Status Solidi (b)*, vol. 250, p. 48, 2013

6. J. Bechter, C. Pietzka, **Ch.Petkov**, P. Reintanz, U. Siemeling, C. Popov, A. Pasquarelli, "Investigation of diamond electrodes for photo-electrochemistry", *Physica Status Solidi (a)*, vol. 211, p. 2333, 2014

7. S. Pehlivanova, **Ch. Petkov**, C. Popov, P. Petkov, V. Boev, T. Petkova, "Nanostructured Diamond Electrodes for Energy Conversion Applications," in Nanoscience Advances in CBRN Agents Detection, Information and Energy Security, Springer, p. 479, 2014

Publications of the author

8. S. Pehlivanova., **Ch. Petkov**, A. Surleva, P. Petkov, C. Popov, T. Petkova, "Diamond electrodes for waste water treatment", *Bulgarian Chemical Communications*, 2015 to be published

9. **Ch.Petkov**, P. Reintanz, W. Kulisch, A. Degenhardt, T. Weidner, J. Baio, R. Merz, M. Kopnarski, U. Siemeling, J.P. Reithmaier, C. Popov, "Functionalization of nanocrystalline diamond films with phthalocyanines", *Applied Surface Science* 2016- submitted

Selbstständigkeitserklärung

Selbstständigkeitserklärung

Hiermit versichere ich, dass ich die vorliegende Dissertation selbstständig und ohne unzulässige bzw. nicht ausdrücklich in der Arbeit genannte fremde Hilfe verfasst habe und dass alle wörtlich oder sinngemäß aus Veröffentlichungen entnommenen Stellen dieser Arbeit unter Quellenangabe einzeln kenntlich gemacht sind. Die Arbeit wurde in gleicher oder ähnlicher Form zu keiner anderen Prüfung vorgelegt und auch noch nicht veröffentlicht.

Kassel, den 15.03.2016

Acknowledgements

First of all, I would like to thank the Institute of Nanostructure Technologies and Analytics, University of Kassel for the opportunity to prepare my doctoral thesis here.

Deep appreciation goes to Priv. Doz. Dr. Cyril Popov for being a marvelous mentor giving me a great start and familiarization in this new environment. He has showed incredible patience helping me to solve various scientific and non-scientific problems, supervising my work and being always on disposal when help is needed.

I would also like to thank Prof. Dr. Ulrich Siemeling, Prof. Dr. Martin Garcia, Prof. Dr. Kilian Singer, for taking part as committee members of my public defense. Next gratitude goes to Professor Dr. Johann Peter Reithmaier for accepting me at INA and giving me the opportunity to be here now.

I also would like to express my special gratitude to my brother, Dr. Emil Petkov, for the support in hard workdays and countenance both professionally and personally. Then, many thanks Florian Schabel for his unconditional assistants in the clean room, teaching me how to work with the various equipment, giving me useful tips, always having a simple answer to my questions. Additionally thanks to the whole "diamond' group- Alexandra Voos, Nina Felgen for the great team work. I would like to express gratitude to Dr. Wilhelm Kulisch, for sharing his unique theoretical knowledge and helping in the thesis improvement.

I cannot end these acknowledgments without thanking my family, their encouragement, support and love which have been a constant throughout my life.

Finally, I want to express my profound gratitude to my dearest Tina who is always there for me, supporting me and giving me strength and love during my work. I am truly thankful for having you in my life.

To my fiancé I dedicate my thesis…